Numerical modelling of the excitation of polyatomic molecules by femtosecond laser beams

by

Ludwig Erasmus de Clercq

Thesis presented in partial fulfillment of the requirements for the degree of Masters of Science

at

the University of Stellenbosch

Physics Department

Faculty of Natural Science

Supervisor: Dr Lourens R. Botha
Co-supervisor: Professor Erich G. Rohwer

March 2011

Declaration

By submitting this thesis electronically, I declare that the entirety of the work contained therein is my own, original work, that I am the sole author thereof (save to the extent explicitly otherwise stated), that reproduction and the publication thereof by Stellenbosch University will not infringe any third party rights and that I have not previously in its entirety or in part submitted it for obtaining any qualification.

Date: 1 March 2011

Abstract

The selective excitation of an arbitrary vibrational level of a polyatomic molecule, without passage through an intermediary electronic excited state is demonstrated. This was achieved by simulating the interaction of a shaped, femtosecond pulse with one vibrational mode of the molecule. The carrier frequency of the pulse is chosen near resonant to the ground-to-first-excited vibrational transition of the mode, and the pulse shape is optimized via closed-loop feedback. The simulation concentrates on the first few vibrationally excited states since the density of states is still low, thus ensuring that the inter-vibrational decoherence time is relatively long compared to the pulse length.

While various molecules were investigated this study focuses onUF_6 for which detailed spectroscopic data for the ν_3 vibrational mode is available in literature. A multilevel model was developed and can be adapted for any number of levels. The model reported here was limited to a vibrational quantum number of four. The spectroscopic data included anharmonic splitting as well as forbidden transitions. The effect of rotational levels was not included. A density matrix approach was followed because this will allow for the introduction of dephasing of the coherent excitation via thermalizing collisions with the reservoir, as well as inter-vibrational relaxation. The time evolution of the density matrix is given by the Von Neumann equations.

Opsomming

Die selektiewe opwekking van 'n arbitêre vibrasionele vlak van 'n poliatomies molekule sonder oorgang na 'n intermediëre elektroniese opgewekte toetstand word gedemonstreer. Dit was bereik deur die interaksie te simuleer van 'n gevormde, femtosekonde pulse met een vibrasionele mode van 'n molekule. Die draer frekwensie van die pulse is so gekies dat dit naby resonansie van die grond-tot-eerste-opgewekte vibrasionele oorgang van die mode is, die puls vorm word geoptimeer deur 'n geslote-lus terugvoer. Die simulasie konsentreer op die eerste paar vibrasionele opgewekte toestande, omdat die digtheid van toestande nog steeds laag is, dus verseker dit dat inter-vibrasionele de-koherensie tyd relatief lank is in vergelyking met die puls se lengte.

Verskillende molekules was ondersoek vir die studie. Die fokus is op UF_6 waarvoor gedetaileerde spektroskopiese data vir die ν_3 vibrasionele beskikbaar is in die literatuur. 'n Multivlak model was ontwikkel en kan aangepas word vir enige aantal van vlakke. Die model wat hier aangemeld is, is beperk tot die vibrasionele kwantum getal van vier. Die spektroskopiese data het anharmonies splitting so wel as nie toegelaatbare oorgange bevat. Die effek van rotasionele vlakke was nie in berekening geneem nie. 'n Digtheids matriks benadering was gevolg, omdat dit toelaat vir die dekoherensie. Die tyd evolusie van die digtheids matriks word gegee deur die Von Neumann vergelykings.

Acknowledgments

I have come to know many people while working to completing my masters who have helped me and guided me during my research. Firstly my thanks goes to Dr Lourens Botha for all the support and time spent to help me finish my masters. His passion for the work we have done ignited my own and we have worked well together on this project. To prof Erich Rohwer, my supervisor at Stellenbosch, thank you for the knowledge you have bestowed upon me during the lectures. Prof Heinrich Schwoerer, thank you for all the time and effort you have spent with me in lectures, discussions on molecular physics and coherent control in general. To Dr Hermann Uys, thank you for helping sort out some of the problems I had during the course of the project. Dr Anton Du Plessis, thank you for helping me keep in touch with the practical side of things.

The time I have spent in the student room, at the NLC, I have come to know new friends and colleagues. Oliver Collett, I really enjoyed our discussions about pretty much everything. Thanks for your help with the infamous Fourier transforms which I just did not know so much as you did, it really helped me quite a lot. Questioning my assumptions and arguing about the validity, kept me sharp during my research. Nicolene Botha, we have really spend a lot of time the past year to discuss spatial light modulators (SLMs), simulations and a lot of other things. Thanks that I can just come and bother you, your willingness to help I greatly appreciate. Malcolm Govendor and Darryl Naidoo, thanks for all your jokes and conversations which really can cheer up a bad mood. Attie Hendriks, my cubicle mate, thanks for all the interesting conversations we had. Cobus Jacobs, our chats about nearly anything, I enjoyed it a lot and thank you for reintroducing me to bubble-bobble. Thanks for your help on Fourier transforms and their applications.

To my family thank you so much for your support in the past years with my studies and keeping me motivated! To two of my best friends Nic Roets and Dawie van der Merwe, you guys are awesome! Lastly Adré Engelbrecht, you have changed my life and my view of it, without your understanding and support I do not know how I would have come this far, I really appreciate it. You will always have a special place in my heart.

To God and my family.

Contents

List of Figures

List of Tables

Chapter 1

Introduction

1.1 Introduction

Controlling chemical reactions and the dynamics through which molecules break up is at the forefront of femtochemistry. From the same reagents in chemical reactions multiple hypothetical products can form, adapted from [1], consider the following possible reactions,

$$A + B \rightarrow C + D \tag{1.1}$$
$$\rightarrow E + F \tag{1.2}$$
$$\rightarrow G + H \tag{1.3}$$

A and B depicts two different molecules and C, D, E, F, G and H represent various products. Each of the combinations, C + D, E + F and G + H represents a product channel, also known as a branch of the reaction. Each of these branches has a different associated reaction rate. If x, y and z are the product percentages corresponding to the branches, C + D, E + F and G + H the branching ratio is defined as

$$x : y : z. \tag{1.4}$$

Thus when the branching ratio is manipulated the amount of the different products are varied.

One might ask how whether branching ratios be controlled? Traditionally, chemists have done this by varying macroscopic thermodynamic parameters, such as temperature, pressure and concentration [2]. For example, the Arrhenius equation [3] gives the dependence of the reaction rate on temperature, while reaction rate equations are concentration dependent. The influence of pressure on the reaction rate of reagents in the solid or liquid state, in general, is minor, while in gas phase pressure dependence can be significant. Changing the reaction rates will result in different branching ratios.

More recently an alternative to controlling branching ratios has been developed [4, 5, 6, 7, 8]. This approach is based on quantum interference between multiple paths, via different intermediate states that link a starting quantum state with the target state [9]. Interference is a coherent phenomenon and as a result this approach is known as quantum coherent control. Coherent control can be applied to the selective excitation of molecules [10, 11] and state selective excitation [12, 13]. All coherent control procedures have one thing in common, the use of lasers.

For the current study, the interest lies in bond selective excitation, specifically within a polyatomic molecule. The idea is to control the population distribution of these molecules in the gas phase such that most are in a preselected vibrational state within a specific vibrational mode after an ultrashort pulse has interacted with the system. This will therefore demonstrate that coherent control could

result in a system that is far from thermal equilibrium and furthermore that this can be done in a selective manner.

The process of photodissociation is a process that is concerned with the breakup of specific bonds in molecules. To achieve this, a single mode within a molecule is excited, as well as a specific vibrational state within this mode. This could lead to selective dissociation of a particular bond within the molecule. The concept of branching ratios still applies to the case, even if there is only one type of molecule present in a gas phase or any other phase. The branching ratio in this case will be the ratio of the different products that can form, from the photodissociation process. Experimental realizations and theoretical descriptions of the photodissociation process could be found in [14, 15].

If the molecule is excited in this specific manner, there is still a problem. A molecule excited in a particular vibrational mode will very quickly distribute its energy among all the other vibrational modes. This is known as inter-vibrational relaxation (IVR) and occurs on timescales of the order of femto- to picoseconds. Narrow band lasers have durations in the order of nanoseconds and more, thus using them to manipulate the excitation of molecules would only be as efficient as using a flame. The dynamics of the molecule should be manipulated at time scales shorter than the IVR timescales. Thus a femtosecond laser would be necessary in order to either observe or manipulate the dynamics of the molecule, before IVR can settle in.

Using femtosecond lasers in order to manipulate the dynamics of molecules solves the problem of IVR that destroy the coherence of the system, but using ultrafast laser present a new problem. It is well known that the time duration and bandwidth of a laser is related by the uncertainty principle. Thus for these ultrafast lasers, large bandwidths exist and these can overlap several vibrational level transitions. In the 1980s two techniques have been developed simultaneously for coherent control, one using continuous wave lasers (although not restricted to their use) and the other using femtosecond lasers. Both of these techniques when applied to femtosecond pulses provide a solution to the problem of IVR. Some of the very earliest coherent control experiments on chemical reactions have used these methods, they are[4, 5],

- Two-pathway control scheme, developed by Brumer and Shapiro.
- Pump-dump control scheme, developed by Tannor, Kosloff and Rice.

Various other methods were developed using variations on the two mentioned techniques to coherently control chemical reactions. It was later realized that these apparently different control methods could all be described within the framework of Quantum Optimal Control Theory (QOCT). QOCT is a theoretical technique used to find a pulse that will optimally control a reaction given an objective. The process leads to equations that can be tedious and difficult to solve. It has also been shown that the pulses obtained by applying the QOCT technique are not always experimentally feasible to implement [16]. Thus QOCT was implemented experimentally as an adaptive feedback control (AFC) type of experiment. In the experiment a pulse shaping device is controlled by a learning loop and some measurement is optimized within the AFC experiment. Adaptive feedback control simulations (AFCS) are a search for optimality within the quantum system, given an objective. AFCS is a numerical process that mimics a real AFC experiment. The details of QOCT, AFC and AFCS are left to the next chapter.

1.2 Objectives

- To create an adaptive feedback control simulation (AFCS) which will be able to simulate the interaction of an ultra short pulse with a cold gas of spherical top molecules.
- To maximize the population of a specific vibrational state within the ground electronic state of a polyatomic molecule and to analyze the obtained pulses with frequency resolved optical gating (FROG) traces and Husimi distributions.

- In addition, issues of importance to optimal quantum control will be investigated, such as the uniqueness and robustness of the obtained solutions.

1.3 Research question

Can a shaped femtosecond pulse be used to selectively excite a specific vibrational state of a polyatomic molecule within the ground electronic state, without making use of intermediary excited electronic states?

1.4 Assumptions

- The medium will be assumed to be completely isotropic.
- The gas of molecules will be extremely cold, formed by cooling by expansion.
- The initial population distribution of the vibrational levels, as a function of temperature, can be described by the canonical distribution. A distribution of the population as a function of temperature is given in appendix B.1.

1.5 Motivation

The work that is presented in this thesis is intended for an experimental physicist to determine whether it is possible to carry out coherent control experiments for molecules in the ground electronic state. Optimizing a specific vibrational state without making use of other excited electronic states must be implemented. This will introduce a new method, to the best of our knowledge, of doing coherent control with the purpose of selective excitation of an arbitrary vibrational state in polyatomic molecules.

Chapter 2

Literature Review

2.1 Introduction

Chemical reactions have classically been manipulated by changes made to parameters, like pressure and temperature or the addition of a catalyst [2]. In molecular chemical reactions the molecular vibrations are what drive the reaction [17]. For a reaction to take place old bonds must break and new ones must form. In order for this to occur, the nuclear positions of the atoms building up the molecule must be rearranged. Since the invention of the laser, scientists have hoped that lasers might assist in controlling chemical reactions [17, 18].

Initially it was thought that to control chemical reactions with lasers would be quite a simple feat [19]. All that was necessary was to excite a particular bond with a laser and the bond should break. It was thought that a narrow band laser could be used to excite a specific bond and that it would lead to mode selective chemistry. It was soon realized, however, that the energy quickly dissipated among all the degrees of freedom [20], thus into all the vibrational modes of the molecule. It would thus have the same effect as heating the molecule using a flame. The dissipation of the energy in the molecule to all the degrees of freedom will lead to breaking of weaker bonds in the molecule based on a statistical process [19]. Obtaining targeted bond breaking is thus lost. This process in which the energy is dissipated among all the degrees of freedom within the molecule is known as, inter-vibrational relaxation (IVR).

The typical timescale of IVR can vary from femto- to picoseconds and depends on the molecule [21], a study of these rates for the lower vibrational levels of a spherical top molecule is given in [22]. To achieve coherent control, manipulation of the system is required before dephasing can set in. Thus femtosecond lasers are ideal, for they act in the timescales before IVR can destroy the coherence within the quantum system. The only problem left is that an ultra short pulse has a large bandwidth and this leads to the excitation of all the states that are covered within the bandwidth of the laser. Coherent control techniques, the subject of this chapter, provide a solution.

The first section of this chapter will describe some of the early coherent control techniques. To follow, a section is devoted to quantum optimal control theory (QOCT). The search for optimal control with laser pulses, in the laboratory, is done by adaptive feedback control experiments (AFC) and will be discussed in a separate section. Adaptive feedback control simulations (AFCS) are also quantum optimal control in which AFC experiments are simulated, a section is devoted to AFCS.

2.2 Early quantum control techniques

Progress toward coherent control of chemical reactions was first made in the late 1980s [4, 23]. Brumer and Shapiro developed the two-pathway quantum interference technique in which lasers are used to control chemical reactions [4, 24]. If, in a quantum system, there are various paths that can be taken to arrive in a final state, then the different routes that could be taken to arrive at the final state can interfere, this is core to Feynman's path integral approach to quantum mechanics [25]. By changing the phases and amplitudes of continuous wave (CW) lasers, the different routes that are taken to arrive at the final state can be controlled in a quantum system. This results in coherent control of the system. Two monochromatic lasers for which the intensities and phases can be varied are used to achieve the two-pathway control. Schematic representations of two different realizations of two-pathway control are shown in Figures 2.1 and 2.2 obtained from reference [24].

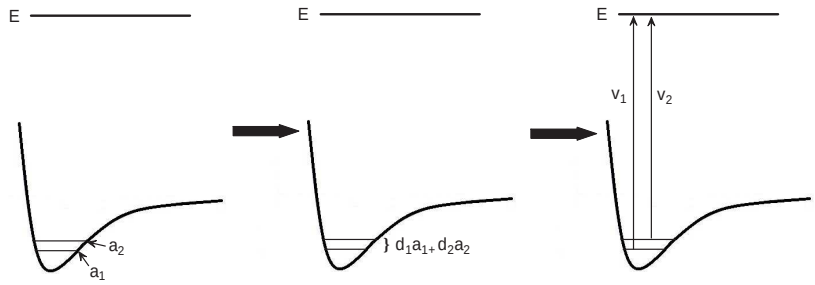

Figure 2.1: The system is first prepared in a superposition of two vibrational states within the ground state. The superposition can be described as, $d_1a_1 + d_2a_2$. Two lasers with frequencies ν_1 and ν_2 of which the phase difference between them can be varied, is used to control the quantum interference on state E that lies in the upper electronic state.

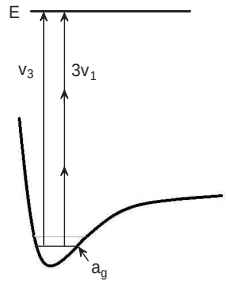

Figure 2.2: The different optical route procedure. No preparation of a superposition of states is necessary. Two lasers with frequencies ν_1 and ν_3 in which the condition, $3\nu_1 = \nu_3$ is fulfilled is used. The laser with frequency ν_1 must be intense enough to allow for the three photon process. The phase difference between the two lasers is used to control the interference on state E that lies in the upper electronic state.

It was shown that by changing the relative phase between the two lasers, it would be possible to control the branching ratios of molecular reactions [24]. This particular method could also be applied to the population transfer between bound states and the control thereof [26, 27]. Either only odd or only even number of photons can be used to control the population dynamics within bound states using the two-pathway technique, the reason for this is explained in terms of parity conservation in [24].

Experimental realization of the two-pathway control technique only came in the 1990s with experiments controlling population dynamics [26], photodissociation of products [28], control of cross sections of photochemical reactions [29] and other. In practice though, it was difficult to obtain the same rate of excitation along different pathways. This could be due to an absorption cross section that was too small, or that competing processes were interfering [19]. In addition, due to the fact that, initially, the process employed CW lasers, de-coherence was still a problem. One needs to operate on time scales shorter than the de-coherence time of the system, which in many cases is limited by the IVR time. Femtosecond lasers which have a natural broad bandwidth provided a solution.

In the 1980s Tannor, Kosloff and Rice simultaneously developed a technique called pump-dump control. In figure 2.3 a schematic representation of this method is given. In this control scheme two time delayed pulses with the same carrier frequency are used [30, 19]. A wave packet is formed, when the population from the ground state is transferred to an excited electronic state. A wave packet forms due to the overlap of the various vibrational levels within the ground electronic state with those in the excited electronic state. The amount by which they overlap is determined by the bandwidth of the laser pulse used [31]. The overlap integrals of the different wave-functions, of the two distinct electronic states, are called the Franck Condon factors. The linear combination of all the vibrational states in which overlap took place, within the excited electronic state, forms a vibrational wave packet. Franck Condon factors are the main contributors of the coefficients that determine how the different vibrational states are added, in the linear combination [31, 32]. The wave packet evolves within the potential well of the excited electronic state, until the dump pulse is used to force the wave-packet back to the ground electronic state. The time delay between the pump and dump pulses can be used to obtain reaction selection, since the time delay determines which reaction channel the wave-packet will evolve into, on the ground electronic state [5, 30].

In general the scheme is called the pump-dump scheme, but the scheme is not limited to the use of only pump and a dump pulses. There are times when two pump pulses could be used to force the wave-packet to a higher electronic state [25] resulting in a pump-repump scheme. There have been various experimental realizations of this scheme [33, 34]. This technique was not only used in coherent control, but also for the investigation of transient molecular states [35] in which case pump-probe spectroscopy could be used. With femtosecond lasers that have become more available over the years, the application of this technique still find many more experimental realizations. The drawback of this scheme is that only transform limited pulses are used.

Various techniques were developed to increase the effectiveness of the pump-dump process. For example, in stimulated emission pumping (SEP), two pulses with different frequencies are used, but the time delay is not necessarily varied [36]. An improvement on this was control via stimulated Raman adiabatic passage (STIRAP), the time delay between the two pulses of possibly different frequencies is varied. What makes STIRAP really different from SEP is that the sequence in which the pump and dump pulses is applied is reversed, which seems to be counter intuitive [37]. Various control techniques, different from the pump-dump scheme and two-pathway control, have been developed to control population dynamics, branching ratios of chemical reactions, controlling photocurrents etc. [19].

2.3 Quantum optimal control theory (QOCT)

Initially, the different control schemes mentioned in the previous section were thought to be fundamentally different. It was later realized that they are all elements within a larger control scheme in which quantum interference within the system is controlled. The limitations of these control schemes are, in general, only a few parameters are varied to control the system. The small degree of freedom available to the control field might be suitable for simple systems, but in general to manipulate more

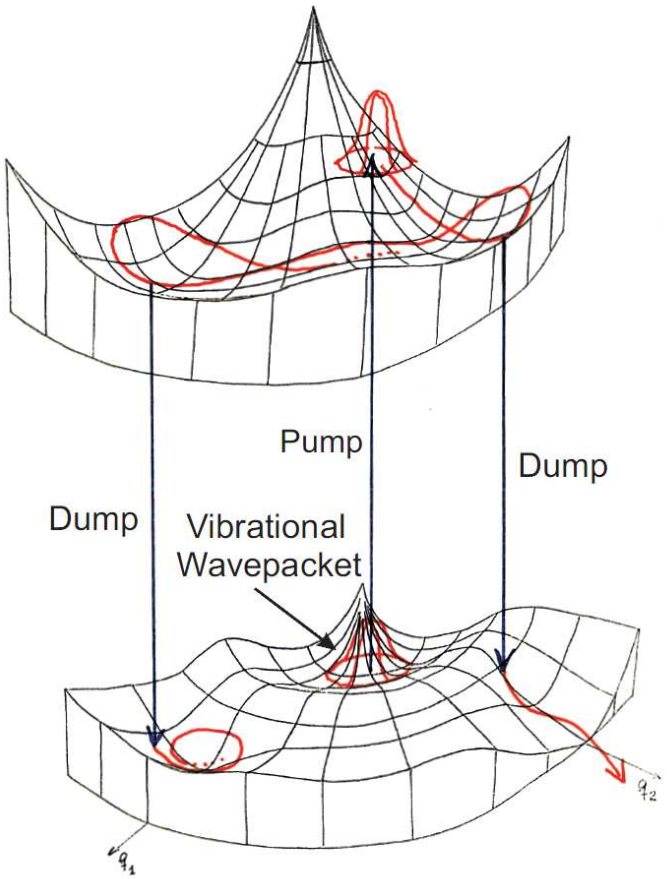

Figure 2.3: The potential surfaces of the lower and upper electronic state with two general quantum coordinates indicated, q_1 and q_2 are shown. For pump-dump control a pump pulse is used to lift the population from the ground vibrational state within the ground electronic state to an excited electronic state (upper potential surface). The wave packet that is formed on the excited electronic state can evolve freely as shown by the red track on this electronic state. Two places where dump pulses could be applied are shown. At these points in time if the dump pulse were to be applied, the wave packet will be de-excited back to the locations shown on the ground electronic level. These locations can represent in this case, an isomerization of a molecule (on the left) or dissociation (on the right). Source: Prof. H. Schwoerer, Stellenbosch University

complex systems, there should be more parameters involved.

Theoretically, it was shown that it is possible to control the evolution of a quantum system to a desired reaction channel by specifically shaping the control field to the characteristics of the system [38, 39]. QOCT could be used to tailor control fields in a manner such that a specific goal could be reached [38, 40]. It is not common that the optimal field has a simple structure. In general the structure is complex both in the time domain and frequency domain [19]. The amplitudes and phases of the frequency components of the initial transform limited pulse are manipulated and a shaped control

field is found. When control in a quantum system is desired, the obtained final control field that is found to reach an objective manipulates the system in a specific manner. The interference among all the different routes is optimized by the control field, such that the routes that are taken interfere constructively.

A typical example of QOCT is setting up equations describing the quantum system to be controlled [19]. In the procedure an objective functional is created. In the function various constraints could be included. There are various types of objective functionals. The types of functionals that have no condition during the time when control is applied to the system and is only interested in the final outcome due to the control, is known as Mayer type functionals [19]. Thus Mayer type of functionals is only dependent on the final time. Three of these types of functionals have been of particular interest these are; evolution-operator control, state control and observable control.

Controllability of a quantum system is defined as the ability that a control function can configure the quantum system from one to another configuration within finite time T [19]. For evolution-operator control a unitary transformation at time T, U(T), is tailored in such a manner that it resembles closely the target unitary transformation W. In state control the objective is to transform the initial state ρ_0 to a target state ρ_f in the limited time T. Lastly for observable control, the probability of observing a specific state is to be maximized.

What is of concern for the current study is state control, also known as density matrix control. This requires a control that would ensure the evolution from density matrix ρ_1 to ρ_2. The equivalence of density matrix control to that of evolution operator control has been established by [41, 42]. There are various methods to obtain an optimal control and in the section on adaptive feedback control simulations (AFCS) another technique will be discussed.

QOCT has been applied to many problems, such as molecular isomerization [43] and other manipulations on molecular systems [38, 39, 40]. The controls that are found by using the QOCT technique are only as good as the amount of detail that is available to describe the system's Hamiltonian which in most instances is not known in great detail. There is also the difficulty implementing theoretical control designs in the laboratory. Optimal controls that are found by the QOCT techniques might differ significantly from that which is found experimentally, for it is usually not possible to include all the factors that can influence the results in the laboratory in QOCT .

2.4 Adaptive feedback control (AFC)

Adaptive feedback control (AFC), is an experimental realization of QOCT. Unlike QOCT, where the degree to which you can describe the system Hamiltonian determines the obtained optimal control, AFC does not require the same prior knowledge in order to control the quantum system [19]. In AFC measurements could be taken and an arbitrary measurement could be used as a fitness function. A fitness function, similar to an objective functional, is the function that is optimized in a learning loop experiment. The Schrödinger equation, subject to control, is solved experimentally and iteratively in AFC to obtain some objective. Figure 2.4 depicts the AFC process in which a learning loop could be used to optimize the objective functional. Typical examples of learning loops are, genetic algorithms, ant colony optimization, evolutionary algorithms and the Nelder Mead algorithm. A pulse shaping device is used in AFC with which the algorithm interacts. The shaping device could be an acoustic optic modulator (AOM) or a spatial light modulator (SLM). Pulse shaping based on a SLM type device will be discussed in chapters to follow. In AFC experiments, a search is done throughout the parameter space for an optimal solution. The theoretical grounding of AFC was done by [44]. A schematic representation of a typical AFC experiment is depicted in figure 2.4 obtained from [19].

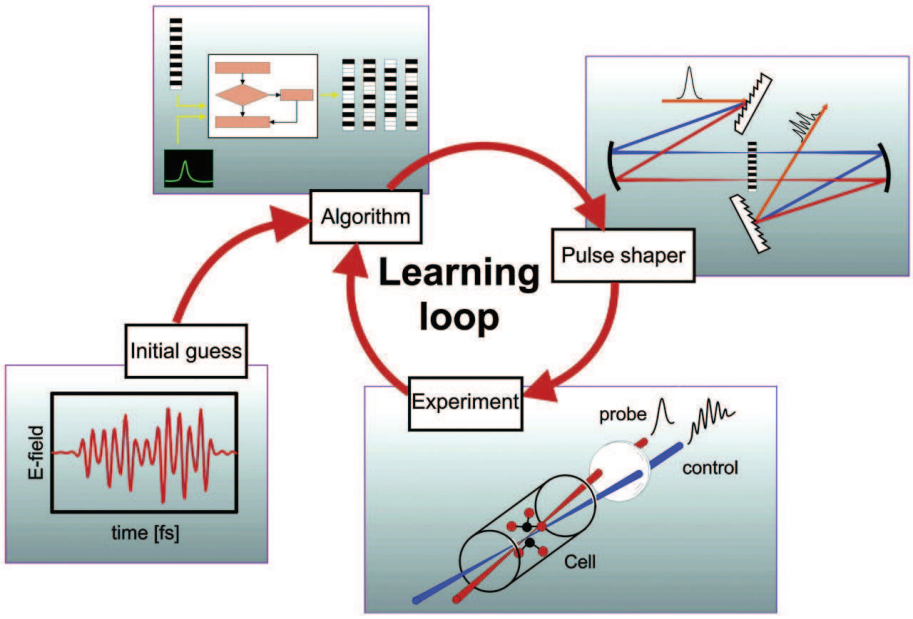

Figure 2.4: An adaptive feedback control (AFC) experiment is a closed loop experiment in which a learning loop shapes pulses with a spatial light modulator (SLM), or any other pulse shaping device, to obtain a certain outcome. The learning loop algorithm requires some initial guess of pulse shapes. In a genetic algorithm this will typically be the initial population. The pulses that are formed with the shaping device interact with the system and measurements are taken and fed back to the algorithm. The process stops when predefined conditions are met, for example when the objective functional is optimal.

2.5 Adaptive feedback control simulation (AFCS)

Simulations are done to bridge the gap between theoretical QOCT and experimental searches for optimal solutions and have been performed on various types of systems [45, 46]. Adaptive feedback control simulations (AFCS) also searches for optimal quantum controls. The only difference between AFCS and QOCT is that in AFCS the quantum mechanical system's interaction with the laser pulse is solved numerically and numeric optimization techniques are used while in the case of QOCT this is usually done analytically. The core of this current study is to use AFCS to find the best possible control to achieve maximum excitation of a particular vibrational state in a polyatomic molecule. With simulations the advantage is that the scheme which is developed can be implemented in the laboratory with more ease than the control techniques found by using QOCT. The difference between AFC and the simulated AFC is that instead of taking measurements, for example measuring a population in a specific state, the density matrix describing the quantum system is solved and the information is extracted from it. A typical AFCS scheme is depicted in figure 2.5.

An AFCS similar to that done by [47, 48] will be carried out for the current study. The manner in which the pulses are shaped will differ significantly. In the mentioned articles the pulse was formed by addition of the transition frequencies and manipulating the amplitudes and phases of these transition frequencies. For the current study, a spatial light modulator (SLM) will be modeled, this should give a higher degree of freedom to the pulses that could be formed. This should enable control over a more

complex system than that studied by [47, 48]. Control over a real molecule with anharmonic splittings will be studied.

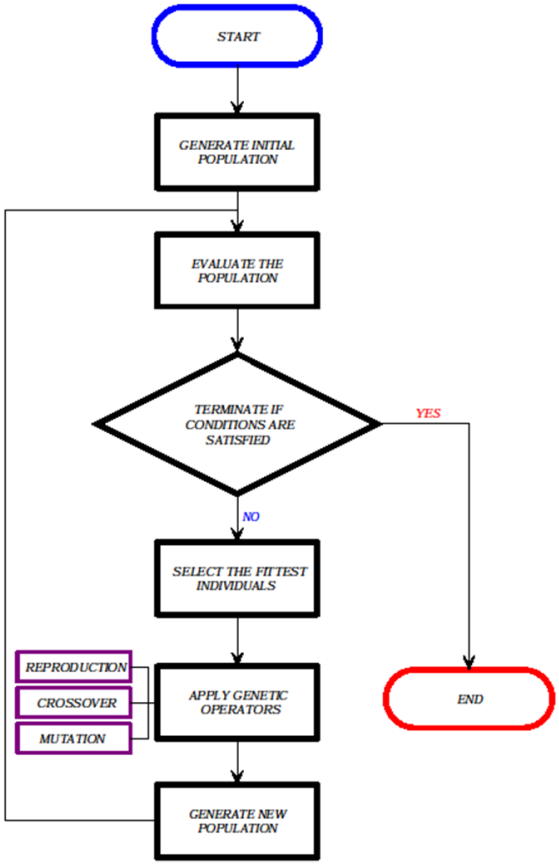

Figure 2.5: Layout of a genetic algorithm (GA) feedback optimization process. In figure 2.4 the experimental realization of a GA is depicted. In this graph evaluation of the population is done by solving the quantum mechanical problem numerically instead of taking measurements experimentally. The pulses are also shaped numerically by simulating an SLM. The process is called an adaptive feedback control simulation.

2.6 General

In this particular study the focus will be on exciting the vibrational modes in the electronic ground state of the molecule. In particular the focus will be to excite only the first few vibrational levels of the molecule. The reason for this is the fact that the density of states at these low lying vibrational levels is still very low the de-coherence time is still much longer than the pulse duration [22]

Adaptive feedback control simulation (AFCS) for selective excitation of a vibrational state within polyatomic molecules will be carried out for this current study. A laser pulse will be shaped and the effect it has on population dynamics of a polyatomic molecules will be investigated making use of the

density matrix formalism. The amount of population in an arbitrary vibrational state will be extracted and will be fed back using a genetic algorithm to optimize the population of this state.

Chapter 3

Method

3.1 Introduction

This project is based on numerical simulations. A brief discussion of the research design, instruments used and the instruments simulated will be given. There are limitations to doing simulations, and these will be discussed as well.

3.2 Research design

The density matrix formalism was used to describe a gaseous system of spherical top molecules. The Von Neumann equation gives the time evolution of a density matrix. A specific set of Von Neumann equations, suitable for solving numerically, was developed to describe how the electromagnetic radiation interacts with the ensemble of particles. These equations were solved numerically and the population in an arbitrary vibrational state was extracted after the pulse interacted with the gas. A feedback loop with a genetic algorithm (GA) manipulating the electromagnetic pulse was used in order to maximize the population of the ensemble in the chosen vibrational state within the molecule. An electromagnetic field is manipulated with a Spatial Light Modulator (SLM) in a closed-loop with a GA by changing the frequency dependent amplitude and phase of the Fourier transform of the pulse and transforming this back. The detail of the pulse shaping via the SLM will be explained and analyzed in the pulse shaping chapter.

3.3 Methodology

Different methods, to simulate the interaction of electromagnetic radiation with the physical system under consideration, were investigated. The evolution of the system using Von Neumann's equations was investigated. Von Neumann's equations were chosen to simulate the interaction of radiation with an ultra cold gas jet of a hexafluoride molecule. All physical information required for the simulations were obtained from literature [49, 50]. Details regarding the molecule will be given in Chapter 6.

3.3.1 Spatial Light Modulator (SLM)

Pulse shape simulations were done for a Jenoptik SLM, details of the specific model used in the simulations are given in Table 3.1 [51]. A schematic representation of an SLM is given in Figure 3.1 adapted from [51].

Property	Value
Active Area	Approx. 63.7 mm x 10.0 mm
Number of strips	2x640
Strip Size	3.8 mil (96.52 μm) x 10.0 mm
Liquid crystal type	nematic
Refractive index of glasses	1.53
Wavelength Range	430 - 1600 nm
Transmission	>75% at 450 - 1100 nm (without polarizers)
Refractive index of glasses	1.53

Table 3.1: JENOPTIK SLM-S640d Optical Data

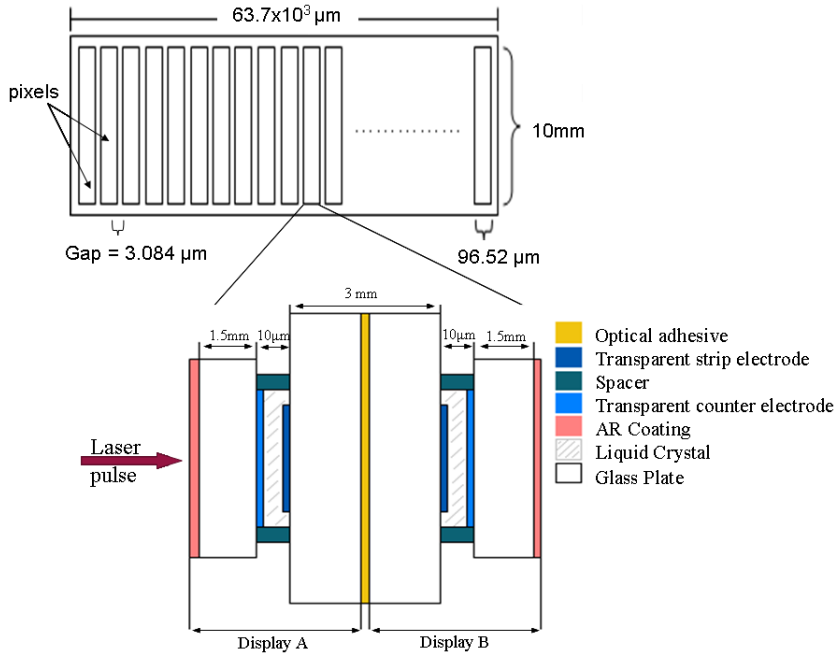

Figure 3.1: Schematic representation of an SLM and the layout of what a pixel consists of.

3.3.2 Data

A numerical model based on Von Neumann's equations was created and simulations were carried out using a parallel processing methodology based on a dual quad core desktop computer and Matlab's "parallel computing" toolbox. The programming was done in Matlab 2008b and the optimizations utilized the "Genetic Algorithm and Direct Search" toolbox.

3.3.3 Error Analysis

In all the simulations all the local and global error estimates are well below 1e-6. Comparison to what is found in the simulations and what is recorded in literature will be analyzed. No experimental confirmation of the model can at this stage be given.

3.4 Limitations

The SLM is constructed out of pixels and there are gaps between them. The influences of the gaps are neglected for the current study. A section in Chapter 4 is given, where it is described how to include gaps into the simulation. The genetic algorithm is implemented theoretically in the computer simulations and the results will vary in laboratory conditions, due to various factors, such as the uncertainty in the exact system Hamiltonian.

Chapter 4

Genetic Algorithms

4.1 Introduction

Genetic algorithms (GAs) are based on the theory of evolution and can be applied to wide variety of optimization problems. In particular genetic algorithms are robust and are ideal for finding global maxima. In some problems other optimization techniques might be faster in finding the minima. However the focus of this study was not the development of the optimization techniques, but rather the proof of principle of coherent control in the excitation of a molecule in the ground electronic state. Therefore it was decided to use the robust, but possibly slower genetic algorithm techniques. The GA searches the parameter space in a random manner and preference is given to parameter sets that start to optimize the objective function of the problem. The objective function is called a fitness function when one works with GA's. The ideas and conceptual understanding of GAs will be explained in this chapter has been adapted from the book [52].

4.2 Evolution and the Genetic Algorithm

Using ideas from the theory of evolution, the genetic algorithm was developed by John Holland. In the book [52] rigorous mathematics was used to prove that GA's do not find optimal solutions by mere chance. It is shown that the search technique is a directed search. The main concepts from the theory of evolution that are incorporated in GAs are: reproduction, crossover and mutation and of course the survival of the fittest.

Genetic algorithms differ from traditional optimization techniques in four ways [52] :

- GAs do not use the parameters themselves, but instead use an encoding of the parameter set based on the problem.
- GAs do not start at a single point, but rather with a certain population of points randomly scattered in the parameter space.
- The way GAs are steered in the correct direction for their search to find an optimal parameter set are by means of a fitness function.
- The evolution of the population is based on probabilistic transition rules, not deterministic ones.

4.3 General Explanation

A genetic algorithm works with a parameter space. A parameter space is the set of all the different values a parameter set can have. For example, to maximize a function over the interval $[t_0,t_F]$ of

integers the parameter space only consists of integers from t_0 to t_F including t_0 and t_F. In a typical GA these integers will be encoded as binary strings. The reason for this is that GA operations cannot be applied to single numbers, thus the values from the parameter space are encoded into bit-strings. Once all the values are encoded the GA can perform manipulations on the encoded set of values which are all bit-strings. The population size is defined as the number of members or elements that are selected in a random fashion from the parameter space. The population size in GAs usually remain the same size throughout their evolution, however, there are more involved GAs that could change the population size during its evolution[53].

An initial population is required by the GA. This initial population can be constructed using a random selection of elements from the encoded parameter space. Each member of the population is assigned a certain value which depends on the fitness function. The GA uses these fitness values to determine what will happen to the bit-strings associated with each of the fitness values.

The length of the bit-string is determined by the bounds of the problem. A typical example would be the search for the largest integer in the interval [0,31]. For this case a bit-string of length 5 would be required. In Table 4.3 it is shown how this bit string is encoded.

It should be noted that for multi-parameter problems, the members that make up the parameter set could still be encoded into a bit-string, even if the parameter set contains multiple parameters. In the multi-parameter case bit-strings are linked together to form a larger bit-string and different parts of the bit-string represents different parameters. A typical example would be if there are two parameters, x and y, where each one requires a bit-string of length five. A new bit-string of length 10 with both the parameters encoded is formed by stringing the two individual bit-strings together. The manner in which the GA operators are applied to the newly formed bit-string might differ however.

Bit string	Definition	Value
11111	$2^0 + 2^1 + 2^2 + 2^3 + 2^4$	31

Table 4.1: A bit string with the decomposition showing how the value for the string is obtained.

The three most important operators that are involved in the GA are: reproduction, crossover and mutation. These operators will be discussed in the sections to follow.

4.4 Reproduction

A genetic algorithm (GA) assigns values to the bit-strings using a fitness function. A fitness function is defined by the user and corresponds to an objective that the user wants to reach. It is the function that describes the problem and as a result of optimizing the fitness function the objective associated with it is reached. The fitness function does not need to be continuous [52].

When each member in the parameter space has a value assigned by the fitness function, a roulette wheel can be constructed with the information. The size of a slice corresponding to a particular member of the parameter space on the roulette wheel is proportional to the ratio of each assigned fitness value to the sum of all the fitness values. Thus, when all the ratios are added the sum total will be equal to one. The wheel is then spun and a member is picked. The spinning of the wheel is done as many times as is necessary to build a new intermediate population of the same size. This results in the buildup of a new intermediate population from the old. The members that have higher fitness values associated with them, has a higher probability to form part of the new intermediate population.

When the process is completed a new population is formed from the intermediate population. Members are paired and mate, this is where the crossover and mutation operators determine the

resulting final population.

4.5 Crossover

The crossover operation determines how two paired members from the intermediate population will mate and form two new members. A member is simply a bit-string and the 0's and 1's have specific positions within the bit-string. In a typical crossover process a random position p within the bit-string is chosen. This random number should lie between one and the bit-strings length minus one. This is done to avoid switching of the bit-string's, for when switching occurs no crossover has technically taken place. If l represents the bit-string's length a random number p is chosen within the interval of integers [1,l-1]. To have p lie within this interval, implies that crossover will take place. The crossover operation is then done by swapping the bits from position p to l of the two bit-strings involved. It should be noted that it is still possible to have replication even though switching is excluded. If it happens that bit-strings, 11001 and 00111 mate and crossover take place at position four the resulting bit-strings would be: 00111 and 11001. Thus, even though crossover took place, the two new resulting members of the final population are the same ones that mated.

As an example to demonstrate crossover the two members 10001 and 00011 will be used. Suppose that the random number that was chosen where crossover should take place, within the interval [0, 4], is 3. The two members and the position where crossover should take place are indicated.

$$S_1 = 1\,0\,0\,|\,0\,1$$
$$S_2 = 0\,0\,0\,|\,1\,1$$

After crossover the result is

$$S_1 = 1\,0\,0\,1\,1$$
$$S_2 = 0\,0\,0\,0\,1$$

4.6 Mutation

The mutation operator changes a 0 to a 1 and vice versa. The probability for mutation to occur is usually chosen so low that it would seldom be observed. It is usually chosen to be $p_m = 0.001$ in simple GAs. In the calculations of the first example no mutation occurred. As an example, if mutation would occur in the first new member after reproduction, at the binary located in position two, 1$\underline{0}$011 it would mutate into 1$\underline{1}$011. The mutation operator increased the diversity of the population and ensures the the GA does not get stuck on a local minimum.

4.7 First GA Example

As a first example of using a GA to optimize a function consider the function $f(x) = x^2$ represented in Figure 4.1. A GA will be used to find the maximum of this function on the interval [0,31]. The first step is to encode the variable x as a bit string. In this case bit-strings of length five must be used. Secondly the population size is specified, in this case an unvarying population size of six.

A member of the initial population is created by a random process, e.g. flipping a coin. For example let heads represent 1 and tails represents 0. Thus flipping a coin a total of five times will result in a bit-string of length five. Thus to create a population with six members this procedure should be performed six times. An example of this procedure and the values that correspond to the generated bit-strings are summarized in Table 4.2.

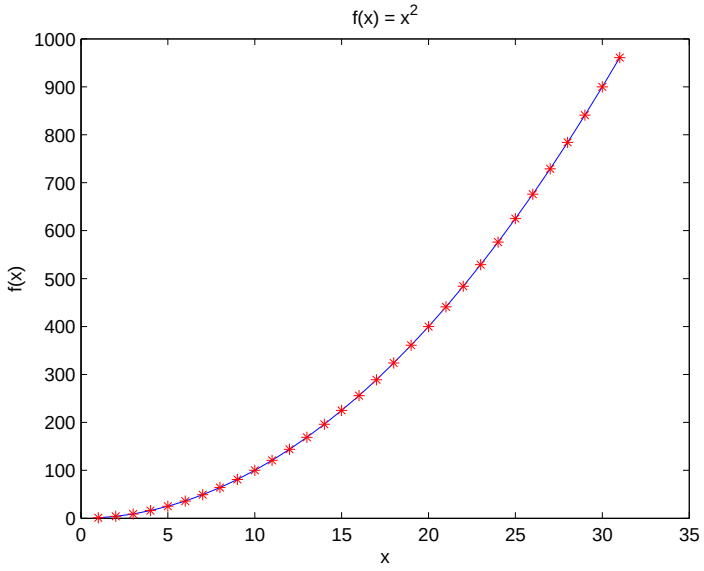

Figure 4.1: The red points indicate the set of function values in the interval [0,31]. The objective of the example is to obtain the maximum value of the function on this set. The continuous function $f(x) = x^2$ is depicted by the blue line.

No.	Bit String	Actual Value
1	10001	17
2	11101	29
3	00011	3
4	10101	21
5	01101	13
6	00111	7

Table 4.2: Initial population of integers that was build up by coin flipping.

A weighted random process, such as a roulette wheel is now constructed from the obtained fitness values. The population size determines the number of segments the wheel should be divided into. For the example the wheel needs to be divided into six parts. The size of a slice is determined by the ratio of its fitness value to the sum of all the fitness values. The process is summarized in Table 4.3.

The roulette wheel is spun and the last column in table 4.3 indicates the number of times a member of the population was chosen. It is clear that the members with the higher fitness values are chosen preferentially. Those members that were not chosen are eliminated from the reproduction process. In terms of the language used in natural evolution only the fittest survived and are allowed to breed. The first part of the genetic algorithm is now complete. The next part in the GA; reproduction, crossover and mutation follows.

In Table 4.4 the number in the second column refers to the numbers in the first column of Table 4.2, these numbers indicate which bit-strings were paired up to form new members by introducing crossover.

No mutation occurred within the population. The reason is simple: there was a 0.001 probability of mutation to take place. There were 30 (6×5) bits which made up the whole population. There were, in total, expected to be $0.001 \times 30 = 0.03$ bits that should have undergone mutation. Thus the

No.	String	Actual Value	Fitness Values (f_i) $f(x) = x^2$	$p_i = \frac{f_i}{\sum f}$ (slice size)	Expected count $\frac{f_i}{\bar{f}}$	Actual count on Roulette Wheel
1	10001	17	289	0.12	0.72	1
2	11101	29	841	0.35	2.09	2
3	00011	25	625	0.26	1.55	2
4	10101	21	441	0.18	1.10	1
5	01101	13	169	0.07	0.42	0
6	00111	7	49	0.02	0.12	0
Sum			2414	1.00	6.00	6.00
Average			402 ($\bar{f}$)	0.25	1.00	1.00

Table 4.3: Initial population of integers that was build up by coin flipping.

Individuals in mating pool after Reproduction	Mate (Randomly Selected)	Crossover Site (Randomly Selected)	New population after Crossover	x Value	Fitness Function $f(x) = x^2$
100|01	1	3	10011	19	361
000|11	3	3	00001	1	1
1|0101	4	1	11101	29	841
1|1101	2	1	10101	25	625
111|01	2	2	11111	31	961
000|11	3	2	00001	1	1
Sum					2790
Average					465

Table 4.4: The part where reproduction, crossover and mutation takes place within the GA.

probability of a mutation is very low.

It can be seen that the new population that has been formed has a new total fitness value and new average fitness values after one generation. It should be noted that the new population from Table 4.4 is the new generation. In the tables one run of the genetic algorithm is recorded, forming a new population which acts as the new generation.

From this example that was adapted from [52] a good intuition of how a GA works has been gained. Two more examples will be covered in the sections to follow. The first will give an example where a new fitness function is defined which will be a function of the objective function, thus $g(f(x))$. In the second example, a two dimensional problem is solved with a genetic algorithm. The latter acts as an example of a multiparameter search for an optimum.

4.8 Second GA Example

The example given next is chosen to introduce the idea that a fitness function could be cast into many different forms but still leads to the objective. It could be that different fitness functions converge quicker to a solution than other fitness functions. The function of which the maximum must be found in this section has many different minimas and maximas. Equation 4.1 represent the function being investigated and it is displayed graphically in Figure 4.2.

$$g(t) = cos(\omega t)e^{-\alpha t^2} \tag{4.1}$$

The maximum value of this function is one, and many methods exist to find the corresponding value of the time parameter. In this section a genetic algorithm (GA) will be used to find the time parameter that maximizes Equation 4.1. The fitness function does not necessarily have to be equal to $g(t)$ itself. In the current study it was realized that Matlab's "Genetic Algorithm and Direct Search" toolbox only minimizes a given fitness function and there is no option to maximize. This is one reason why re-structuring of the fitness function is sometimes necessary in order to reach the objective of the problem.

As an example the fitness function could be defined as

$$f(t) = (1 - g(t))^2. \tag{4.2}$$

For completeness, any function $p(t)$ can be maximized using matlab's GA if the fitness function is cast into the form -$p(t)$. The problem is changed by introducing the search for the minimum of the fitness function $f(t)$. The best fitness values, as well as the mean fitness values corresponding to $f(t)$ as a function of generation run by the GA is given in Figure 4.2. It is clear that in order to minimize $f(t)$ the function $g(t)$ should be close to one. It should also be clear that in finding the value of t that minimizes the fitness function the value that maximizes $g(t)$ is found.

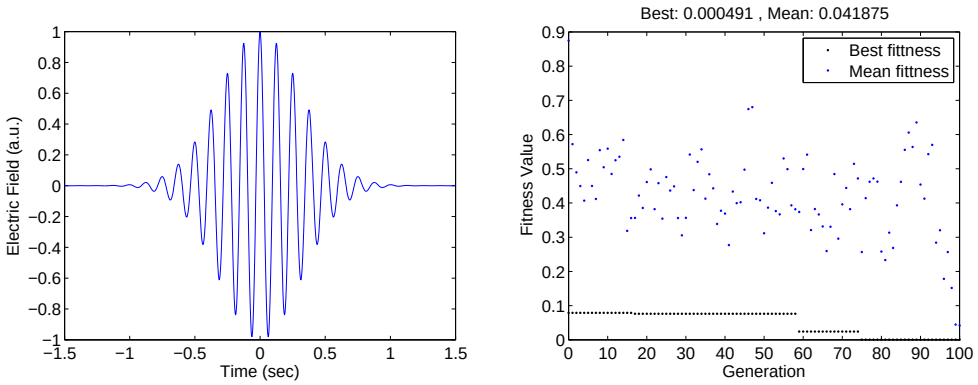

Figure 4.2: (Left) Pulse with parameters $\omega = 50$ and $\alpha = 5$ are used in the example. (Right) The evolution of the best and mean fitness values throughout the generations of the genetic algorithm as the fitness function $f(t) = (1 - g(t))^2$ is optimized.

4.9 Third GA Example

In this example the capability of the genetic algorithm (GA) to work with multiple parameters will be illustrated. The particular form of the sinc function that is going to be used is quite interesting, since it has many local minimas and maximas in two dimensions. Finding where the maximum is located is not necessarily a simple task. The derivatives can be calculated and be set equal to zero and the search for where the maximum is located can be done analytically, however this could result in finding one of the local maximas and might miss the global maxima. Instead of solving the problem analytically, a GA could be used to solve the problem numerically, thus removing the need to do all the tedious calculations. A genetic algorithm (GA) might not give the global optimum precisely, but it will come very close.

Finding the minimum of equation 4.3 analytically will not be attempted. The idea of this chapter is to show that a GA algorithm can work with multiple parameters and can find the maximum of a two dimensional problem.

The function that will be optimized is given by

$$f(x,y) = \frac{sin(\sqrt{x^2+y^2})}{\sqrt{x^2+y^2}}. \tag{4.3}$$

The function is shown graphically in Figure 4.3. A fitness function similar to that of section 4.8 will be used, i.e. equation 4.2. Figure 4.4 displays the best fitness values. as well as the mean fitness values as a function of generations of the GA. It can clearly be seen from Figure 4.4, that the fitness function is optimized.

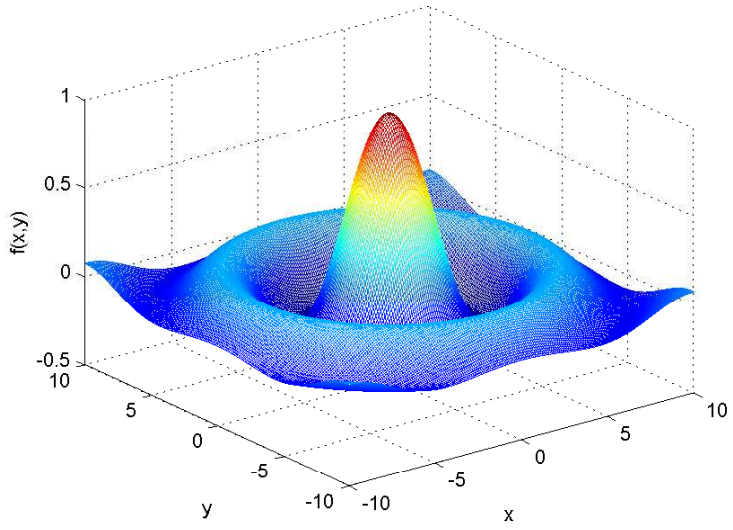

Figure 4.3: The two dimensional sinc function as defined as in equation 4.3.

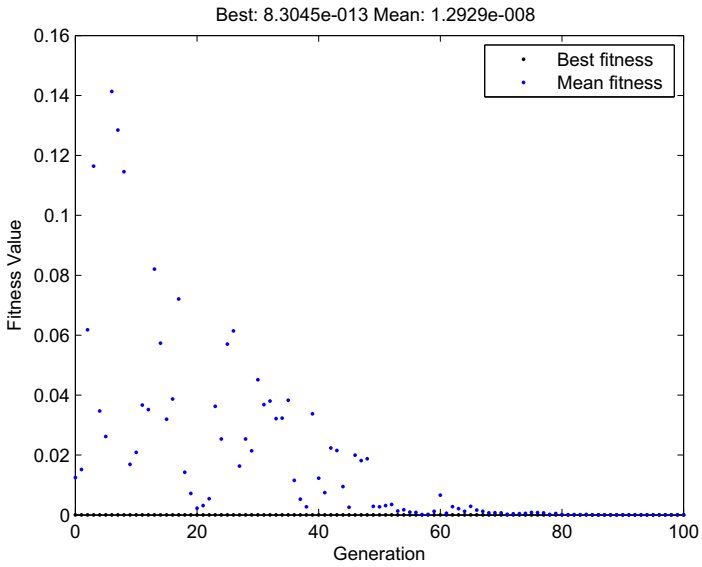

Figure 4.4: The evolution of the best fitness value and average fitness value throughout the generations of the genetic algorithm, as fitness function $f(t) = (1 - g(t))^2$ is optimized.

Chapter 5

Pulse Shaping

5.1 Introduction

Since the first laser was build 50 years ago, interest grew in the generation of ultrashort pulses of which the typical timescales are pico- to femtoseconds. Pulses with durations of less than 100 femtoseconds were consistently generated in the early 1980s. These pulses were created with a colliding pulse modelocked (CPM) ring dye laser. Even shorter pulses have been obtained using nonlinear pulse compression on pulses produced from the CPM laser [54]. In the 1990s it was shown that femtosecond pulses can be generated from solid-state lasers [55]. The advantages of using solid-state lasers rather than liquid dye lasers are: higher output power, stability and new methods for producing even shorter pulses [54].

Experimentally the use of shaped pulses provided novel tools for the investigation of molecules and atoms, for example, ultrafast spectroscopy. Examples of fields in which shaped pulses are experimentally applied are nonlinear fiber optics and high-field physics [54]. Shaping of femtosecond pulses in particular had a large impact on coherent control of quantum systems [56]. Ultrashort pulses have a large bandwidth due to the uncertainty principle. Shaping of these pulses implies a phase or amplitude or phase and amplitude modulation of their frequencies in order to obtain a shaped pulse [57]. Shaped pulses are required in the control of quantum systems where the shaped field guides the system from an initial state to a final, predetermined state.

Experimentally, the most success in shaping pulses with high flexibility came from using spatial light modulators (SLMs) in a 4f zero-dispersion setup [54, 57]. A pulse is spatially Fourier transformed into its different frequency components and the SLM can then be used to modulate the phase and amplitude of these components. If this modulated pulse is transformed back to the time domain the pulse would have a different shape in time than the incoming pulse. Shaping of ultrashort pulses are analogous to electronic function generators in the terminology of electronic instrumentation. It has become common to use SLMs in adaptive feedback control (AFC) experiments where some learning algorithm is used to guide the shaping of a pulse in such a manner that a certain objective is obtained, be it excitation of a specific vibrational state or any other goal. There are many published results which used these types of setups [16, 58, 59, 60, 61].

This chapter will contain a brief introduction to ultra short pulses (USP) and will be followed by discussion of time domain pulse shaping. The focus will be on a 4f-configuration. In this setup a pixelated device, called a spatial light modulator (SLM) shapes pulses in the Fourier plane. Other elements that contribute in building up the 4f-configuration will be discussed as well.

5.2 Ultra Short Pulses

An ultra short pulse (USP) is constructed from many frequencies with different phases and amplitudes. Typical examples are Gaussian, square and top-hat pulses. The shorter the duration of a pulse the larger the bandwidth according to the uncertainty principle. Short pulse lasers are multimode lasers. The discrete Fourier transform (FT) pairs of a pulse that is described in the time domain by $f(t)$ and in the frequency domain by $F(\omega)$ is given by [62]

$$F(\omega) = \frac{1}{N}\sum_{t=0}^{N-1} f(t)e^{-i(\frac{2\pi\omega t}{N}+\phi(t))} \tag{5.1}$$

$$f(t) = \sum_{\omega=0}^{N-1} F(\omega)e^{i(\frac{2\pi\omega t}{N}+\varphi(\omega))} \tag{5.2}$$

In the frequency domain $F(\omega)$ is the amplitude and $\varphi(\omega)$ is the phase of the associated frequencies. The discrete Fourier pairs give an intuitive approach to how an USP is build up. The continuous Fourier pairs are given by [62],

$$F(\omega) = \int_{-\infty}^{\infty} f(t)e^{-i(\omega t+\phi(t))}dt \tag{5.3}$$

$$f(t) = \frac{1}{2\pi}\int_{\infty}^{\infty} F(\omega)e^{i(\omega t+\varphi(\omega))}d\omega \tag{5.4}$$

Examples of how equations 5.1 and 5.2 could be used to construct pulses are shown in Figure 5.1. Six frequencies were used to construct a pulse. In this case these frequencies were all in phase as can be seen in the middle of the three figures. This can be noted by observing that there is a maximum of each frequency at time $t = 0$. It should be noted that the discrete FT of the input pulse consist of replica pulses. This is due to a discrete sum of frequencies that are used to build up the pulse.

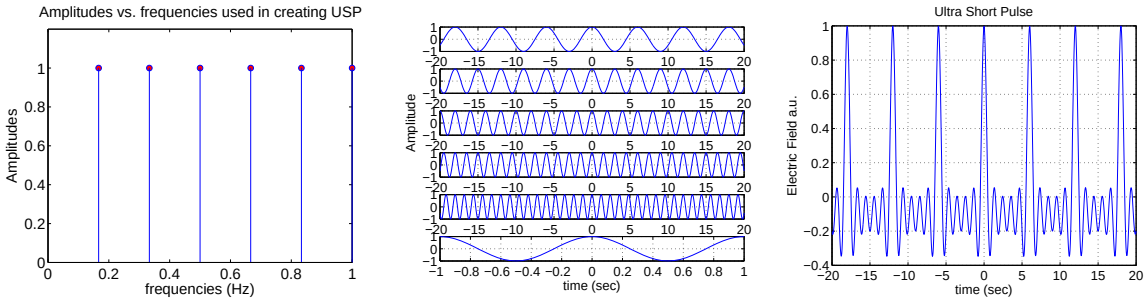

Figure 5.1: Using equations 5.1 and 5.2 USPs were generated. (Left) A linear amplitude distribution with all the frequencies in phase. (Middle) The six frequencies used to construct the pulse. (Right) Resulting electric field.

5.3 Pulse Characterization

Modern electronic response times are in the orders of nanoseconds (10^{-9}s). To take measurements of ultra short pulses (USP) quicker response times are required. Electronic equipment is not quick enough and therefore other methods are required to measure the pulses. An example is intensity auto-correlation, where the pulse that needs to be measured is split in two. This process is demonstrated in Figure 5.3. One pulse is time delayed with respect to the other and both pulses are focused in a second harmonic generation (SHG) crystal. The light produced by the crystal is frequency doubled. With τ, the time delay between the two pulses, the intensity of the field is then proportional to

$$I_{signal}^{SHG}(t,\tau) \propto I(t)I(t-\tau). \tag{5.5}$$

In this setup a detector with a slow response time is used and thus the following measurement is made.

$$A^{(2)}(\tau) = \int_{-\infty}^{\infty} I(t)I(t-\tau)dt. \tag{5.6}$$

This is known as the intensity auto-correlation or just the auto-correlation and the bracketed 2 indicates that this is a second order auto-correlation. Using the intensity auto-correlation the phase information is lost and only the intensity information acquired. Therefore if the amplitude and phase information is required, a different measurement technique is needed. To resolve a pulse in the time and frequency domain a spectrogram can be constructed using the following function [63],

$$S(\omega,\tau) = \left|\int_{-\infty}^{\infty} E(t)g(t-\tau)e^{-i\omega t}dt\right|^2. \tag{5.7}$$

The gating function could be any other pulse or the pulse itself. A graphical depiction is given on how the spectrogram is formed in Figure 5.2. The spectrogram can be described as a set of spectra where each set corresponds to the gated part of the electric field $E(t)$ at a specific time delay, τ. Thus information of both time and frequency is now simultaneously contained within the spectrogram.

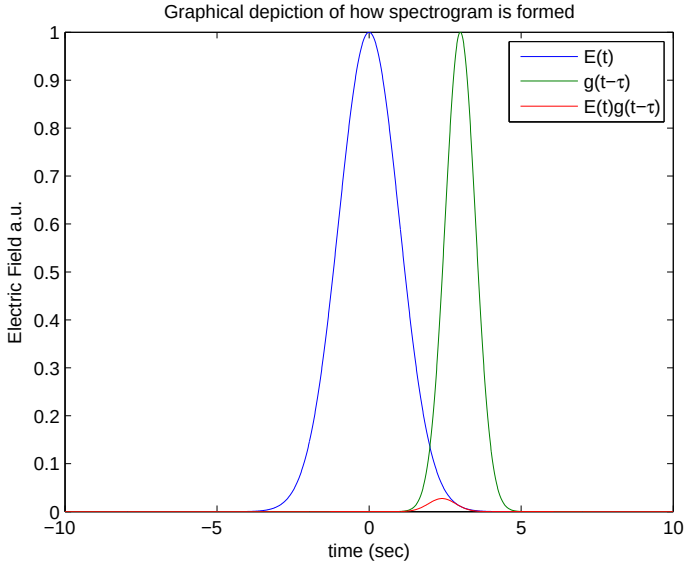

Figure 5.2: The arbitrary electric field and the gating function used in the construction of an auto-correlation trace is shown, as well as the signal produced by the product of the two.

Second harmonic generation (SHG) Frequency Resolved Optical Gating (FROG) measurements are taken, by using the pulse $E(t)$ itself as the gating function. Splitting a formed pulse in two equal pulses and using a time delay stage to separate the pulses in time, a FROG trace can be taken by using the one pulse to trace, in time, over the other pulse. This is schematically demonstrated in Figure 5.3. This is similar to the intensity auto-correlation, but instead of using a detector to take the measurements, a spectrometer is used. This is the only difference in the experimental setup of measuring a SHG-FROG and an intensity auto-correlation.

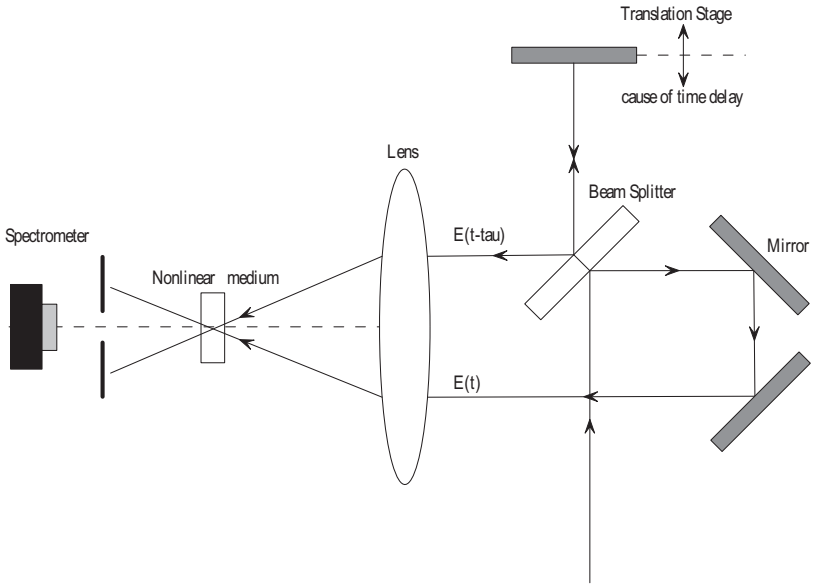

Figure 5.3: Experimental setup to measure a FROG trace.

The second harmonic generation-gate (SHG) FROG is given by [63]

$$I_{FROG}^{SHG}(\omega,\tau) = \left|\int_{-\infty}^{\infty} E(t)E(t-\tau)e^{-i\omega t}dt\right|^2. \tag{5.8}$$

The polarization-gate (PG) FROG is another type of FROG trace and is given by [63]

$$I_{FROG}^{PG}(\omega,\tau) = \left|\int_{-\infty}^{\infty} E(t)|E(t-\tau)|^2 e^{-i\omega t}dt\right|^2. \tag{5.9}$$

There are various other types of FROG traces as well, for example the transient-grating (TG)-FROG [63]. All FROG traces completely describes the measured field, thus with any of the FROG traces the electric field can be reconstructed. If a FROG trace is available, the intensity and phase information can be extracted and via algorithms [63]. For the current study a PG-FROG trace was chosen.

It is commented in [64] that optimal pulse shapes are best described by Husimi distributions and has been used in other theoretical papers [65]. The Husimi distribution cannot be directly measured experimentally, but from the information obtained from any FROG trace a Husimi distribution can be created [64]. The Husimi distribution is proportional to the absolute value square of $G(\omega,t)$ given as [25, 66] ,

$$G(\omega,t) = \int_{-\infty}^{\infty} e^{-i\omega(\tau-t)}e^{-\alpha(\tau-t)^2}\varepsilon(\tau)d\tau. \tag{5.10}$$

$G(\omega,t)$ can be viewed as the overlap of the pulse, $\varepsilon(t)$ with a set of Gaussians of which the centers in both the time and frequency domain changes continuously [25]. The α parameter determines the width of the Gaussians that are used and can be set according to the corresponding width of the pulse that is measured. The Husimi distribution depicts where the energy is located within the pulse as

function of time and frequency [67].

As a typical example, chirp will now be considered and the PG-FROG and Husimi distribution will be numerically evaluated for both cases. Chirp describes how frequencies follow one another in time. For positive chirp, the lower frequencies come first followed by the higher frequencies [68], for negative chirp the order in which the frequencies follow is reversed.

Assume a Gaussian chirped pulse [69] ,

$$\varepsilon(t) = e^{-\frac{t^2}{2\tau^2}} e^{i(\omega_0 t + \alpha \frac{t^2}{2})} \tag{5.11}$$

where α is the linear chirp and $\tau\sqrt{ln16}$ is the Full Width at Half Maxima (FWHM) of the intensity of the pulse. Consider the following pulse

$$E(\omega) = e^{\frac{-(\omega-\omega_0)^2}{2\Gamma^2}} e^{i\alpha' \frac{(\omega-\omega_0)^2}{2}} \tag{5.12}$$

where α' is the linear spectral chirp and $\Gamma\sqrt{ln16}$ is the frequency bandwidth at FWHM of the intensity of the pulse. The instantaneous angular frequency of the pulse is given by [70]

$$\omega_i = \frac{d\phi_{tot}(t)}{dt}. \tag{5.13}$$

The phase of the Gaussian chirped pulse of equation 5.11 is given by,

$$\phi_{tot}(t) = \omega_0 t + \frac{\alpha t^2}{2}. \tag{5.14}$$

The instantaneous angular frequency is then [70]

$$\omega_{inst}(t) = \omega_0 + \alpha t, \tag{5.15}$$

thus it can be seen that the pulse is linearly chirped. Pulses with positive and negative chirp are shown in Figures 5.5 and 5.6 respectively. The spectral phase defined as the phase of equation 5.12 is given as

$$\varphi(\omega) = \alpha' \frac{(\omega-\omega_0)^2}{2} \tag{5.16}$$

The linear temporal chirp and linear spectral chirp are coupled by the following equations [69]

$$\alpha = \alpha' \frac{\Gamma^4}{(1+(\alpha')^2\Gamma^4)}$$

$$\alpha' = \alpha \frac{\tau^4}{(1+\alpha^2\tau^4)}$$

The chirp parameters are commonly varied in coherent control experiments [14, 69, 71] to achieve some objective.

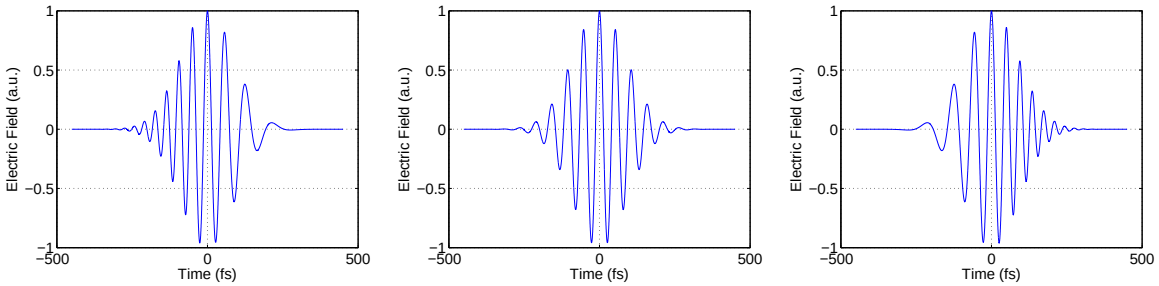

Figure 5.4: The electric field of three chirped pulses. (Left) α = -3x10^{-4} fs^{-2} (negatively chirped), α=0 (zero chirp) and α = +3x10^{-4} fs^{-2} (positively chirp) of a 150fs pulse with a center frequency, 628 cm^{-1}.

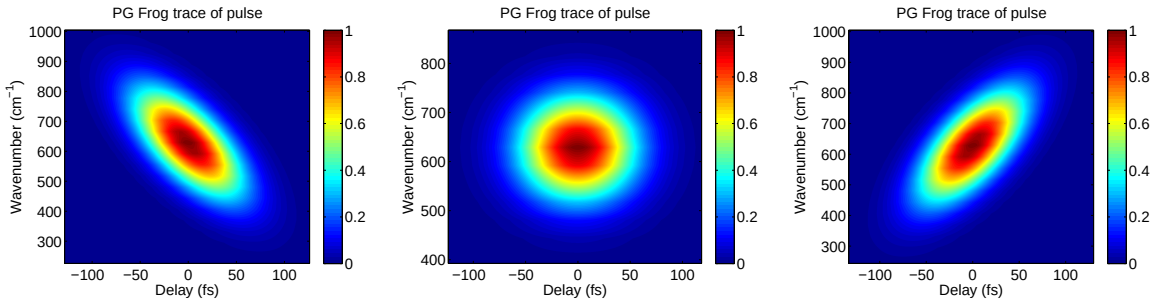

Figure 5.5: Polarized gating, frequency resolved optical gating (PG-FROG) distributions of the three chirped pulses. (Left) α = -3x10^{-4} fs^{-2} (negatively chirped), α=0 (zero chirp) and α = +3x10^{-4} fs^{-2} (positively chirp) of a 150fs pulse with the center frequency, 628 cm^{-1}.

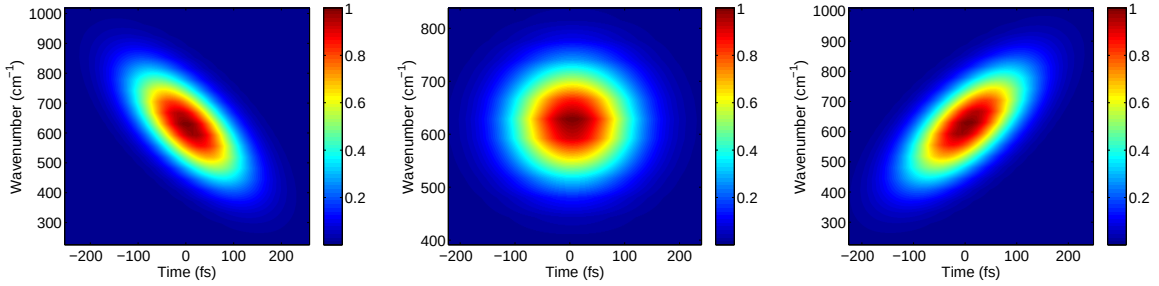

Figure 5.6: Husimi distributions of the three chirped pulses. (Left) α = -3x10^{-4} fs^{-2} (negatively chirped), α=0 (zero chirp) and α = +3x10^{-4} fs^{-2} (positively chirp) of an 150fs pulse with the center frequency, 628 cm^{-1}.

The difference between the PG-FROG and the Husimi distribution is not that clear from the chirp plots, Figures 5.5 and 5.6, for only the time axis is different. From the Husimi distribution, the slope of the graph gives the chirp. In the case of the PG-FROG it is more difficult to get the numerical value of the chirp. Thus using a Husimi plot is advantageous as it represents the pulse more intuitively. The difference in the Husimi distribution and PG FROG for a double pulse is clear in Figure 5.7. The Husimi distribution gives a more intuitive representation of a pulse. Consider the two representations of a double pulse in Figure 5.7 where the time and frequency separations are clear to distinguish in the Husimi plot and not for the PG-FROG trace.

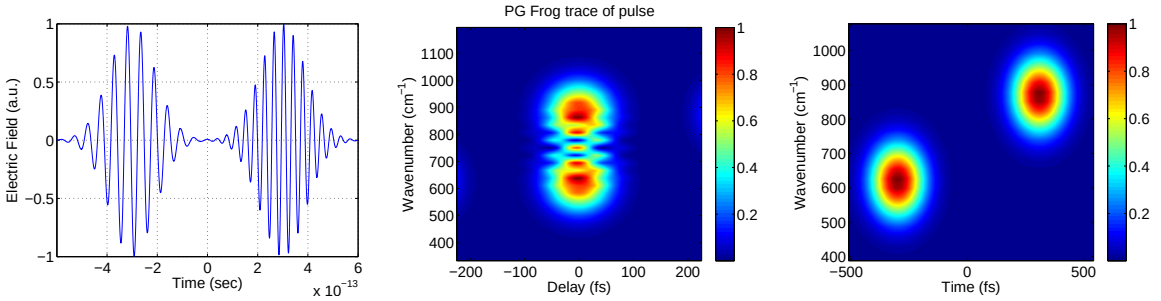

Figure 5.7: The PG-FROG (left) and Husimi distribution (right) of a double pulse which are separated 600 fs from each other and of which one pulse has a center frequency corresponding to the wavenumber 628 cm^{-1} and the other pulse with a wavenumber of 878 cm^{-1}.

5.4 Femtosecond Pulse Shaping Basics

Femtosecond pulse shaping as described here, is based on linear filtering. In electronics linear filtering is done on signals ranging from audio to microwave frequencies. As was discussed in the previous section, electronics are not fast enough to measure femtosecond pulses nor is it fast enough to directly modulate the beams in the time domain. Therefore different methods need to be employed to do pulse modulation [54].

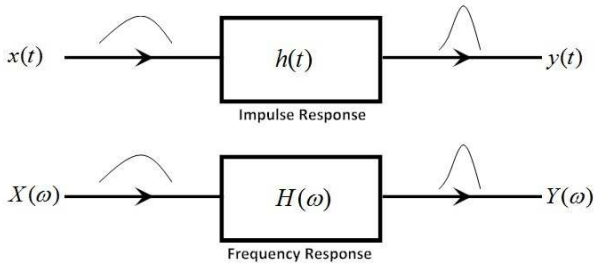

Figure 5.8: Using linear filtering to shape pulses. (Top) Time domain perspective (Bottom) Frequency domain perspective.

A graphical depiction of linear filtering is given in Figure 5.8. In the time domain the linear filter is characterized by the impulse response function $h(t)$. In response to an incoming pulse $\varepsilon_{in}(t)$, the resulting output of the filter $\varepsilon_{out}(t)$ is given by [54]

$$\varepsilon_{out}(t) = \varepsilon_{in}(t) * h(t) = \int \varepsilon_{in}(t')h(t-t')dt' \tag{5.17}$$

Thus in the time domain the output of the filter is the convolution of the input pulse and the impulse response function. The frequency response $H(\omega)$ describes the filter in the frequency domain perspective. The output of a filter $E_{out}(\omega)$ in the frequency domain is described by [54],

$$E_{out}(\omega) = E_{in}(\omega)H(\omega) \tag{5.18}$$

which amounts to the product of the input signal and the frequency response.

Theoretically if the input pulse $\varepsilon_{in}(t)$ is a Dirac delta function the output pulse will be the impulse response function, $h(t)$. Thus, the problem of creating a specific output pulse reduces to making a linear filter with the correct impulse response.

The impulse response and the frequency response functions are the Fourier transform pairs of each other and is given by [54]

$$H(\omega) = \int h(t)e^{-i\omega t}dt \tag{5.19}$$

$$h(t) = \frac{1}{2\pi}\int H(\omega)e^{i\omega t}d\omega. \tag{5.20}$$

For the current study it will be assumed that the input pulse is a 150 femtosecond transform-limited pulse. The carrier frequency can be varied and in this case it was assumed that the carrier frequency is equal to the first transition frequency of the vibrational levels of the molecule.

5.5 Pulse Shaping Apparatus

In order to shape pulses the phases and/or amplitudes of the frequencies that are contained within the pulse itself needs to be manipulated. This section will focus on shaping pulses using a so-called 4f-shaper.

The elements within the 4f-configuration setup that alters the electric field will be discussed. Finally a formulation will be derived which can be used to simulate pulse shaping with pixelated devices, such as a spatial light modulator (SLM) for a given 4f-configuration.

5.5.1 4f-Configuration

In order to arrive at the final equation which can be used to simulate pulse shaping in a numerical model, the 4f-configuration will be analyzed. In Figure 5.9 there are three elements which alters the electric field, these are: a grating, a lens and a SLM (pixelated device).

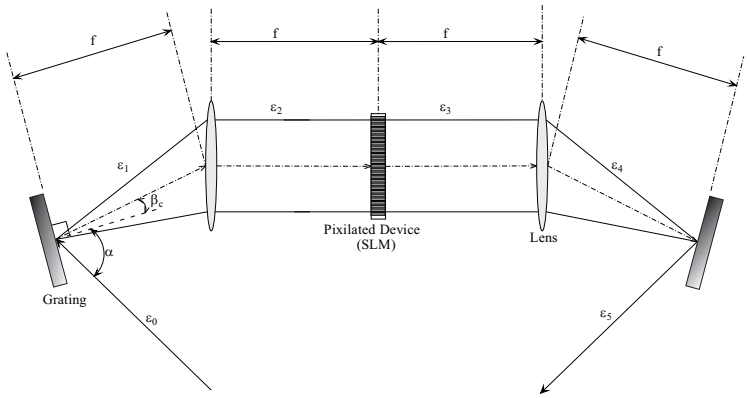

Figure 5.9: Schematic representation of the 4f-configuration used for pulse shaping. The various variables that are used in the equations, within the chapter, are indicated. The 4f-configuration consists of a grating to disperse the light, a lens to collimate the light and an spatial light modulator (SLM) to shape the light by modulating the amplitudes and phases of it.

Explanations and the equations are adapted from [57] and lecture notes by T. Feurer [72] are used. The slowly varying electric field approximation will be used in the derivation to follow. The frequency associated with the slowly varying electric field is given by the relative frequency

$$\Omega = \omega - \omega_c. \tag{5.21}$$

Here ω_c is the center frequency of the laser pulse and ω the instantaneous frequency of the electric field. Only the positive frequency components will be investigated and it will be indicated with the $+$ symbol.

The slowly varying electric field in the time domain is represented by $\varepsilon_i^+(x,t)$ and in frequency domain by $\tilde{\varepsilon}_i^+(x,\Omega)$. These describe the complex envelope associated with the laser pulse, which enters the 4f-configuration.

The electric field that traveled a distance z through free space and that was initially described as $\tilde{\varepsilon}_i(k_x,\Omega)$ can be described by using Fresnel diffraction equation from Fourier optics. It modifies $\tilde{\varepsilon}_i(k_x,\Omega)$ as follow [57]

$$\tilde{\varepsilon}_o^+(k_x,\Omega) = \tilde{\varepsilon}_i^+(k_x,\Omega)e^{-ikz+i\frac{zk_x^2}{2k}}. \tag{5.22}$$

In the above equation k is the propagation direction of the instantaneous frequency ω. The wave vector, k_x is the x-component of k and z is the thickness of the medium. A linear dispersion grating would change the outgoing electric field according to [57],

$$\tilde{\varepsilon}_o^+(x,\Omega) = \sqrt{b}\tilde{\varepsilon}_i^+(bx,\Omega)e^{-i\gamma\Omega x}. \tag{5.23}$$

The constants b and γ are defined as follow [72]

$$b = \frac{cos(\alpha)}{cos(\beta_c)} \tag{5.24}$$

$$\gamma = \frac{2\pi m}{\omega_c G cos(\beta_c)}, \tag{5.25}$$

where α is the angle of incidence, m the diffraction order, G the grating constant and c the speed of light. Lastly, a perfect lens modifies the pulse as [57],

$$\tilde{\varepsilon}_o^+(x,\Omega) = \tilde{\varepsilon}_i^+(x,\Omega)e^{i\frac{kx^2}{2f}}, \tag{5.26}$$

where the focal length f is assumed to be independent of the wavelength. If a plane wave of unit amplitude entered the lens the exponential term can be interpreted as an approximation to a spherical wave. If f is positive, the wave converges to a point a distance f behind the lens and when f is negative, it is diverging about the point f in front of the lens. The way in which a pixelated device alters the electric field will be described shortly, but first the masking function needs to be introduced that is associated with the pixelated device. The masking function

$$M(x) = \sum_{k=-\frac{N}{2}}^{\frac{N}{2}-1} rect\Big[\frac{x-x_n}{\Delta x_p - \Delta x_g}\Big]M_n e^{-i\Phi_n} + \sum_{k=-\frac{N}{2}}^{\frac{N}{2}-1} rect\Big[\frac{x-x_n+\frac{\Delta x_p}{2}}{\Delta x_g}\Big]M_g e^{-i\Phi_g}, \tag{5.27}$$

describes a device with N pixels of which the width of a single pixel is Δx_p and the separation between the different pixels is Δx_g. The pixels and gaps are represented with amplitude modulations M_n and M_g respectively. The same holds for Φ_n and Φ_g to describe the phase modulation of the pixels and the gaps. Lastly $rect(x)$ is the normal rectangular function defined by

$$rect(x) = \begin{cases} 1 & \text{for} \quad |x| < \frac{1}{2} \\ \frac{1}{2} & \text{for} \quad |x| = \frac{1}{2} \\ 0 & \text{for} \quad |x| > \frac{1}{2} \end{cases} \tag{5.28}$$

It is now known what each of the elements in the 4f-configuration does to the electric field and the output pulse can be analyzed for an initial incoming pulse $\varepsilon_0^+(x,\Omega)$. The derivations contained in this section will be sufficient to understand how certain elements change the electric field and how they, as a whole, manipulate pulses.

Assume that the input is given by

$$\varepsilon_0^+(x,\Omega) \tag{5.29}$$

The action of the grating on the field is given by equation 5.26 therefore after the grating the field can be written as

$$\tilde{\varepsilon}_1^+(x,\Omega) = \sqrt{b}\tilde{\varepsilon}_0^+(bx,\Omega)e^{i\gamma\Omega x}. \tag{5.30}$$

After the field passes through the lens the field that is obtained just before it enters the SLM is

$$\tilde{\varepsilon}_2^+(x,\Omega) = \sqrt{\frac{ik}{2\pi bf}}e^{-i2kf}\tilde{\tilde{\varepsilon}}_1^+(\frac{kx}{f},\Omega) \tag{5.31}$$

$$\tilde{\varepsilon}_2^+(x,\Omega) = \sqrt{\frac{ik}{2\pi bf}}e^{-i2kf}\tilde{\tilde{\varepsilon}}_0^+(\frac{kx}{fb}+\frac{\gamma\Omega}{b},\Omega). \tag{5.32}$$

The pulse now goes through the pixelated device (SLM) and after the SLM it is given by$\varepsilon_3^+(x,\Omega)$ with

$$\tilde{\varepsilon}_3^+(x,\Omega) = \tilde{\varepsilon}_2^+(x,\Omega)M(x). \tag{5.33}$$

After the field has propagated again through the lens, the electric field just before it reaches the last grating is given by

$$\tilde{\varepsilon}_4^+(x,\Omega) = \sqrt{\frac{ik}{2\pi f}}e^{-i2kf}\tilde{\tilde{\varepsilon}}_3^+(\frac{kx}{f},\Omega) \tag{5.34}$$

$$\tilde{\varepsilon}_4^+(x,\Omega) = \frac{ik\sqrt{b}}{f}e^{-4ikf}\int dx'\tilde{\varepsilon}_0^+(-bx',\Omega)e^{-i\gamma\Omega x'}\tilde{M}(-\frac{k}{f}(x-x')). \tag{5.35}$$

Finally the description of the field, after the last grating in the spatial domain is then given by

$$\tilde{\varepsilon}_5^+(x,\Omega) = \frac{1}{\sqrt{b}}\tilde{\varepsilon}_4^+(\frac{x}{b},\Omega)e^{i\frac{\gamma\Omega x}{b}} \tag{5.36}$$

$$\tilde{\varepsilon}_5^+(x,\Omega) = \frac{ik}{bf}e^{-4ikf}\int dx'\tilde{\varepsilon}_0^+(-x',\Omega)\tilde{M}(-\frac{k}{bf}(x-x'))e^{i\frac{\gamma\Omega}{b}(x-x')}. \tag{5.37}$$

This could be described in the time domain as

$$\tilde{\varepsilon}_5^+(x,t) = \frac{1}{2\pi}\int \tilde{\varepsilon}_5^+(x,\Omega)e^{i\Omega t}d\Omega \tag{5.38}$$

$$\tilde{\varepsilon}_5^+(x,t) \approx \frac{ik_c}{bf}e^{-4ikf}\int dx'\tilde{\varepsilon}_0^+(-x',t+\frac{\gamma}{b}(x-x'))\tilde{M}(-\frac{k_c}{bf}(x-x')). \tag{5.39}$$

With equation 5.39, an initial incoming pulse could be shaped by using the masking function of the pixelated device (SLM) to construct an output pulse from the 4f-configuration.

A discretization of the transform limited pulse in the frequency domain can be made by

$$\tilde{\varepsilon}_0^+(\Omega) = \sum_{n=-\frac{N}{2}}^{\frac{N}{2}-1} rect\frac{\Omega-\Omega_n}{\Delta\Omega}A_n. \tag{5.40}$$

The set of amplitudes A_n are the spectral amplitudes of the laser that corresponds to the different pixels of the SLM. With equation 5.40 representing the approximated incoming electric field in the frequency domain, the output pulse (time domain) could be found by using the masking function described in equation 5.27. The result is given by

$$\varepsilon^{+}_{output}(t) = \frac{\Delta\Omega_p - \Delta\Omega_g}{2\pi} sinc\frac{(\Delta\Omega_p - \Delta\Omega_g)t}{2} \sum_{n=-\frac{N}{2}}^{\frac{N}{2}-1} A_n M_n e^{i\Omega_n t - i\Phi_n} + \frac{\Delta\Omega_g}{2\pi} sinc\frac{\Delta\Omega_g t}{2} \sum_{n=-\frac{N}{2}}^{\frac{N}{2}-1} A_n M_g e^{i\frac{\Omega_n - \Delta_p}{2}t} \quad (5.41)$$

The last equation could be used to describe a shaped pulse form by a SLM. Two examples are given and displayed in Figures 5.10, 5.11 and 5.12.

In the current study some assumptions and approximations are made to equation 5.41. The SLM that is simulated has pixel sizes of approximately 97 μm and gap sizes of 3 μm. In this particular simulation the effect of the gaps was neglected. The second term in equation 5.41 thus approaches zero and the equation reduces to

$$\varepsilon^{+}_{output}(t) = \frac{\Delta\Omega_p}{2\pi} sinc\frac{(\Delta\Omega_p)t}{2} \sum_{n=-\frac{N}{2}}^{\frac{N}{2}-1} A_n M_n e^{i\Omega_n t - i\Phi_n}. \quad (5.42)$$

The envelope factor on the left of the summation is approximated by a square function of value one around the summation. This can be done, since the factor only scales the solution around time $t = 0$. The pulses are formed around $t = 0$ and the width of the pulses are narrower than the width of the envelope factor. Therefore the function that was used in this simulation is given by

$$\varepsilon^{+}_{output}(t) = \sum_{n=-\frac{N}{2}}^{\frac{N}{2}-1} A_n M_n e^{i\Omega_n t - i\Phi_n}. \quad (5.43)$$

Thus, by Fourier transforming the incoming pulse a mask can be applied to the spectrum and then inverse Fourier transformed back to the time domain, resulting in a shaped electric field in the time domain. Obtaining the frequency response $H(\omega)$ such that the resulting electric field excites a particular vibrational state of the chosen polyatomic molecule will be done by a genetic algorithm.

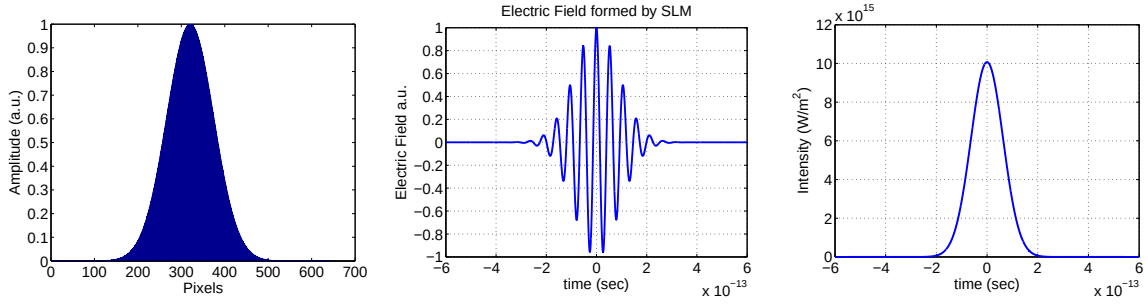

Figure 5.10: All applied phases are zero and the applied amplitude modulations are all equal to one. (Left) Amplitudes of the frequency components at the pixels (Middle) The output electric field. (Right) Intensity of the output pulse.

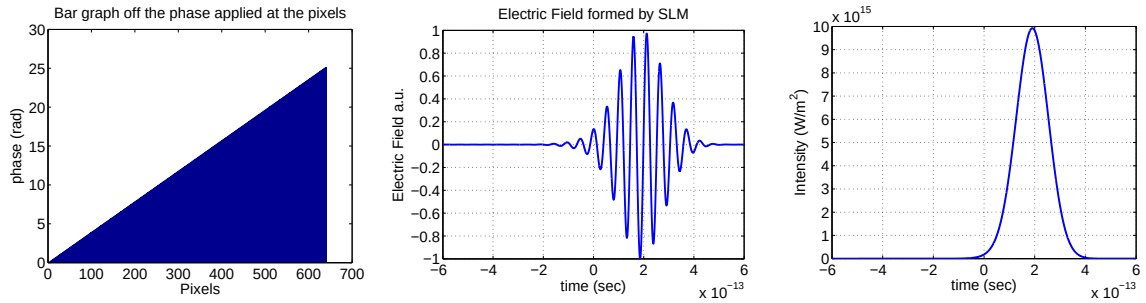

Figure 5.11: The amplitude modulation which was applied at all the pixels are all equal to one. (Left) Phases applied to the SLM at each pixel. (Middle) The output electric field. (Right) Intensity of the output pulse. The result is a pulse that is shifted in time.

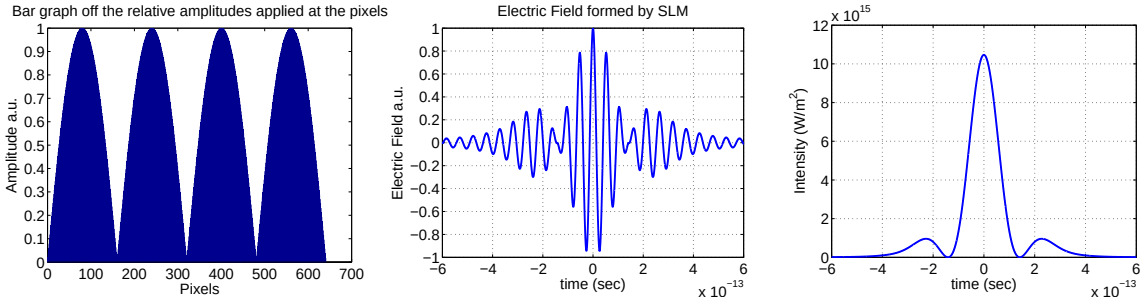

Figure 5.12: The phase modulation which was applied at all the pixels are all equal to zero. (Left) The amplitude modulation applied to the SLM at each pixel. (Middle) The output electric field. (Right) Intensity of the output pulse.

In Figures 5.10, 5.11 and 5.12 examples are shown where certain amplitude and phase modulations are simulated with the resulting effects it has on the field shown. From Figure 5.11, it is clear that when a linear phase modulation is applied the pulse shifts in time, which corresponds to the shift theorem in Fourier analysis [62]. The phase was changed linearly over the range $[0, 8\pi]$. From Figure 5.12, amplitude modulations which correspond to an absolute sine modulation were applied at the SLM and the effect it has is displayed in the figure.

Chapter 6

Electromagnetic Radiation and Matter Interaction

6.1 Introduction

In this chapter the theory of laser-matter interaction is introduced and the equation necessary for simulating the interaction of an ultrashort laser pulse with a hexafluoride molecule is developed. The purpose of the current study is to selectively excite a specific vibrational state in the electronic ground state of the molecule without making use of excited electronic states. This objective will be achieved by using shaped pulses which interact with the molecules and then searching for the shape that result in optimizing the transition. The pulses that will be used are in the order of femtoseconds to picoseconds.

For the current study a molecule was chosen of which the spectroscopic data appears in the literature. This was done in order to simplify the problem. Based on this information, the molecular Hamiltonian could be set up. The energies that were found in the literature were chosen to be the eigenvalues of the molecular Hamiltonian. The eigenvectors associated with the energies diagonalize the molecular Hamiltonian. These eigenvectors form the basis of the molecular Hamiltonian. The total Hamiltonian that describes the system can be written as a sum of the molecular Hamiltonian and the interaction Hamiltonian. It will be shown that the time evolution of the system can be described as the effect that the interaction Hamiltonian has on the basis vectors.

This chapter begins with a discussion of the time-dependent Schrödinger equation and its solutions. To follow, the Hamiltonian that will be used to describe the physical system and how it is setup will be discussed. The model that will be developed must be able to account for dephasing due to thermalizing collisions and inter-vibrational relaxation (IVR). Therefore the density matrix formalism will be used. A section is devoted to the density matrix and its time evolution. Towards the end of the chapter a discussion comparing the Schrödinger and density matrix formalisms will be given.

6.2 The Molecular System

There are a total of $3N$ degrees of freedom associated with a molecule consisting of N atoms. Three of these are the translational degrees of freedom in the x, y and z directions. Another three degrees of freedom are for the rotation of the molecule around the x,y and z-axes. The remaining $3N-6$ degrees of freedom are associated with the internal motions of atoms within the molecule which are called vibrations. For any non-linear molecular structure there are thus $3N$-6 normal modes associated with vibrations [73]. In anharmonic oscillators the normal modes are coupled and IVR causes the energy

to redistribute over these different modes.

Molecules can, under certain conditions, be considered harmonic oscillators, but in general they are more accurately described by anharmonic oscillators. In the anharmonic potential the vibrational energy level spacing becomes smaller as you move up the potential. The region where the levels become very dense is called the quasi-continuum. In Figure 6.1 the quasi-continuum is represented as a single level and in the model it is added phenomenologically as one level.

For the simulations the energy levels of the molecule, as well as the transition probabilities are required. In Figure 6.1 the energy level diagram is shown which will be used in the simulation. During the literature survey it was found that Uranium Hexafluoride, UF_6, has been studied extensively and that all the required spectroscopic data were found for the vibrational mode ν_3. In Table 6.1 some of the relative dipole moments required for the simulations are given [49, 50, 74]. The transitions are shown in Figure 6.1 and 6.2.

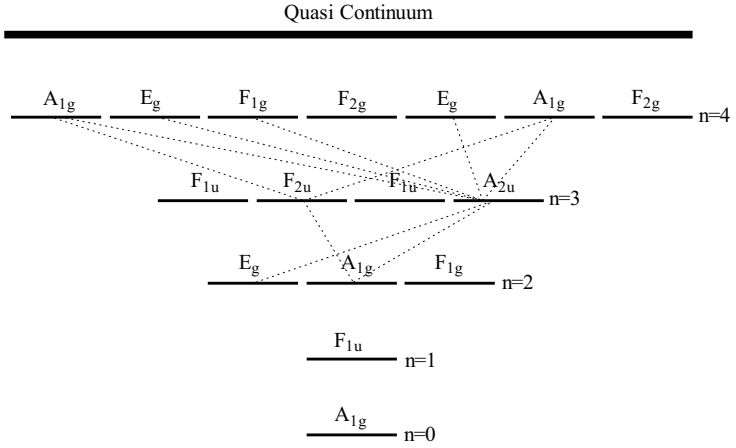

Figure 6.1: The vibrational levels of the Uranium Hexafluoride molecule in mode ν_3 with the vibrational levels and the anharmonic splitting in the levels indicated.

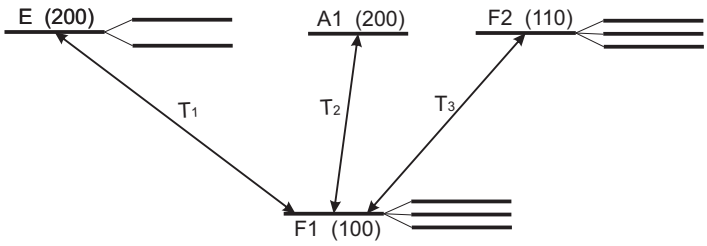

Figure 6.2: The transitions between vibrational levels $|1\rangle$and $|2\rangle$ with the transition probabilities indicated as T_1, T_2 and T_3. The calculated transition probabilities are given in Table 6.1.

Transition	Relative Dipole moment	Matrix Element	Transition	Relative Dipole moment	Matrix Element
$\|0,A_{1g}\rangle \rightarrow \|1,F_{1u}\rangle$	1.000	H_{12}	$\|2,A_{1g}\rangle \rightarrow \|3,F_{1u}(1)\rangle$	$\sqrt{0.5}$	H_{46}
			$\|2,A_{1g}\rangle \rightarrow \|3,F_{2u}\rangle$	0	H_{47}
$\|1,F_{1u}\rangle \rightarrow \|2,E_g\rangle$	$\sqrt{0.\dot{4}}$	H_{23}	$\|2,A_{1g}\rangle \rightarrow \|3,F_{1u}(2)\rangle$	$\sqrt{0.5}$	H_{48}
$\|1,F_{1u}\rangle \rightarrow \|2,A_{1g}\rangle$	$\sqrt{0.\dot{2}}$	H_{24}	$\|2,A_{1g}\rangle \rightarrow \|3,F_{2u}\rangle$	0	H_{49}
$\|1,F_{1u}\rangle \rightarrow \|2,F_{2g}\rangle$	$\sqrt{0.\dot{6}}$	H_{25}			
			$\|2,F_{2g}\rangle \rightarrow \|3,F_{1u}(1)\rangle$	0	H_{56}
$\|2,E_g\rangle \rightarrow \|3,F_{1u}(1)\rangle$	$\sqrt{0.5}$	H_{36}	$\|2,F_{2g}\rangle \rightarrow \|3,F_{2u}\rangle$	$\sqrt{0.643}$	H_{57}
$\|2,E_g\rangle \rightarrow \|3,F_{2u}\rangle$	$\sqrt{0.5}$	H_{37}	$\|2,F_{2g}\rangle \rightarrow \|3,F_{1u}(2)\rangle$	$\sqrt{0.643}$	H_{58}
$\|2,E_g\rangle \rightarrow \|3,F_{1u}(2)\rangle$	$\sqrt{0.5}$	H_{38}	$\|2,F_{2g}\rangle \rightarrow \|3,F_{2u}\rangle$	$\sqrt{0.214}$	H_{59}
$\|2,E_g\rangle \rightarrow \|3,F_{2u}\rangle$	0	H_{39}			

Table 6.1: Calculated relative dipole moments for the first few vibrational transitions in the mode ν_3. Given dipole moments are relative to the first transition $|0,A_{1g}\rangle \rightarrow |1,F_{1u}\rangle$ which has a dipole moment of 0.394 Debye (1 Debye = 3.3356×10^{-30} C.m). All other transition dipole moments can be calculated similarly to the example given in the text.

To calculate the required relative dipole moments for the spherical top molecule of the current study, the system was approximated as a triply degenerate harmonic oscillator. Consider as an example the excitation from the first to the second excited state as shown in Figure 6.1. From group theory it is known that A1, E and {F1,F2} are irreducible representations that are non-degenerate, double degenerate and triply degenerate respectively, this is indicated in Figure 6.1. From [75] the following equality should hold when calculating dipole moments in the triply degenerate harmonic oscillator regime:

$$\sum_i T_i^2 = \frac{m+n}{m} \tag{6.1}$$

where T_i is the relative dipole moment associated with a transition from one vibrational level to another. Both m and n are associated with the higher lying vibrational level, where m is the degeneracy of that level and n is the vibrational quantum number of it. When using this equation it is assumed that the intensity is distributed equally among the degeneracies of a vibrational level. It is also assumed that all the transition intensities among the degeneracies are equal and this will be represented by a^2.

As an example, the dipole moments will be calculated for the transitions shown in Figure 6.2. For this example equation 6.1 produces

$$T_1^2 + T_2^2 + T_3^2 = \frac{3+1}{3} = \frac{3}{2}. \tag{6.2}$$

The assumptions that are made then lead to

$$\begin{aligned} T_1^2 &= a^2 + a^2 \\ T_2^2 &= a^2 \\ T_3^2 &= a^2 + a^2 + a^2 \end{aligned}$$

It follows that a is given by

$$a = \sqrt{\frac{2}{9}} \tag{6.3}$$

and therefore

$$\begin{aligned} T_1 &= \sqrt{0.444} \\ T_2 &= \sqrt{0.222} \\ T_3 &= \sqrt{0.666} \end{aligned}$$

The calculated transition probabilities are relative to the 0→1 transition dipole moment which is equal to 0.394 Debye. In a similar fashion all the other transition probabilities can be calculated. These appear in table 6.1.

6.3 Time-dependent Schrödinger equation

The interaction of the electric field with the molecular system is a time dependent process and our interest lies in the state of the system after interaction has taken place. The evolution of a quantum state in the absence of an perturbing field is described by the time-dependent Schrödinger equation which is given by [25]

$$i\hbar\frac{\partial}{\partial t}\Psi(x,t) = H\Psi(x,t) \tag{6.4}$$

with Hamiltonian operator

$$H = -\frac{\hbar^2}{2m}\nabla^2 + V. \tag{6.5}$$

In the case of molecules, m is the reduced mass. The potential can be a function of both space and time, but here it will be assumed to be time independent: $V = V(x)$. Another assumption that will be made to simplify the discussion is that the problem is one-dimensional. This allows us to replace ∇^2 with $\frac{\partial^2}{\partial x^2}$.

The wavefunction $\Psi(x,t)$ contains the information about the system prior to measurement, but can only describe the system to the degree of accuracy with which the Hamiltonian was set up. When the wavefunction is normalized $|\Psi(x,t)|^2$ is the probability density of finding the particle at x at the time t.

6.3.1 Solving the Time-dependent Schrödinger equation

To solve equation 6.4 we make the assumption that the solution can be written as a product of functions. One function will depend only on time and the other only on the spatial coordinate. Setting [25]

$$\Psi(x,t) = \psi(x)\chi(t), \tag{6.6}$$

and using this form as a trial solution of equation 6.4 one obtains [25]

$$i\hbar\frac{\dot{\chi(t)}}{\chi(t)} = \frac{H\psi(x)}{\psi(x)}. \tag{6.7}$$

It is clear that one side contains the spatial dependence (right-hand side) while the other the time dependence. For this equality to hold both the left-hand and right-hand sides of the equation should equal a constant. Two differential equations are then obtained [25]:

$$i\hbar\dot{\chi}(t) = E\chi(t). \tag{6.8}$$

$$H\psi(x) = E\psi(x). \tag{6.9}$$

From this set of equations solutions to 6.4 can be found. The solution to equation 6.8 is given as [25]

$$\chi(t) = \chi_0 e^{-\frac{i}{\hbar}Et}. \tag{6.10}$$

The factor χ_0 is a constant about which more will be said in the text to follow. Equation 6.9 now remains to be solved. It should be noted that this is an eigenvalue equation, with E the eigenvalue and $\psi(x)$ the eigenstate. Together equations 6.6 and 6.10 produces the wavefunction, $\Psi(x,t)$ that satisfies equation 6.4

$$\Psi(x,t) = \psi(x)\chi_0 e^{-\frac{i}{\hbar}Et}. \tag{6.11}$$

If the wave equation is normalized then

$$\Psi(x,t) = \int_{-\infty}^{\infty} |\Psi(x,t)|^2 dx = 1 \tag{6.12}$$

and that fixes the factor χ_0 up to a trivial phase. Thus a particular solution to equation 6.4 can be written as [25]

$$\Psi(x,t) = \psi(x)e^{-\frac{i}{\hbar}Et}. \tag{6.13}$$

From this the probability density can be determined as

$$|\Psi(x,t)|^2 = |\psi(x)|^2, \tag{6.14}$$

which is independent of time, since eigenstates of H are stationary. This is due to the fact that the probability density was taken of only one particular solution to equation 6.4. It is well known that any linear combination of particular solutions is again a solution and it is due to the factors with which all of the particular solutions are multiplied and added that causes time to enter the probability density. The general solution to equation 6.4 when H has a discrete spectrum is [25]

$$\Psi(x,t) = \sum_{n=1}^{\infty} a_n \psi_n(x) e^{-\frac{i}{\hbar}E_n t}. \tag{6.15}$$

As an example, consider the linear combination of two particular solutions

$$\Psi(x,t) = a_1\psi_1(x)e^{-\frac{i}{\hbar}E_1 t} + a_2\psi_2(x)e^{-\frac{i}{\hbar}E_2 t}. \tag{6.16}$$

The probability density is given by

$$|\Psi(x,t)|^2 = |a_1|^2|\psi_1(x)|^2 + |a_2|^2|\psi_2(x)|^2 + 2Re\{a_1^* a_2 \psi_1^* \psi_2 e^{-i\frac{E_2-E_1}{\hbar}t}\} \tag{6.17}$$

which is explicitly time dependent whenever $E_1 \neq E_2$ and $a_1, a_2 \neq 0$.

6.4 Setting up Hamiltonian

The Hamiltonian $\hat{H}$ that describes the system is the sum of $\hat{H}_{mol}$ which represents the molecule in the unperturbed state and $\hat{H}_I$ which represents the perturbation:

$$\hat{H} = \hat{H}_{mol} + \hat{H}_I \tag{6.18}$$

The idea is to use published spectroscopic data in order to construct the level system. Many molecules were investigated and it was found that uranium hexafluoride UF_6 in the vibrational mode ν_3 has been extensively studied. The required spectroscopic data to set up the level system was obtained from literature [49, 50, 74]. All the energies associated with the vibrational levels in the vibrational mode ν_3, thus all the transition wavelengths are known. The transition probabilities are calculated

according to the method presented in Section 6.2. With the energy levels known, the molecular Hamiltonian can be set up and a set of orthogonal eigenvectors, $\{\psi_n\}$, that corresponds to the set of energies, $\{E_n\}$, that are the energies corresponding to the different vibrational energy levels.

$$H_{mol} = \sum_j \hbar\omega_j |\psi_j\rangle\langle\psi_j| \tag{6.19}$$

The electric field that interacts with the molecule can be written as

$$\mathbf{E} = E_0\varepsilon(t)\hat{\epsilon}, \tag{6.20}$$

and is assumed to be polarized in the $\hat{\epsilon}$ direction. The parameter $\varepsilon(t)$ is the normalized complex electric field and E_0 is the electric field amplitude.

All that remains is a description of the interaction Hamiltonian H_I. In this case only dipole interactions will be studied. The model to follow only deals with these types of interactions and the perturbation of stationary vibrational states. The interaction Hamiltonian couples the electric field to the unperturbed vibrational states of the molecule. It is possible to approximate the interaction Hamiltonian in the same manner as it is defined for coupling electronic states,

$$\hat{H}_I = e\mathbf{D} \bullet \hat{\epsilon}E_0\Re[\varepsilon(t)], \tag{6.21}$$

where $\mathbf{D}$ is the sum of the position vectors of the nuclei in the molecule:

$$\mathbf{D} = \sum_j \mathbf{r}_j. \tag{6.22}$$

Next we define[76]

$$X_{ab} = \hat{\epsilon} \cdot \mathbf{D_{ab}} \tag{6.23}$$

with

$$\mathbf{D}_{ab} = \int \psi_a^* \mathbf{D} \psi_b dV \tag{6.24}$$

Where ψ_a and ψ_b are elements of a complete set of orthogonal eigenstates $\{\psi_n\}$ with eigenvalues $\{E_n\}$ of H_{mol}. The matrix elements for the interaction Hamiltonian can be written as

$$I_{ab} = \int \psi_a^* \hat{H}_I \psi_b dV, \tag{6.25}$$

and by using equation 6.21 and 6.24 this becomes

$$I_{ab} = e\Re[\varepsilon(t)]E_0 X_{ab}. \tag{6.26}$$

The dipole moments between the different vibrational states are eX_{ab}. The interaction Hamiltonian now reads

$$H_I = eE_0\Re[\varepsilon(t)] \sum_{i,j} X_{ij} |\psi_i\rangle\langle\psi_j|. \tag{6.27}$$

6.5 Setting up the model.

The interest of the current study lies in manipulating the population distribution among the vibrational levels within a gas phase of spherical top molecules, specifically Uranium Hexafluoride, UF_6. The model should allow for dephasing due to thermalizing conditions as well as inter-vibrational relaxation to be added at a later stage. Working with large numbers of particles and including the

above mentioned effects is not possible using only the Schrödinger equation. Using the density matrix formalism and the Von Neumann equation now becomes essential.

In the density matrix formalism the Von Neumann equations determine the time evolution of the density matrix, just as the Schrödinger equation determines the time evolution of a wavefunction. The density matrix can represent both pure states and mixed states, whereas the Schrödinger equation deals with the evolution of a single wavefunction.

In the next section we investigate the properties of the density matrix also explain why a single average state vector cannot describe a statistical mixture of states.

6.6 The Density Matrix

In this section the time evolution of the density matrix will be derived for the pure case and then it will be shown that this is also applicable to a mixed state.

6.6.1 Pure Case

Some of the arguments and equations in this section were adapted from [77]. The state of a system is described by a state vector $|\Psi(t)\rangle$ which can be expanded in an orthonormal basis $\{|u_n\rangle\}$ as

$$|\Psi(t)\rangle = \sum_n c_n(t)|u_n\rangle. \tag{6.28}$$

we require that

$$\sum_n |c_n(t)|^2 = 1 \tag{6.29}$$

which indicates that the state vector is normalized. The pure state density operator that corresponds to the state vector in equation 6.28, is defined by [77]

$$\rho(t) = |\Psi\rangle\langle\Psi|. \tag{6.30}$$

The matrix elements of the density operator in the orthonormal basis, $\{|u_n\rangle\}$ can be written as

$$\rho_{pn}(t) = \langle u_p|\rho(t)|u_n\rangle = c_p(t)c_n^*(t). \tag{6.31}$$

Using equations 6.29 and 6.31, we find that

$$Tr(\rho(t)) = \sum_n \rho_{nn}(t) = \sum_n |c_n(t)|^2 \tag{6.32}$$

and it is clear that the population information of the various levels is contained in the diagonal elements of the density matrix. The state vector evolves according to the Schrödinger equation as

$$i\hbar\frac{d}{dt}|\Psi(t)\rangle = H(t)|\Psi(t)\rangle. \tag{6.33}$$

The Hamiltonian is Hermitian as it represents a physical observable. The Hermitian conjugate of equation 6.33 is

$$-i\hbar\frac{d}{dt}\langle\Psi(t)| = \langle\Psi(t)|H^\dagger(t) = \langle\Psi(t)|H(t). \tag{6.34}$$

Deriving the evolution of the operator with the help of equations 6.33 and 6.34, $\rho(t)$ [77],

$$\frac{d}{dt}\rho(t) = \frac{d|\Psi(t)\rangle}{dt}\langle\Psi(t)| + |\Psi(t)\rangle\frac{d\langle\Psi(t)|}{dt} \tag{6.35}$$

this transforms in, using equation 6.34 ,

$$\frac{d}{dt}\rho(t) = \frac{1}{i\hbar}H(t)|\Psi(t)\rangle\langle\Psi(t)| + \frac{1}{-i\hbar}|\Psi(t)\rangle\langle\Psi(t)|H(t) \tag{6.36}$$

which reduces to,

$$\frac{d}{dt}\rho(t) = \frac{1}{i\hbar}(H(t)\rho(t) - \rho(t)H(t)) \tag{6.37}$$

and finally can be written in a compact form given by,

$$\frac{d}{dt}\rho(t) = \frac{1}{i\hbar}[H(t), \rho(t)]. \tag{6.38}$$

Equation 6.38 is known as the Von Neumann equation. The Von Neumann equation has a classical counterpart called the Liouville equation and it is key to classical statistical mechanics [20]. The expectation value of an observable A is given [77] by

$$\langle A\rangle(t) = Tr(A\rho(t)) = Tr(\rho(t)A). \tag{6.39}$$

Another useful formula [77] which gives the probability to find the system in the state $|u_n\rangle$ is given by

$$P(a_n) = Tr(P_n\rho(t)), \tag{6.40}$$

where P_n is the projector operator

$$P_n = |u_n\rangle\langle u_n|. \tag{6.41}$$

Two important relations for the pure state case of the density operator is

$$\rho^2(t) = \rho(t) \tag{6.42}$$

$$Tr\rho^2(t) = 1 \tag{6.43}$$

These relations can be used as a check within the model to determine in each time step of the evolution whether the system is in a pure state or not.

6.6.2 Mixed States

Care should be taken when working with statistical mixtures of states and it will be shown why an average state vector cannot be used to describe such a mixture. Arguments and equations to follow are adapted from [77].

Suppose that there are two orthogonal and normalized states $|\psi_1\rangle$ and $|\psi_2\rangle$. Assume the system is in the state corresponding to $|\psi_1\rangle$. It is possible to calculate the probabilities for the results associated with performing a measurement for an observable A. Let the set $\{u_n\}$ be a set of normalized eigenvectors of A with corresponding eigenvalues $\{a_n\}$. The eigenvalues are assumed to be non-degenerate. The probability of finding a_n when A is measured for the system in state $|\psi_1\rangle$ and $|\psi_2\rangle$ respectively are

$$P_1(a_n) = |\langle u_n|\psi_1\rangle|^2 \tag{6.44}$$

$$P_2(a_n) = |\langle u_n|\psi_2\rangle|^2. \tag{6.45}$$

Consider a state vector which is a linear superposition of $|\psi_1\rangle$ and $|\psi_2\rangle$, as in

$$|\psi >= \lambda_1|\psi_1\rangle + \lambda_2|\psi_2\rangle \tag{6.46}$$

$$|\lambda_1|^2 + |\lambda_2|^2 = 1. \tag{6.47}$$

If this state vector is interpreted as a statistical mixture of the states $|\psi_1\rangle$ and $|\psi_2\rangle$ with weights $|\lambda_1|^2$ and $|\lambda_1|^2$ this would lead to incorrect results. One can calculate the total probability of obtaining the eigenvalue a_n and it is given by the weighted sum of the probabilities,

$$P(a_n) = |\lambda_1|^2 P_1(a_n) + |\lambda_2|^2 P_2(a_n), \tag{6.48}$$

The proper way to calculate the probability is by using

$$P(a_n) = |\langle u_n|\psi\rangle|^2, \tag{6.49}$$

which results in

$$P(a_n) = |\lambda_1|^2|\langle u_n|\psi_1\rangle|^2 + |\lambda_2|^2|\langle u_n|\psi_2\rangle|^2 + 2Re\{\lambda_1\lambda_2^*\langle u_n|\psi_1\rangle\langle u_n|\psi_2\rangle^*\}. \tag{6.50}$$

This is clearly different from equation 6.48. An extra non-zero term appears in equation 6.50 which is not present in equation 6.48. Thus, it is clear that it is not possible to construct an average type of state vector for a statistical mixture of states. It will now be shown how to apply the pure case to the mixture of states using the density matrix approach.

Consider a system described by a statistical mixture of states, where there are a set of probabilities that describe in which state a system can be in. If these probabilities are p_1,p_2,...p_k corresponding to the states ψ_1, ψ_2, ... ψ_k satisfying the conditions [77],

$$0 \leq p_1, p_2, ...p_k \leq 1 \tag{6.51}$$

$$\sum_k p_k = 1 \tag{6.52}$$

With these conditions a derivation for the density matrix for a system of mixed states can be made. The probability associated with a measurement of an observable A resulting in obtaining the eigenvalue a_n if the state is $|\psi_k>$ is given by

$$P_k(a_n) = \langle\psi_k|P_n|\psi_k\rangle. \tag{6.53}$$

The total probability of finding the value a_n, when a measurement for an observable A is made, for the mixed state case can be written as

$$P(a_n) = \sum_k p_k P_k(a_n). \tag{6.54}$$

Here the density operator properties obtained for the pure case are used, specifically equation 6.40 and 6.30. The latter can be redefined for a mixture of states so that it corresponds to an state vector of a sub ensemble. Only an index is added in the redefinition:

$$\rho_k = |\psi_k\rangle\langle\psi_k|. \tag{6.55}$$

All the equations are now in place to derive the density matrix for a mixture of states. With the given equations 6.40 and 6.54 we see that

$$P(a_n) = \sum_k p_k Tr(\rho_k P_n) \tag{6.56}$$

which can be written as

$$P(a_n) = Tr\sum_k p_k \rho_k P_n \tag{6.57}$$

after making a substitution of the summation over k, this equation becomes

$$P(a_n) = Tr(\rho P_n) \tag{6.58}$$

with the definition given in equation 6.54 which corresponds to the probability of measurement relating to mixed states, using the equations in 6.58 the density matrix can then be written as

$$\rho = \sum_k p_k \rho_k. \tag{6.59}$$

The density matrix elements for a mixture of states are as follow:

$$\rho_{np} = \sum_k p_k c_n^k (c_p^k)^* \tag{6.60}$$

The ensemble in question is build up from many sub ensembles. The k^{th} sub-ensemble can be described by a state vector $|\psi_k\rangle$. In general all the different sub-ensembles have different sets of coefficients which builds up the state vector in the orthonormal basis $\{u_n\}$. If the entire system is in the state that corresponds to $|\psi_k\rangle$, the probability of finding this system in state $|u_n\rangle$ after an measurement has been carried out is $|c_n^k|^2$. The set of probabilities, $\{p_k\}$ contained in equation 6.60 states that there is no full knowledge of this system available, but there exists certain probabilities that the system will be in different states. Taking this into account, the meaning of the diagonal elements, ρ_{nn} are that they represent the populations of the states, $|u_n\rangle$, since it corresponds to the average probability of finding the system in the state $|u_n\rangle$.

The off-diagonal elements represent interference terms. The terms $c_n^k c_m^*$ represent the interference between the states $|u_n\rangle$ and $|u_m\rangle$. Thus the off diagonal elements ρ_{nm} represents the average of the cross-terms. It can average out to zero even when the single terms $c_n^k c_m^*$ are non-zero. It should be noted that the Von Neumann equation 6.38 also holds for mixed states. The off-diagonal elements represent the coherence of the system. When the off-diagonal elements are zero, coherence is lost.

6.7 Von Neumann Equations applied to light matter interactions

It was shown in Section 6.6 that the Von Neumann equation,

$$i\hbar \frac{d\hat{\rho}}{dt} = [\hat{H}, \hat{\rho}] \tag{6.61}$$

describes how a density operator evolves in time. The Hamiltonian that will be used to describe the physical system was described in section 6.4. The Von Neumann equations that are found by describing light matter interactions are sometimes called the optical Bloch equations after the rotating wave approximation (RWA) has been made. It should be noted that in setting up the model for the current study no RWA is made. A general n-level model will be developed that can be used to simulate radiation matter interaction.

The matrix elements for the Von Neumann equations that has been calculated for a pure state, equation 6.28, can be written as

$$i\hbar \frac{d\rho_{ab}}{dt} = \sum_{l=1}^{n} (I_{al}\rho_{lb} - \rho_{al} I_{lb}) + \rho_{ab}(E_a - E_b) \tag{6.62}$$

$$\frac{d\rho_{ab}}{dt} = \frac{-i}{\hbar} \sum_{l=1}^{n} (I_{al}\rho_{lb} - \rho_{al} I_{lb}) - i\rho_{ab}\omega_{a,b}. \tag{6.63}$$

These equations hold for the case of mixed states as well. In general for a complicated system an analytic solution cannot be obtained and therefore a numerical solution is usually required. However it was found that numerical solutions to equation 6.63, is unstable due to a very fast oscillating term that is the result the large value for $\omega_{a,b}$. Thus numerical integration of equation 6.63 requires a very small step size which is very time consuming. An alternative method was developed that allowed much larger step sizes to be used and consequently were much faster to solve

6.7.1 Alternative approach

Equation 6.63 is prone to instability when integrated numerically due to the factor, $-i\rho\omega_{a,b}$. In this section an alternative equation will be derived that is lends itself to faster numerical solutions. The arguments and equations to follow are adapted from [78, 76, 77].

The time-dependent Schrödinger equation restated,

$$i\hbar\frac{\partial}{\partial t}\Psi(\mathbf{x},t) = H\Psi(\mathbf{x},t) \tag{6.64}$$

has a general solution of the form equation 6.15 for a n-level system,

$$\mathbf{\Psi}(\mathbf{r},t) = \sum_{l=1}^{n} c_l(t)e^{\frac{-iE_l t}{\hbar}}\psi_l(\mathbf{r}). \tag{6.65}$$

Define,

$$\mathbf{\Psi}_n(\mathbf{r},t) = e^{\frac{-iE_n t}{\hbar}}\psi_n(\mathbf{r}). \tag{6.66}$$

The Hamiltonian under investigation was previously discussed in this chapter and can be written as 6.18,

$$\hat{H} = \hat{H}_{mol} + \hat{H}_I, \tag{6.67}$$

where it is given that,

$$\hat{H}_{mol}\psi_n = E_n\psi_n. \tag{6.68}$$

Substituting equation 6.67 into equation 6.64 one obtains,

$$(\hat{H}_E + \hat{H}_I)\sum_{l=1}^{n} c_l(t)\Psi_l(\mathbf{r},t) = i\hbar\frac{d}{dt}\sum_{l=1}^{n} c_l(t)\Psi_l(\mathbf{r},t) \tag{6.69}$$

$$(\hat{H}_E + \hat{H}_I)\sum_{l=1}^{n} c_l(t)\Psi_l(\mathbf{r},t) = i\hbar\sum_{l=1}^{n}(\frac{dc_l(t)}{dt}\Psi_l(\mathbf{r},t) + c_l(t)\frac{d\Psi_l(\mathbf{r},t)}{dt}). \tag{6.70}$$

From equations 6.68 and 6.64 it is found that,

$$\hat{H}_E\sum_{l=1}^{n} c_l(t)\Psi_l(\mathbf{r},t) = \sum_{l=1}^{n} E_l c_l(t)e^{\frac{-iE_l t}{\hbar}}\psi_l(\mathbf{r}). \tag{6.71}$$

Investigating the rightmost term in equation 6.70,

$$i\hbar\sum_{l=1}^{n} c_l(t)\frac{d}{dt}\Psi_l(\mathbf{r},t) = i\hbar\sum_{l} c_l(t)\frac{d}{dt}(e^{\frac{-iE_l t}{\hbar}}\psi_l(\mathbf{r})) \tag{6.72}$$

$$i\hbar\sum_{l=1}^{n} c_l(t)\frac{d}{dt}\Psi_l(\mathbf{r},t) = \sum_{l=1}^{n} E_l c_l(t)e^{\frac{-iE_l t}{\hbar}}\psi_l(\mathbf{r}). \tag{6.73}$$

Finally concluding from equations 6.71 and 6.73 equation 6.70 reduces to,

$$\hat{H}_I \sum_{l=1}^{n} c_l(t)\Psi_l(\mathbf{r},t) = i\hbar \sum_{l} \frac{dc_l(t)}{dt}\Psi_l(\mathbf{r},t). \tag{6.74}$$

Calculate the expectation values relative to the state, $\psi_k(\mathbf{r})$. Multiply from the left with $\psi_k^*(\mathbf{r})$ and then integrate over all space. These are now measurable quantities.

$$\int \sum_{l=1}^{n} c_l(t)\Psi_k^*(\mathbf{r},t)\hat{H}_I\Psi_l(\mathbf{r},t)dV = i\hbar \int \sum_{l=1}^{n} \frac{dc_l(t)}{dt}\Psi_k^*(\mathbf{r},t)\Psi_l(\mathbf{r},t)dV \tag{6.75}$$

Using equation 6.66 the following is obtained,

$$\sum_{l=1}^{n} c_l(t)e^{\frac{i(E_k-E_l)t}{\hbar}} \int \psi_k^*(\mathbf{r})\hat{H}_I\psi_l(\mathbf{r})dV = i\hbar \sum_{l=1}^{n} \frac{dc_l(t)}{dt}e^{\frac{i(E_k-E_l)t}{\hbar}} \int \psi_k^*(\mathbf{r})\psi_l(\mathbf{r})dV. \tag{6.76}$$

Reducing this further using the completeness relation (orthogonal states),

$$\sum_{l=1}^{n} c_l(t)e^{\frac{i(E_k-E_l)t}{\hbar}} \int \psi_k^*(\mathbf{r})\hat{H}_I\psi_l(\mathbf{r})dV = i\hbar \sum_{l=1}^{n} \frac{dc_l(t)}{dt}e^{\frac{i(E_k-E_l)t}{\hbar}}\delta_{kl}. \tag{6.77}$$

The problem can be simplified by using equation 6.26. After summation on the left hand side equation 6.77 reduces to,

$$\sum_{l=1}^{n} c_l(t)e^{\frac{i(E_k-E_l)t}{\hbar}} I_{kl} = i\hbar\frac{dc_k(t)}{dt}. \tag{6.78}$$

Define,

$$\omega_{k,l} = \frac{E_k - E_l}{\hbar} \tag{6.79}$$

then equation 6.78 reduces to,

$$\sum_{l=1}^{n} c_l(t)e^{i\omega_{k,l}t} I_{kl} = i\hbar\frac{dc_k(t)}{dt}. \tag{6.80}$$

For a given pure state the density operator elements are given by equation 6.31 and are restated here,

$$\rho_{ab}(t) = c_a(t)c_b^*(t). \tag{6.81}$$

The equation of motion for a density matrix element can be written as [76],

$$\frac{d\rho_{ab}}{dt} = c_a\frac{dc_b^*}{dt} + c_b^*\frac{dc_a}{dt} \tag{6.82}$$

Using equation 6.80 and 6.82

$$\frac{d\rho_{ab}}{dt} = c_a(\frac{i}{\hbar}\sum_{l=1}^{n} c_l^* e^{-i\omega_{b,l}t} I_{bl}^*) + c_b^*(\frac{-i}{\hbar}\sum_{l=1}^{n} c_l e^{i\omega_{a,l}t} I_{al}) \tag{6.83}$$

This can be further reduced to,

$$\frac{d\rho_{ab}}{dt} = \frac{-i}{\hbar}\sum_{l=1}^{n} (c_b^* c_l e^{i\omega_{a,l}t} I_{al} - c_a c_l^* e^{-i\omega_{b,l}t} I_{lb}). \tag{6.84}$$

And by using equation 6.81 it reduces to,

$$\frac{d\rho_{ab}}{dt} = \frac{-i}{\hbar}\sum_{l=1}^{n} (\rho_{lb} e^{i\omega_{a,l}t} I_{al} - \rho_{al} e^{-i\omega_{b,l}t} I_{lb}). \tag{6.85}$$

These equations are sometimes called the optical Bloch equations (OBE's) for an n-level system, when a rotating wave approximation (RWA) has been made. For the simulations that will be done, these equations (equation 6.85) will be used within the numerical model. Both equations 6.63 and 6.85 were derived for a pure state vector. For the case of a mixture of states, equation 6.85 still applies and is proved in reference C.

6.7.2 Decay

The standard model for the coherent excitation of the vibrational modes of a polyatomic molecule introduces a so-called quasi-continuum of states at a certain vibrational quantum number [75]. This state is called the stochastization limit of the molecule. According to this model IVR in the quasi-continuum is extremely fast. This process is introduced into the model developed here by assuming that as soon as a molecule is excited into the quasi-continuum it will be lost to the process. Therefore the quasi-continuum will be approximated as a non-return trap. In this model the onset of the quasi-continuum (QC) was assumed to be vibrational level 5. The QC state is phenomenologically introduced into the model [75]. By adding an additional term to equation 6.80, the level that will represent the QC can be written it in a different form for simplicity.

$$\frac{dc_{QC}(t)}{dt} = -\frac{i}{\hbar}\sum_{l=1}^{n} c_l(t)e^{i\omega_{k,l}t}I_{kl} - \gamma c_{QC}(t). \tag{6.86}$$

γ, is the decay rate and it can either be calculated theoretically, or values from literature can be used. Thus equation 6.85 can be written as,

$$\frac{d\rho_{ab}}{dt} = \begin{cases} \frac{-i}{\hbar}\sum_{l=1}^{n}(\rho_{lb}e^{i\omega_{a,l}t}I_{al} - \rho_{al}e^{-i\omega_{b,l}t}I_{lb}) - 2\gamma\rho_{ab} & \text{for} \quad a = b = QC \\ \frac{-i}{\hbar}\sum_{l=1}^{n}(\rho_{lb}e^{i\omega_{a,l}t}I_{al} - \rho_{al}e^{-i\omega_{b,l}t}I_{lb}) - \gamma\rho_{ab} & \text{for} \quad a \neq b \text{ and } a = QC \text{ or } b = QC \\ \frac{-i}{\hbar}\sum_{l=1}^{n}(\rho_{lb}e^{i\omega_{a,l}t}I_{al} - \rho_{al}e^{-i\omega_{b,l}t}I_{lb}) & \text{for} \quad a \neq QC \text{ and } b \neq QC \end{cases} \tag{6.87}$$

Equation 6.87 is a set of coupled differential equations which were solved numerically using a simple Euler integration technique. For the specific structure shown in Figure 6.1 where excitation up to level n = 5 (QC is level five) was modeled this meant that taking all the energy levels into account resulted in 289 (17^2) coupled equations to be solved.

Chapter 7

Results and Discussion

7.1 Introduction

In this chapter, the different methods that were used to obtain selective excitation of a vibrational state within Uranium Hexafluoride (UF_6) are discussed. The methods which were investigated did not make use of any intermediary electronic states in order to selectively excite a vibrational state in the ν_3 mode. In all cases except one, a fluence of 600 J/m^2 was used. This was done in order to allow for meaningful comparisons of the different pulse shapes obtained from the simulations. For all cases where Husimi plots are given the α value is chosen to correspond to the initial pulse's full width at half maximum (FWHM).

The first section will test the numerical procedure for the case of a two level system for which an analytical solution of the dynamics is available. To follow, the effect that change of the carrier frequency has on the population dynamics are discussed, again for a two level system. The multiple levels of the UF_6 molecules and the effect different pulse shapes have on the population dynamics with selectivity of a vibrational state in mind is then studied. First the effect that the change of chirp has on the system is studied. This is followed by a multiple pulse approach (pulse train) to selectivity, after which a closed-loop feedback with a GA to control a spatial light modulator (SLM) is investigated and discussed. Initially simulations assume temperatures less than 120 Kelvin. In this case the ground vibrational state can be assumed to be fully populated. See Appendix B for details on the temperature dependence of the population dynamics. Phase only and amplitude only shaping of the SLM will be investigated and lastly phase and amplitude shaping. The scheme that works best whether it is phase only, amplitude only or phase and amplitude, will then be used to determine whether selectivity is still possible even at room temperature, 300 Kelvin. The uniqueness of a solution found by the genetic algorithm (GA) will be tested, by running three simulations in succession and comparing the results. Lastly the stability will be investigated by applying 10% noise to both the amplitude and phase masks.

7.2 Two level system - Comparison to known dynamics

A two level system was set up in which no damping is present and the rotating wave approximation (RWA) was not made. The analytic solutions to the differential equations was found in [76]. The equations were solved numerically using an Euler algorithm and compared to the solutions found by solving of equations 6.85 analytically for the same initial conditions. The Rabi frequency is given as [76]

$$V = \frac{X_{12}e}{\hbar}E_0. \tag{7.1}$$

For this example the Rabi frequency was chosen to be $V = 2(\omega_L - \omega_0)$, thus the amplitude and

transition probabilities where chosen to correspond to this value.

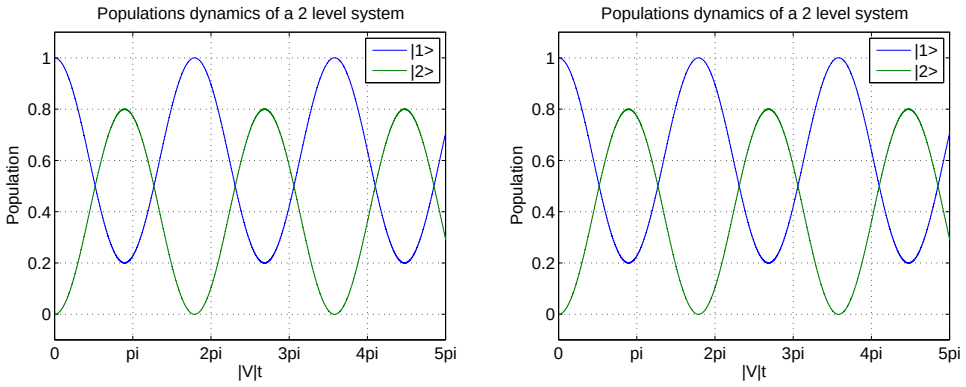

Figure 7.1: Numerical solutions of the differential equations that describe the two level system that interacts with a continuous wave laser. $\rho_{11} = 0$, V $= 2(\omega_L - \omega_0)$ with $\omega_0 = 628$ cm^{-1} and $\omega_L = 625$ cm^{-1}, thus giving $V = 1.3813 \times 10^{13}$ Hz. (Left) Analytic solution to the differential equations . (Right) Solution to equations 6.85 for the same involved conditions.

Figure 7.1 shows both the numerical and analytical solution to a continuous wave laser that interacts with a two level system. The Rabi frequency for the specific case shown here is $V = 2(\omega_L - \omega_0)$ where $\omega_0 = 628$ cm^{-1} and $\omega_L = 625$ cm^{-1} which resulted in a Rabi frequency of $V = 1.3813 \times 10^{13}$ Hz. The initial conditions used were, $\rho_{11} = 0$ and $\rho_{22} = 1$. From the Figure 7.1 it is clear that the two solutions are in excellent agreement. The Rabi oscillations can clearly be observed in both cases and the error was much less than 1×10^{-6} in the Rabi frequency. The simulation acted as first test of the validity and accuracy of the numerical procedure of the model.

7.3 Two level system - Pulse with center frequency varied

If a laser is utilized to excite a two level system it is expected that the on-resonance and off-resonance population dynamics would be different. In particular if the laser excitation frequency is far from the two level transition frequency, i.e. off-resonance, then very little of the population will be excited from the ground state to the upper state. Conversely when the laser frequency is on resonance then it is expected that a significant fraction of the population will be exited. As a further test of the numerical model the excitation of a two level system with a laser pulse was simulated. The center frequency of the laser pulse was scanned across the two level transition frequency. This, in effect, simulates the measurement of the two level absorption spectra of the system. If the intensity of the laser is chosen such that its value is below the saturation intensity of the transition then the expected bandwidth of the simulated absorption peak should be very close to the bandwidth of the laser pulse. The intensity of the laser pulse was chosen such that complete population inversion was achieved, which was 1100 J/m^2. Using the time-bandwidth product of Gaussian form

$$\Delta\nu\Delta t = 0.441 \tag{7.2}$$

the frequency bandwidth associated with a pulse with a FWHM of 150 fs pulse is found to be 98 cm^{-1}. In Figure 7.2 the population in the ground state as a function of the fluence is shown. From the information gained it was possible to use the minimum value of the intensity of the laser pulse to produce a complete population inversion when the pulse was on resonance. This ensured that the intensity of the laser pulse was below the saturation value. As can be seen in Figure 7.2 the FWHM of the transition predicted by the simulated was 94 cm^{-1} compared to the 98 cm^{-1} bandwidth of the

laser pulse and the difference in the absorption given in Figure 7.2 is approximately 4 cm^{-1}, which is less than 5 % difference.

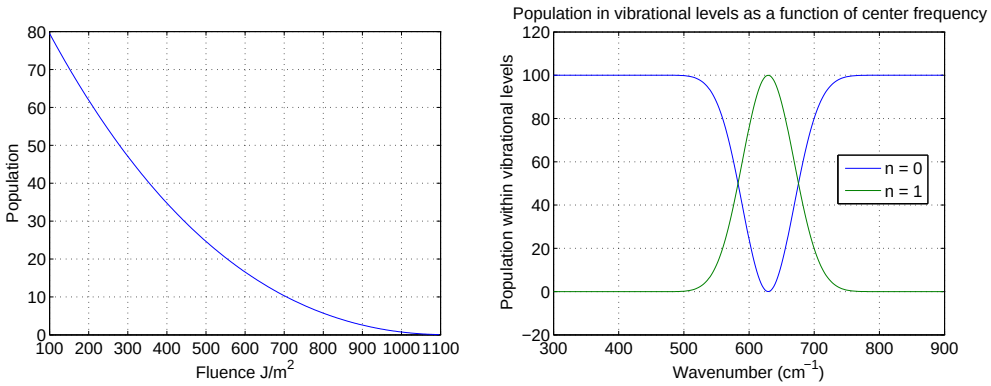

Figure 7.2: A two level system of which the transition frequency is $\omega_0 = 628$ cm^{-1}. (Left) The population in the ground state as a function of fluence. (Right) The center frequency of a transform limited 150 fs pulse is varied as shown in the graph. The fluence was kept constant at 1100 J/m^2. The transition dipole moment is 0.394 Debye (1 Debye = 3.3356x 10^{-30} C.m).

7.4 Transform limited pulse

As a starting point of the search for an optimum pulse that can selectively excite a targeted vibrational state within the ν_3 vibrational mode, the interaction with a transform limited pulse was simulated. This will be used as a benchmark to compare the results obtained with shaped pulses. The interaction was simulated with a 150 fs transform limited pulse with fluence of 600 J/m^2.

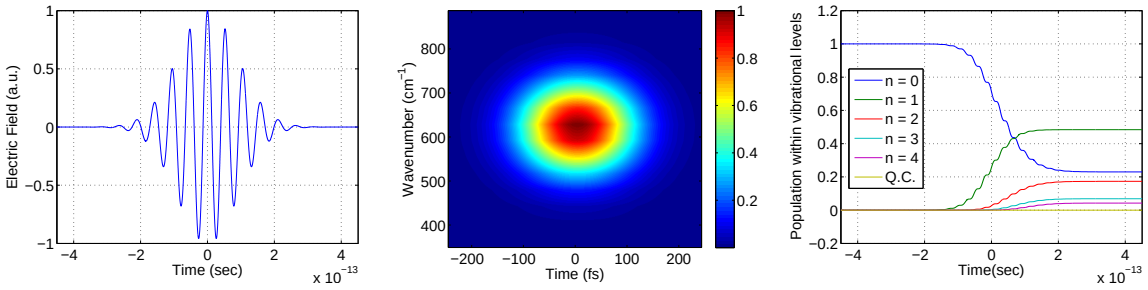

Figure 7.3: The center frequency of a transform limited (TF) pulse of 150fs is chosen to be, $\omega_l = 628$ cm^{-1}. (Left) Electric field in the time domain. (Middle) Husimi distribution of the pulse. (Right) Resulting population dynamics.

After the interaction of the transformed limited pulse, the final population within the vibrational level n=2, is 18%. From Figure 7.3 it is seen that the transform limited pulse has a highly symmetric Husimi distribution. The transform limited pulse has a perfectly symmetric Gaussian form in both the time and frequency domains, it is clear that the Husimi distribution displays both these features simultaneously. The pulse excites the population to the first excited state initially and as it becomes populated some of the population from the first excited state is excited to the second excited state. Similar dynamics can be observed from the second to third and third to fourth, only when there are population within the lower excited state can the population be transferred to a higher state. This is

a typical ladder climbing process. The difference in wavenumbers between adjacent levels is only a few wavenumbers, therefore a resonance condition is maintained.

The goal is to obtain higher selectivity, i.e a higher fraction of the population in a chosen vibrational state, in this case level 2, than can be obtained with the transform limited pulse.

7.5 Chirp variation and its effect

Chirp is often varied in experiments as a control parameter, because depending on the sign of the chirp; either the higher or lower frequencies follow in time. Chirp was investigated to determine whether there is a specific chirp value that can maximize the population in the targeted vibrational state $n = 2$. The fluence was kept constant throughout. Varying the chirp stretches the pulse. The pulse was chirped both negatively and positively to determine whether there exist a linear chirp that causes high vibrational excitation of vibrational level 2. All vibrational level populations were recorded after interaction with the pulses and the data is recorded in Figure 7.4.

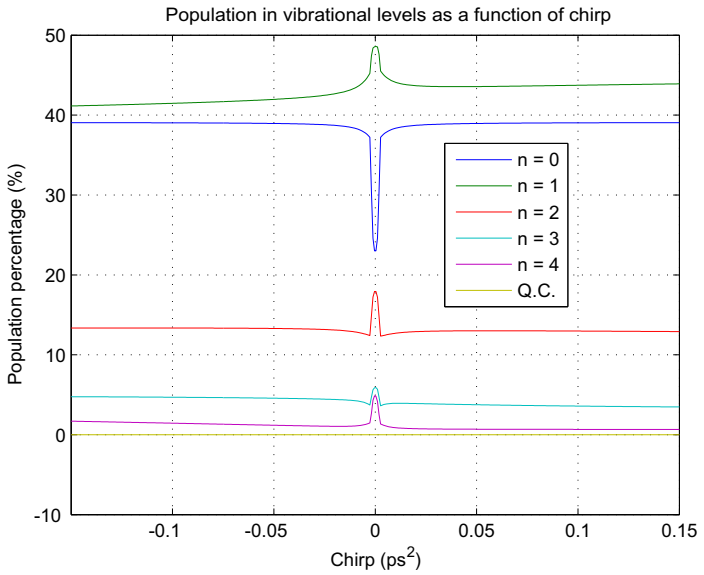

Figure 7.4: The chirp of a 150 fs pulse has been varied and the fluence was kept constant at 600 J/m^2. The center frequency of the transform limited pulse of a 150 fs, which is chirped is, $\omega_l = 628$ cm^{-1}

It can be observed from the Figure 7.4 that there is a non-symmetrical dependence on the sign of the chirp. This shows the difference when higher or lower frequencies first reach the system. Here it is clear that if the frequency increases in time, in the case of positive chirp, the transitions follow each other in a ladder climbing process, because the levels become closer in the higher part of the spectrum. As can be seen from Figure 7.4, the amount of control using only chirp as a varying parameter is very limited.

7.6 Multiple pulses

From the observed ladder climbing process in the simulation of the transform limited pulse interaction, a possible solution to obtaining a larger fraction of the population in the second vibrational state, could be the use of multiple pulses following each other. A step wise process, in which higher adjacent levels

are subsequently excited by using delayed pulses, could be a solution to the selectivity. An investigation was carried out to determine whether multiple pulses (pulse trains) which follow each other in time, could have the effect of exciting a particular vibrational state to a level higher than can be achieved with a transform limited pulse. This is similar to what was done in [79]. However in their model the phase of the individual pulses as well as the center frequency of each pulse could be varied. In our case only the timing and the amplitude of the pulses could be varied. In addition in their model the level that was optimized was the highest vibrational level and their model did not include anharmonic splitting. In our case vibrational level $n = 2$ was again the targeted state for optimization. The multiple pulses that were used, is either two, three or five 150 fs pulses with the center frequencies all set $\omega_l = 628$ cm^{-1}. The manner in which the multiple pulses was constructed and the parameters involved are given in Figure 7.5.

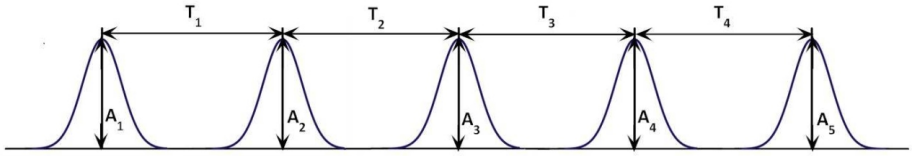

Figure 7.5: Pulse train with the time separation variables and amplitude variables indicated.

A schematic illustration of the pulse train used in the simulation is given in Figure 7.5. The time delays $\{T_i\}$ between the pulses can be varied as well as the amplitudes of each pulse. For example when only three pulses are used, A_1 and A_2 are set to zero. These parameters are manipulated by a genetic algorithm (GA) to obtain the configuration of the pulses that would optimize the fitness function. The fitness function has the form,

$$f = -p(t_{final}) \tag{7.3}$$

where $p(t_{final})$ is the population in the vibrational level $n = 2$ after the pulse has interacted with the molecule.

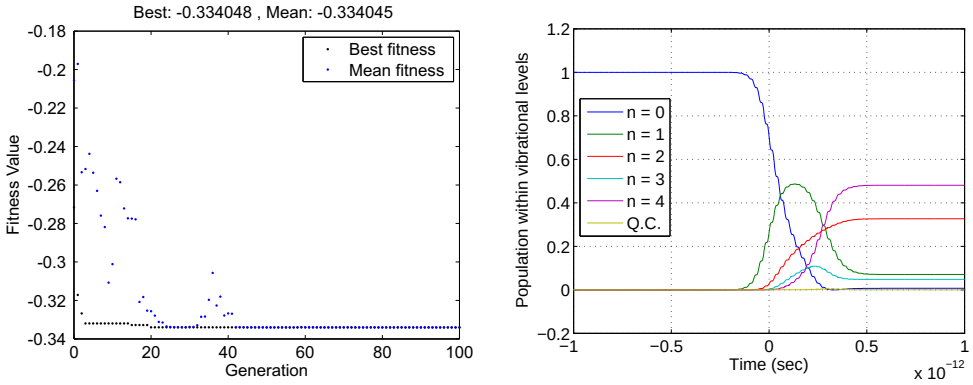

Figure 7.6: Double pulse simulation result with ground state is initially fully populated. (Left) The best and mean fitness as a function of generation. (Right) The resulting population dynamics of the system.

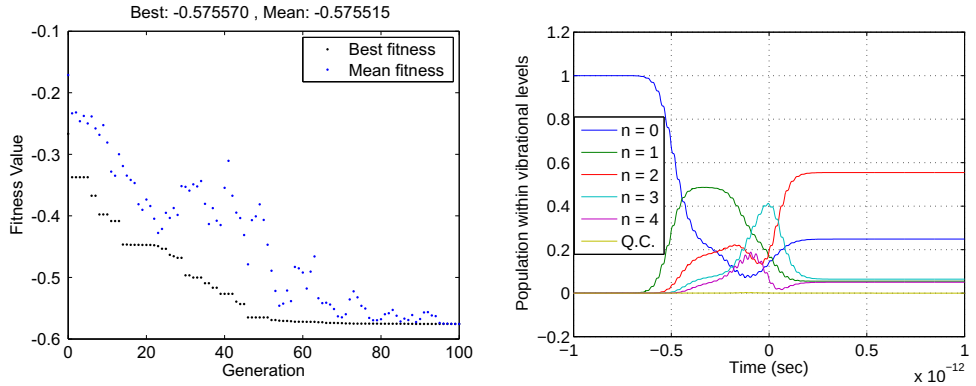

Figure 7.7: Triple pulse simulation result with ground state initially fully populated. (Left) The best and mean fitness as a function of generation. (Right) The resulting population dynamics of the system.

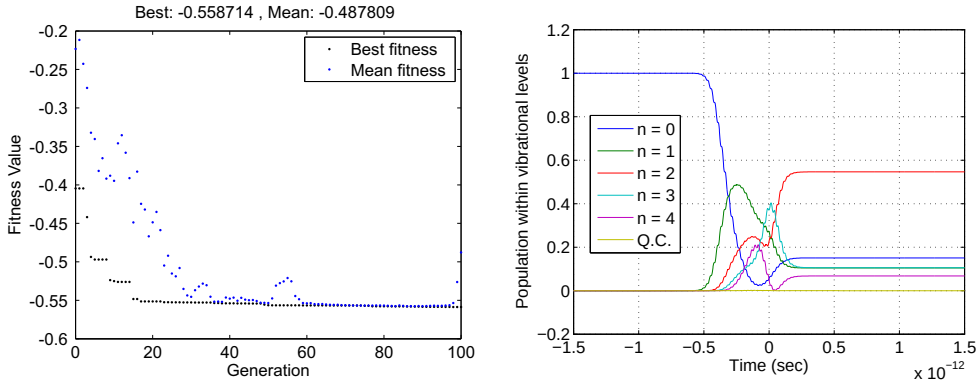

Figure 7.8: Five pulses simulation result with ground state initially fully populated. (Left) The best and mean fitness as a function of generation. (Right) The resulting population dynamics of the system.

Figures 7.6, 7.7 and 7.8 show the best fitness function as function of generation, as well as the resulting population dynamics of the best pulse. In Figure 7.6 the final population in the vibrational level $n = 2$ is 33%. From this figure it can also be seen that the optimum pulse first excites the population into the first excited state and as the state is more populated the next excited state is populated. This trend is similar to that of the transform limited interaction case. The difference comes in after the initial excitation, the second pulse, see Figure 7.11 excites the population from the first excited state to the second and fourth excited states, seemingly skipping the third excited state. This could be a first indication that the process is indeed coherent and not step-wise, for if it were step wise the second pulse should have excited the second and a short time later the third excited state.

The remaining three and five pulses cases have similar final dynamics. In Figure 7.7 the final population for the vibrational level, n = 2, is 56% and for the five pulses case in Figure 7.8 55%. The dynamics of both shows that the first excited state is excited first and then the second, third etc. The final shape pulse obtained by the genetic algorithm are shown in Figures 7.9, 7.10 and 7.11 for the double, triple and five pulse cases respectively. As can be seen the separate pulses in all three cases merged to form a single pulse with a rather complicated form.

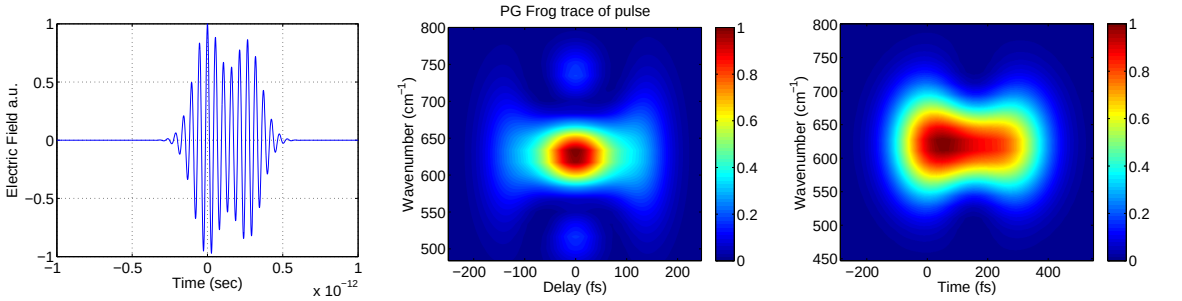

Figure 7.9: The results obtained from when a double pulse is initialized and with the ground state initially fully populated. The final shape resembles a single shaped pulse. (Left) Electric field in the time domain. (Middle) PG FROG trace of the pulse. (Right) Husimi distribution of the pulse.

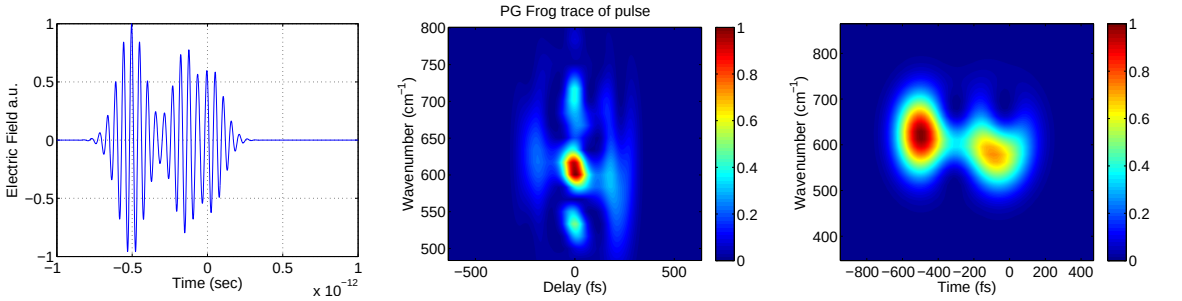

Figure 7.10: The results obtained from when a triple pulse is initialized and with the ground state initially fully populated. The final shape resembles a single shaped pulse. (Left) Electric field in the time domain. (Middle) PG FROG trace of the pulse. (Right) Husimi distribution of the pulse.

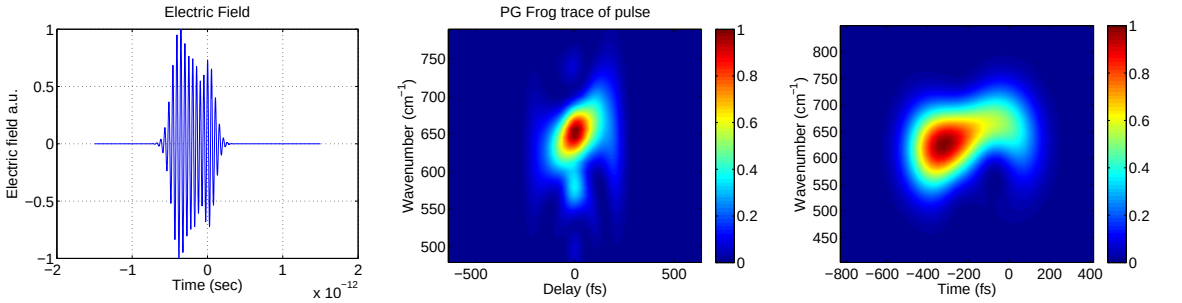

Figure 7.11: The results obtained from when five pulses is initialized and with the ground state initially fully populated. The final shape resembles a single shaped pulse. (Left) Electric field in the time domain. (Middle) PG FROG trace of the pulse. (Right) Husimi distribution of the pulse.

For the 3 cases studied here, the final population percentages after the system interacted with the double, triple and five pulses are, 33%, 56% and 55% respectively. In all three cases they outperform the transform limited interaction case.

It follows that the combination of three pulses, Figures 7.7 and 7.10, with specific time delays and amplitudes result in the shape of the electromagnetic field that optimizes the fitness function. The effect that the combination of the five pulses has on the population dynamics is very similar to that

of the three pulses. It should be noted that all possible combinations of the triple pulse sequence is also contained within the parameter space of the five pulse sequence. It would be expected that after longer periods of evolution allowed for the GA using the five pulse combination should result in the best possible pulse shape. The solutions given in this section is only for a single run, although the triple pulse show better selectivity, nevertheless the obtained solutions of the triple and five pulses are very close and differs by a mere 1%.

From the different multiple pulses simulations the results showed that the pulses are separated by less than 500 fs. This resulted in the overlapping of pulses and formed shaped pulses, instead of a train of pulses where the pulses do not overlap. Obtaining selectivity is thus possible when using combinations of pulses giving better results than using a single transform limited pulse. From the results obtained, it seems that a single shaped pulse could enhance that selectivity of the chosen vibrational level $n = 2$. From the Husimi plots it is clear that the resulting pulse has a primary pulse centered at the set wavelength of $\omega_l = 628$ cm^{-1} on the left, but also a secondary pulse on the right, thus slightly later in time, smaller but slightly shifted in frequency. From the result from the double pulse sequence this pulse is very slightly blue shifted with by only a few wavenumbers. In the experimentation with the triple pulse the shift is more significant 50 cm^{-1}. The five pulse sequence had a secondary structure that seems red shifted by approximately 50 cm^{-1}. It is unclear why this would occur for there is no subsequent transition in the model that has a wavenumber difference in this region.

In these multiple pulses simulation the time separation parameters that could be varied by the genetic algorithm were limited to a range of [-600 fs,600 fs] and the amplitude parameters to a range of [0,1]. The results here suggest that it is not possible to use separated combinations of transform limited pulses to significantly enhance the population in a specific vibrational state.

7.7 SLM simulation

Spatial light modulators (SLMs) are commonly used to shape pulses experimentally [54, 57]. The theory and equations developed in chapter 5 to simulate an spacial light modulator (SLM) were used in combination with a genetic algorithm (GA) to control the shaping of pulses in order to optimize the fitness function in equation 7.3.

Due to the random nature of the GA, sharp discontinuities appear in both the phase and amplitude masks of the SLM. A smoothing function were developed that is used to eliminate discontinuities in both the amplitude and phase. This is used in combination with the GA as follow: the GA generates a random set of amplitudes and phases. The smoothing function then uses these values as input. For an amplitude associated with a specific pixel, i, the smoothing function assigns a new value to it. The new value is the average of the amplitudes associated with its neighboring pixels, $i - 1$ and $i + 1$. This process can be carried out a few times, if necessary, but is never applied so many times to result in a constant amplitude or phase distribution. In the simulations it was performed ten times. It is only done to eliminate noise-like behavior and to have a localized pulse as final product. If noise like behavior is present, for instance in the phase, this will cause disturbances in the sidebands of the pulse that seem noisy as well.

7.7.1 Phase only shaping

In this case only the phase was varied and the amplitude was kept constant during the GA run. The results are shown in Figures 7.12, 7.13.

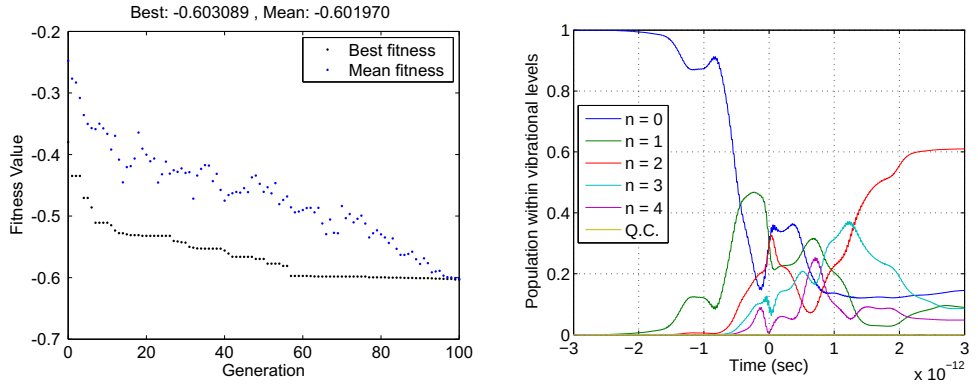

Figure 7.12: For the case of phase only shaping with the ground state initially fully populated. (Left) The best and mean fitness as a function of generation. (Right) The resulting population dynamics of the system.

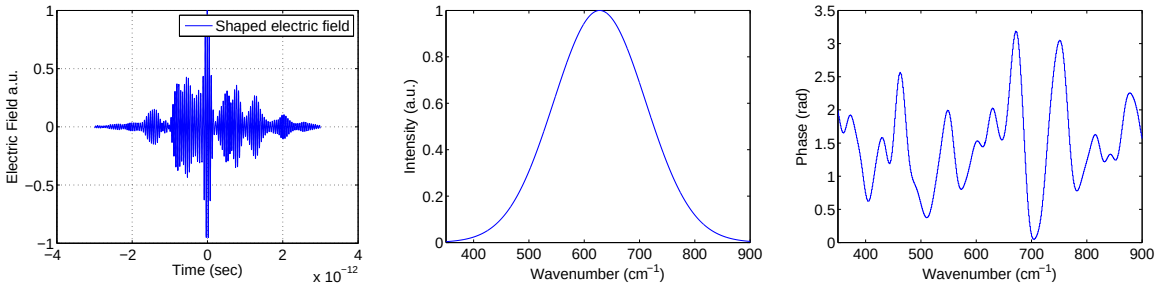

Figure 7.13: For the case of phase only shaping with the ground state initially fully populated. (Left) The shaped electric field that was formed by shaping a 150fs pulse with a fluence of 600 J/m^2. (Middle) The amplitude profile and, (Right) the phase profile of the spectrum of the pulse.

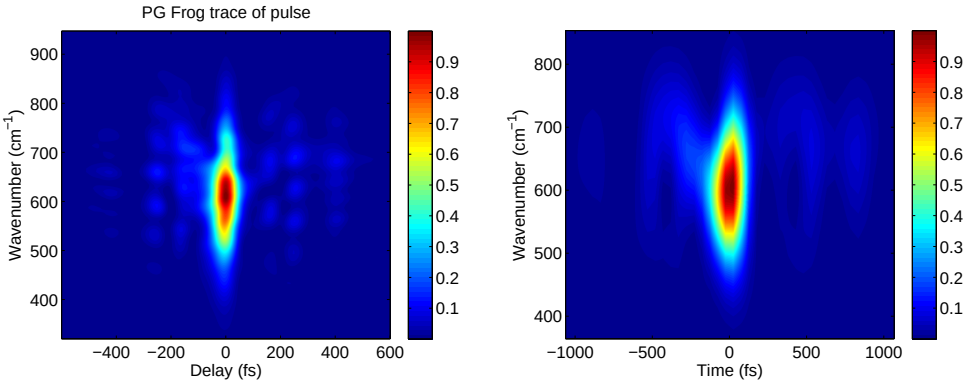

Figure 7.14: For the case of phase only shaping with ground state initially fully populated. (Left) PG FROG trace of the pulse. (Right) Husimi distribution of the pulse.

In Figure 7.12 the fitness value as a function of generation, as well as the resulting population dynamics for the best found pulse is given. From the population dynamics it is seen that the first excited state is initially populated, followed by the second and short time later the third and fourth

states. Just before $t = 0$ the third and fourth state is de-populated and the difference is apparently transferred to the targeted state. After $t = 0$ the population is again taken from the targeted state and all others are being populated and around 1ps the targeted state is filled again to a final value of 60%. The shape of the pulse in the time domain, as well as the amplitude and phase distribution of its frequencies are shown in Figure 7.13. Only the distinguishable areas of the PG-FROG and Husimi plots are shown in Figure 7.14.

From the results, the final population within vibrational level, n = 2, is approximately 60%. The simulation indicates that selectivity can be obtained by using phase only shaping of pulses. The selectivity found here was much greater than that obtained using the transformed limited pulse or the multiple pulse sequences. These results strongly suggest that the process involved is indeed a coherent process.

7.7.2 Amplitude only shaping

Phase only shaping had some success in the specific excitation of the vibrational level $n = 2$ and it would be interesting to investigate amplitude only shaping. Indeed it would be interesting to determine whether the optimum pulse obtained from the genetic algorithm would reflect the resonant structure of the molecule, i.e. at first resonant with the first transition, then the second etc. Thus a ladder climbing type of process that does not depend on a coherent process. Only the masking function associated with the amplitude mask varied by the genetic algorithm (GA). The phase modulations applied to the pixels were all zero.

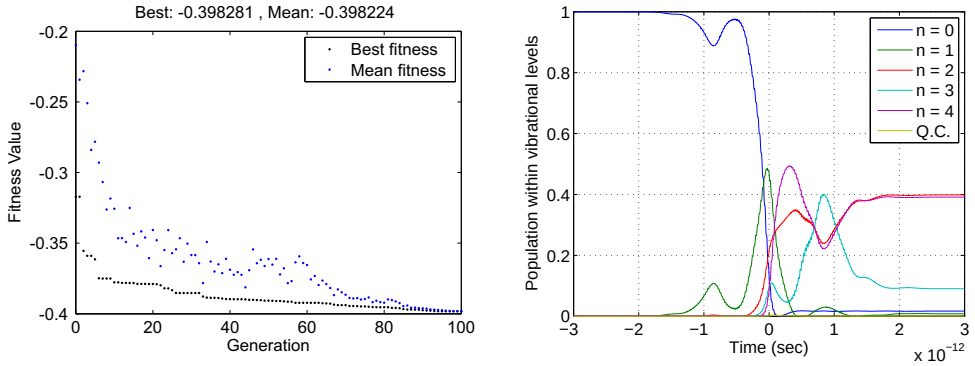

Figure 7.15: For the case of amplitude only shaping with ground state initially fully populated. (Left) The best and mean fitness as a function of generation. (Right) The resulting population dynamics of the system.

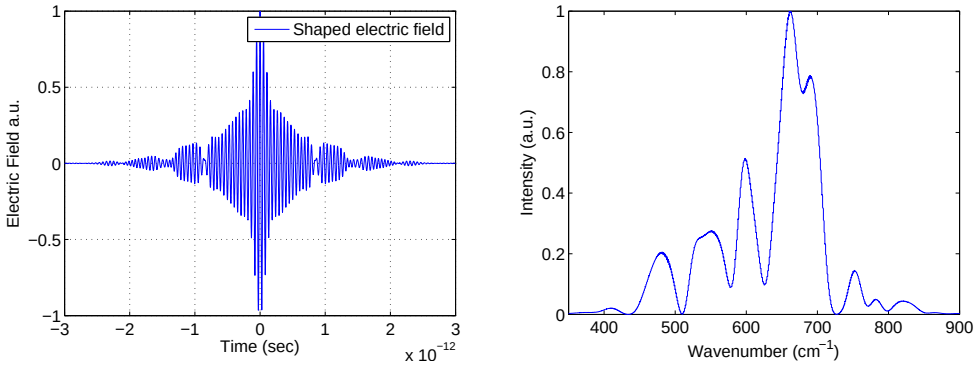

Figure 7.16: For the case of amplitude only shaping with ground state initially fully populated. (Left) The shaped electric field that was formed by shaping a 150fs pulse with a fluence of 600 J/m^2. (Right) The amplitude profile.

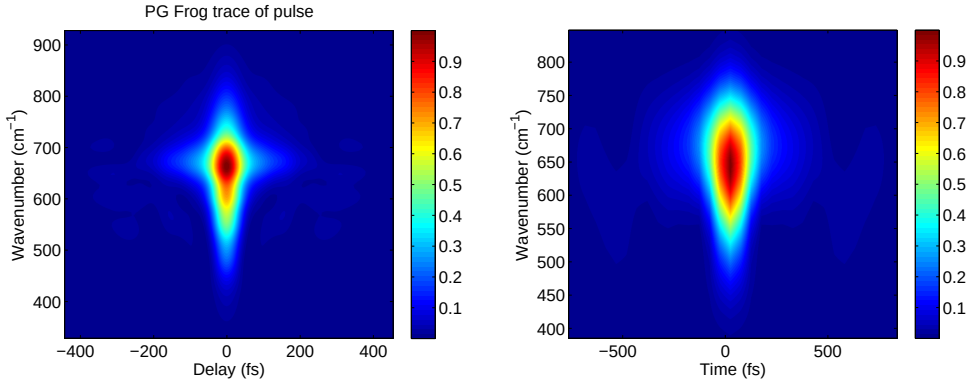

Figure 7.17: For the case of amplitude only shaping with ground state initially fully populated. (Left) PG FROG trace of the pulse. (Right) Husimi distribution of the pulse.

As can be seen in Figure 7.15, the pulse excites most of the population out of the ground vibrational state. In the process it is at first largely pumped into the second excited state. Just before a maximum is reached in the second excited state, levels two and four starts being populated, as level four reaches its limit population from levels two and four are partially pumped into level three. When there is a maximum for level three and equality is reached between level two and four and the population from level three is repumped into levels two and four equally. As can be seen from Figure 7.17 the shaped pulse is symmetric on the time dependent frequency structure and there is no indication of a ladder climbing process. It therefore seems that even in the case of amplitude only modulation the process is still coherent and a result of an interference process rather than ladder climbing.

The PG-FROG trace and Husimi distribution show symmetry only with respect to the time domain. From the results, a worse selectivity was obtained than with the phase only shaping. Only 40% of the population was finally in the vibrational level $n = 2$. Amplitude only shaping and phase only shaping worked in obtaining selectivity and in the following section simultaneous phase and amplitude shaping will be investigated to determine whether this could result in an even higher degree of selectivity.

7.7.3 Phase and Amplitude shaping

Since phase only and amplitude only shaping did manage selectivity, it could be expected that even better selectivity could be obtained if both are varied. Thus both the phase and amplitude masks were varied by the GA. The results obtained are given in Figures 7.18, 7.19 and 7.20. Initially the ground vibrational state is fully populated. This is assumed to hold for temperatures below 120 Kelvin, see Appendix B.

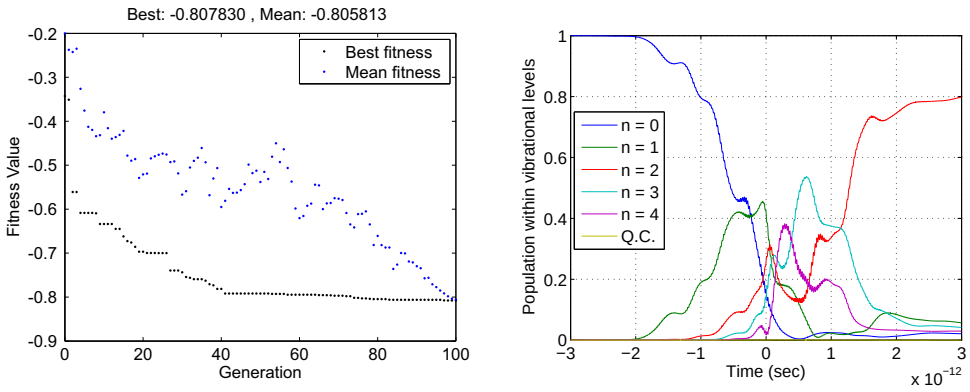

Figure 7.18: Phase and amplitude shaping with ground state initially fully populated. (Left) The best and mean fitness as a function of generation. (Right) The resulting population dynamics of the system.

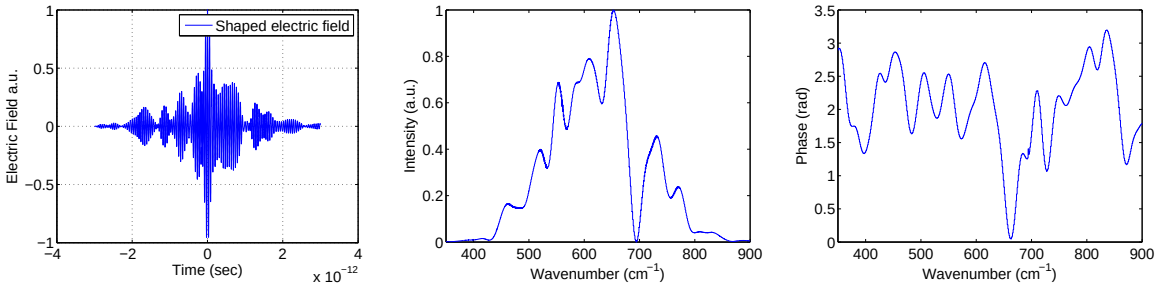

Figure 7.19: Phase and amplitude shaping with ground state initially fully populated. (Left) The shaped electric field that was formed by shaping a 150fs pulse with a fluence of 600 J/m^2. (Middle) The amplitude profile and, (Right) the phase profile of the spectrum of the pulse.

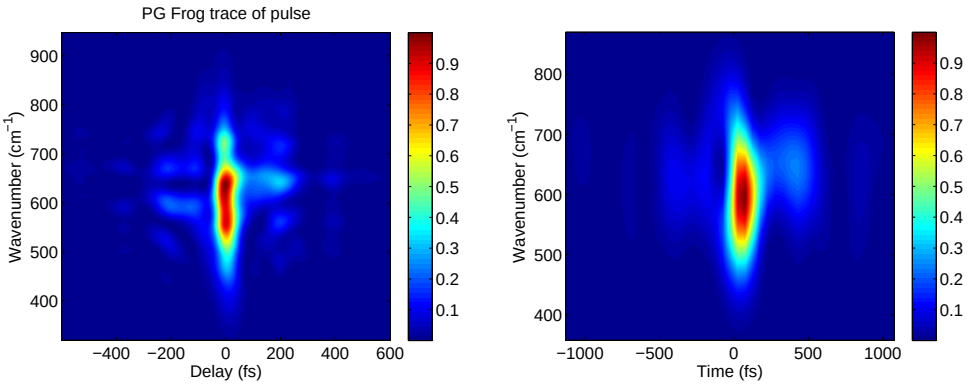

Figure 7.20: Phase and amplitude shaping with ground state initially fully populated. (Left) PG FROG trace of the pulse. (Right) Husimi distribution of the pulse.

In Figure 7.18, the fitness value as a function of generation clearly indicates convergence. The resulting population dynamics of the best pulse found, shows initially again how the first, second, third and fourth excited levels are excited as its neighbor is becoming populated. After $t = 0$ (which is the center of the pulse), all the levels shows a decrease in their population, except for the targeted, second excited state. The final amount of population trapped in the targeted state, is 80 %. This is a significant increase from all the previous simulations of the transform limited pulse, multiple pulse sequences, phase only and amplitude only shaping.

The optimum pulse is not symmetric at all, as in the case of amplitude only shaping. From the PG-FROG and the Husimi plot in Figure 7.20 there are distinguishable characteristics compared to phase only and amplitude only case. In the PG-FROG case the structure still has the dominant features centered around time, $t = 0$ and 628 cm^{-1}, which is the resonant 0-1 transition. For the Husimi plots similar structure is found as well around time $t = 0$ and 628 cm^{-1}.

A higher selectivity was found than in all the previous cases. This shows that the greater freedom of shaping enabled by using both the phase and amplitude to shape pulses, results in the best selectivity thus far. From the simulation, the total population trapped within the vibrational level $n = 2$ is 80 %. An investigation to determine whether selectivity will still be possible at room temperatures will follow.

7.8 Temperature and multiple GA runs

In this section, the simulation was carried out for the molecules at room temperature T = 300 K. The partition function was used as shown in Appendix B to determine the initial population distribution among the different vibrational levels. With these initial conditions the simulation will be carried out to determine whether selectivity is still possible. It was carried out three times in order to examine whether the solutions that are found are unique. The same fitness function as in the previous sections are used.

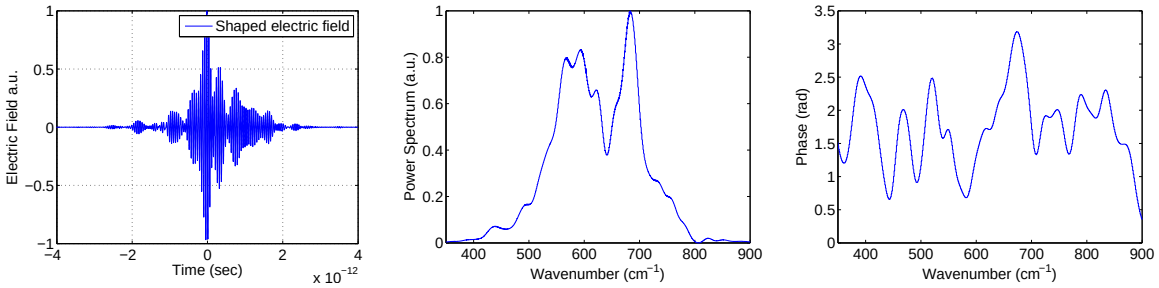

Figure 7.21: First Run : (Left) Electric field in the time domain. (Middle) The amplitude profile and (Right) the phase profile of the spectrum of the pulse.

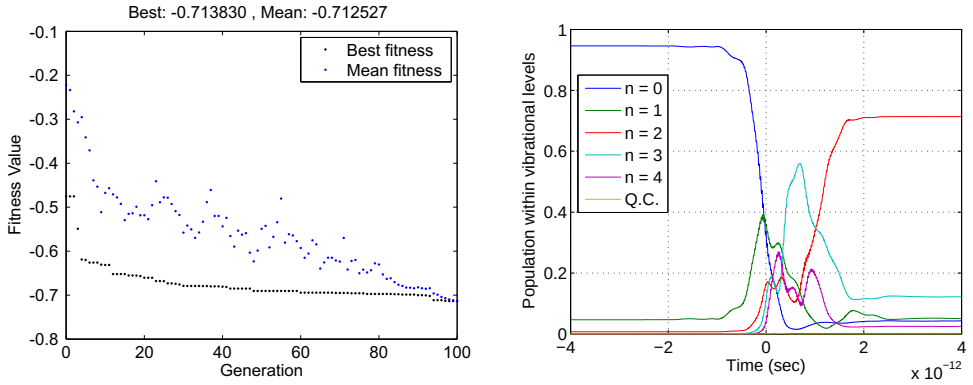

Figure 7.22: First Run : (Left) The best and mean fitness as a function of generation. (Right) The resulting population dynamics of the system.

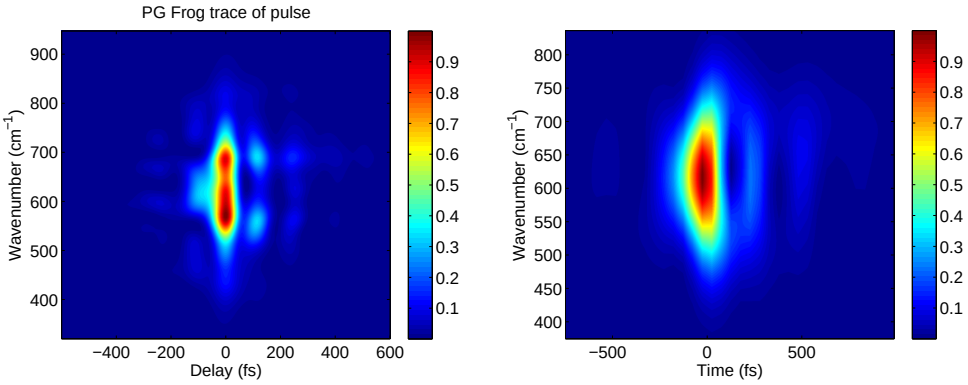

Figure 7.23: First Run : (Left) PG FROG trace of the pulse. (Right) Husimi distribution of the pulse.

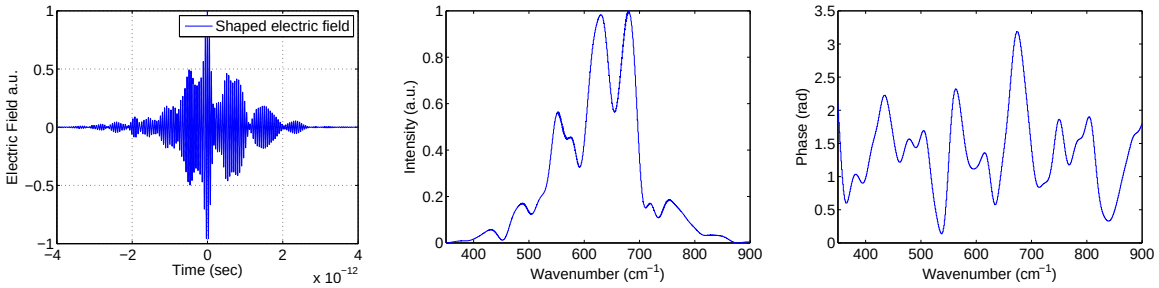

Figure 7.24: Second Run : (Left) Electric field in the time domain. (Middle) The amplitude profile and (Right) the phase profile of the spectrum of the pulse.

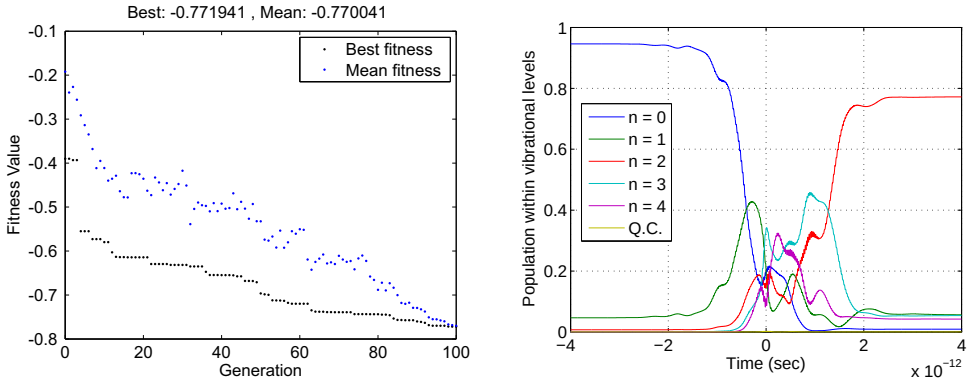

Figure 7.25: Second Run : (Left) The best and mean fitness as a function of generation. (Right) The resulting population dynamics of the system.

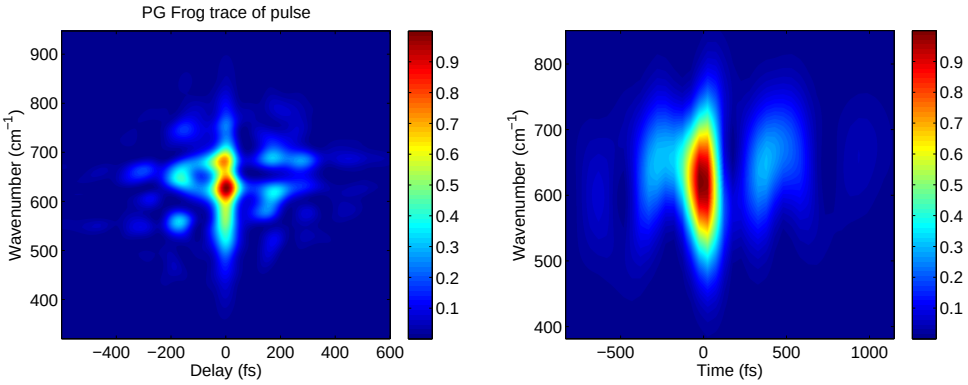

Figure 7.26: Second Run : (Left) PG FROG trace of the pulse. (Right) Husimi distribution of the pulse.

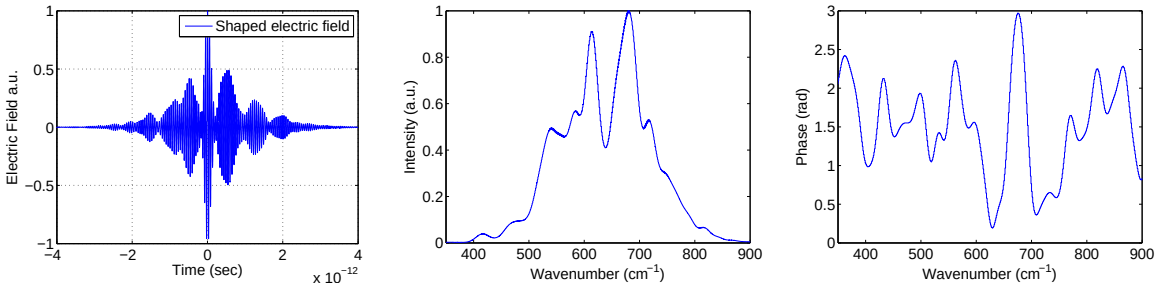

Figure 7.27: Third Run : (Left) Electric field in the time domain. (Middle) The amplitude profile and (Right) the phase profile of the spectrum of the pulse.

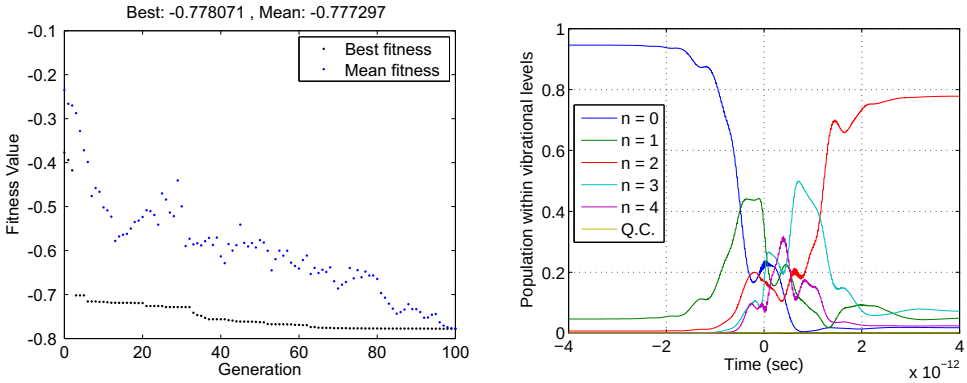

Figure 7.28: Third Run : (Left) The best and mean fitness as a function of generation. (Right) The resulting population dynamics of the system.

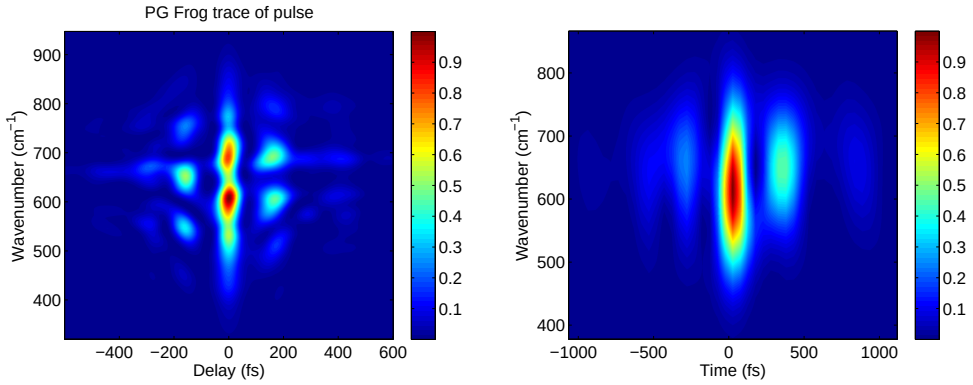

Figure 7.29: Third Run : (Left) PG FROG trace of the pulse. (Right) Husimi distribution of the pulse.

It follows clearly from the obtained results that selectivity is still possible, even at room temperatures. From Figures 7.23, 7.26 and 7.29 the obtained final populations are 71%, 77% and 78% respectively for the first, second and third run. From the results the pulse shapes are different from each other as can be observed from the PG FROG traces and Husimi distributions. Although they differ there are still some similarities. From the second and third run a definite structure around -200fs

and 200fs can be observed as seen in the PG-FROG traces, Figures 7.26 and 7.29. The structure is not clearly observed in the PG-FROG trace of the first run, Figure 7.23. Whether the pulse shape is unique could not be confirmed from these multiple runs. In 100 generations different best values were found, and it may be argued that if the GA was run for a longer period, the solutions might have converged to the same shape. Additionally it could be that the genetic algorithm found different local maxima that all gave comparable selectivity values. This was predicted by Rabitz in [80] and needs to be examined further. Another possibility could be that, because of the starting population that was not the same and the random behavior of the GA resulted in different population dynamics that are not equal.

7.9 GA stability

The results obtained from the first run of the multiple GA runs, was used to test the stability of the pulse shape that was found. Approximately ten percent noise is added to the amplitudes and phases of the masking functions. This was done by using$\Delta A = 0.1$ and $\Delta\phi = 0.3$ and multiplying it by a random number in the interval [0,1]. The obtained values are then added to the original amplitude and phase modulations of the result found for the first run in the previous section. The fitness function in equation 7.3 was used in the simulation. This has been done and the results are given in Figures 7.30 and 7.31.

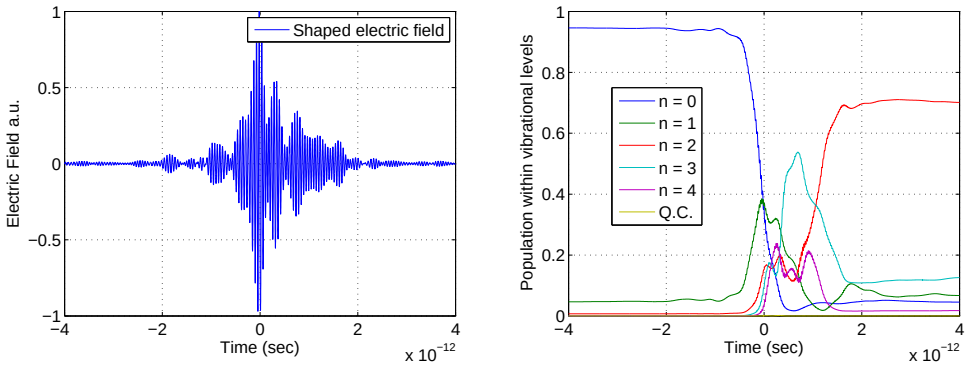

Figure 7.30: First test with ten percent noise added: (Left) Electric field in the time domain. (Right) The resulting population dynamics of the system.

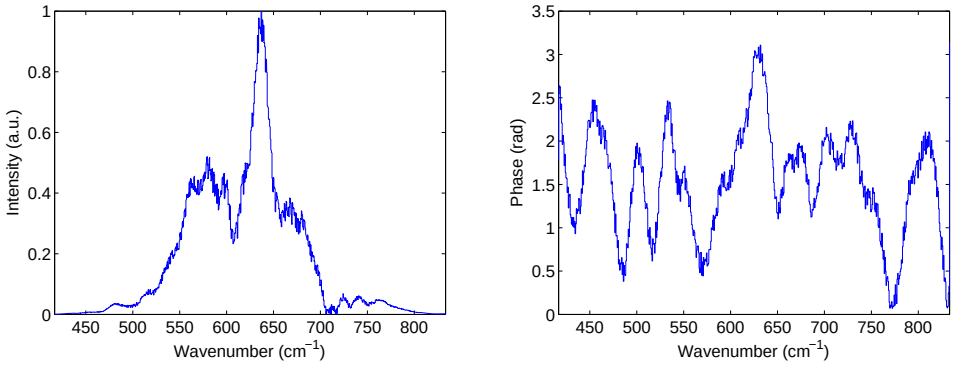

Figure 7.31: First test with ten percent noise added : (Left) The amplitude profile and (Right) the phase profile of the spectrum of the pulse.

As can be seen even with the noise added to the masking functions selectivity is not lost, although it is reduced. The final population before noise was added was 71.5% and after noise was added 70%. This 1.5% drop is not significant compared to the 10% noise increase on both the amplitude and phase masks. The reduction is due to the side bands which formed around the shaped pulse. The noise causes the pulse to be not as well localized as in the noiseless case.

Chapter 8

Conclusion

8.1 Summary of findings

The results obtained from the simulations with multiple pulses, found that the combination of the pulses resulted in shaped pulses that produced an increased population in a chosen vibrational state compared to that obtained with a transform limited pulse. The best selectivity that was found from these simulations had 56% of the population trapped in the vibrational state that was chosen compared to 18% obtained with a transform limited pulse. The simulations of the SLM show that it is possible to obtain an even higher fraction of the population in the chosen vibrational level $n = 2$ in a feedback loop experiment with a genetic algorithm (GA) algorithm. From the SLM simulations, phase only and amplitude only pulse shaping were able to find selectivity. The phase only shaping resulted in 60% of the population trapped in the vibrational level$n = 2$ and the amplitude only shaping only 40%. Using amplitude and phase shaping in combination, it is seen that the pulse shape that was found by iteratively changing it by means of a GA, found a pulse shape that resulted in 80% of the population being trapped in the vibrational level $n = 2$. All these simulations were carried out below 120 Kelvin, for then only the lowest vibrational state is assumed to be fully populated.

Simulations were carried out again, but with a temperature of 300 Kelvin. The results showed that excitation of the vibrational level $n = 2$ is still possible even at room temperature. The best obtained excited population in level two was 77.8%. The uniqueness of the solutions was tested by doing three consecutive runs and comparing the optimum pulses that were achieved. Similarities were found between the pulses, but the pulses were not identical. A proper metric needs to be developed to determine whether these pulses are close to each other in the parameter space or far removed.

The stability of one of the solutions that was obtained at a temperature of 300 Kelvin was tested, by applying noise to the masking functions. It was found that even with approximately 10% noise to both masking functions, the high fraction of the population remained within the vibrational level two. The degree is slightly less than that of the noise-free signal, but not significantly. The population in the vibrational level $n = 2$ dropped from 71.5% to 70%. The maximum possible population of a specific state was not established in the current study and is left for further study.

8.2 Conclusions

From the simulations that were done, it is clear that it is indeed possible to trap most of the population within a specific vibrational level within a spherical top molecule, without making use of an intermediary electronic state. This is also possible even at room temperatures and showed only approximately 2% decrease. The simulations were carried out for Uranium Hexafluoride, UF_6, since this molecule

is well studied and all the spectroscopic data required to do the simulations were found in literature. There are two ways in which the selectivity of a vibrational level can be reached, without making use of an intermediary electronic state. One method is to make use of pulse trains in which the pulses are allowed to overlap each other. Secondly making use of a SLM and a genetic algorithm (GA) to control the phase and amplitude masks, a pulse shape could be found subject to obtaining a specific goal.

From the simulations using pulse trains to selectively excite the targeted, vibrational state $n = 2$ the best solution found, resulted in 56% of the population being trapped in the targeted state. The case where the initial starting pulse was the three pulse train, gave the best solution, although for the simulation of the five pulse sequence the final difference was only 1%. It is interesting to note that from the three and five pulse sequences, the resulting population dynamics strongly suggests that the process is indeed coherent. Further study was carried out to find a method for achieving even better selectivity.

Simulations of an SLM were made in order to enable amplitude and or phase shaping of pulses. At first only phase shaping was done and the best solution found by the GA resulted in 60% population trapped in the vibrational state $n = 2$. The success of phase only shaping strongly suggests that the process is coherent and based on interference of multiple pathways. Amplitude only shaping was also investigated, in order to establish whether there is a step wise ladder climbing solution to the problem. A step-wise solution means exposing the molecules to the subsequent transition frequencies at certain time intervals. From the simulation only a 40% of the population was finally trapped within the targeted state. What was interesting was that no evidence of step wise excitation could be found by investigating the Husimi plots, again it seems that the process was a coherent process based on multiple path interference. Finally both amplitude and phase shaping were done simultaneously. The obtained best pulse resulted in a final population within the targeted vibrational state $n = 2$ of 80%. This is the highest value obtained with the various methods that were investigated. The results obtained for all the different methods are summarized in Table 8.1.

Method used	Population in vibrational level, n = 2 (%)	Comparison
Transform limited pulse	18	1.00
Multiple pulse sequences	56	3.11
Phase only shaping	60	3.33
Amplitude only shaping	40	2.22
Amplitude and Phase only shaping	80	4.44

Table 8.1: Comparison of the different methods used in relation to the transform limited pulse excitation (ground state fully populated) to obtain selective excitation of the vibrational level, n = 2 in the ν_3 vibrational mode of the spherical top molecule.

It was attempted to test the uniqueness of the obtained solutions. Are there multiple solutions, or only a single solution to the problem? The simulations in this case assumed a temperature of 300 Kelvin and the GA were ran three times to check for uniqueness. Various pulse shapes was found when the genetic algorithm was run multiple times with different initial populations, different populations dynamics resulted each time. There were some resemblances between them and it could be that the GA did not have sufficient time to run which could mean that the results did not converge to each other. Another possibility could be that due to different initial populations, the final results might never converge and are in fact different maxima. A proper metric needs to be developed to investigate this.

8.2.1 Implementation recommendation

A Spatial Light Modulator (SLM) which can shape pulses at 16 μm with closed loop feedback an which is controlled by a genetic algorithm (GA) is required to do the experiments. Smoothing over both the amplitude mask and phase mask is required to avoid the creation of possible sidebands in the shaped pulse.

8.3 Future research

It was shown theoretically using an adaptive feedback control scheme that it is possible to selectively excite a targeted vibrational state within a ground electronic state of a polyatomic molecule without making use of any other electronic states. Only vibrational transitions were included, however rotational levels should be included and the effect they might have on the selectivity of excitation of a vibrational level should be investigated.

The uniqueness of the control fields that were found should be investigated and compared to the case where there is complete controllability as in [80]. A comparison between full and partial controllability of the control fields should be done. The effect that a field has on a simple molecule should then indicate whether this field that cause complete population transfer is unique or not.

The genetic algorithm is very robust, but it requires lots of evaluations before convergence can be observed. Experimentally this is not necessarily ideal, for it could take hours before an optimum pulse for a specific goal is reached. The optimization procedure itself should be investigated as well as various other techniques that will speed up the search for a control field. A study of the optimization space related to the control method might lead to insight of the physical problem.

Appendix A

Pulse Intensity

A.1 Intensity calculations

The electric field shape we chose is

$$\epsilon(t) = e^{-\alpha t^2} e^{-i(\omega_L t + \beta t^2)}. \tag{A.1}$$

The fluence of a pulse is defined to be

$$Fpulse = \int_0^\infty I(t)dt. \tag{A.2}$$

We can write the intensity of the electric field as

$$I(t) = I_0|\epsilon(t)|^2 \tag{A.3}$$

$$I(t) = I_0 e^{-2\alpha t^2} \quad . \tag{A.4}$$

From this we obtain the relation between the full width at half the maximum (FWHM) and α as

$$\alpha = \frac{ln2}{(\frac{FWHM}{2})^2} \tag{A.5}$$

From equation A.4 we obtain

$$F_{pulse} = I_0 \int_0^\infty e^{-2\alpha t^2} dt \tag{A.6}$$

$$F_{pulse} = I_0 \sqrt{\frac{\pi}{8\alpha}} \tag{A.7}$$

Now using equation A.5 we obtain the following after a lot of simplifications

$$I_0 = \frac{F_{pulse}}{FWHM}\sqrt{\frac{32ln2}{\pi}} \tag{A.8}$$

$$I_0 \approx 2.657\frac{F_{pulse}}{FWHM} \tag{A.9}$$

Appendix B

Canonical Distribution for Uranium Hexafluoride

In this part of the appendix the canonical distribution for UF_6 will be investigated. The proof for why a pure state can be used in the numerical simulation will be given here.

A system where the number of particles and the volume is fixed and only the energy can fluctuate is described by the canonical ensemble. The canonical distribution is given by [20]

$$P_r = \frac{< n_r >}{N} = \frac{e^{-\beta E_r}}{\sum_r e^{-\beta E_r}}, \tag{B.1}$$

Where N is the number of particles in the system E_r are the energies associated with the energy levels in the system and β is given by

$$\beta = \frac{1}{kT}, \tag{B.2}$$

where k is the Boltzmann constant. The canonical distribution was calculated taking into account the nine levels of UF_6 which are simulated in the numerical models. Only the ground vibrational and first vibrational excited state are plotted in Figure B.1. It is clear from the graph that if the gas of UF_6 is colder than 150 Kelvin that the entire gas can be considered as being in a pure state and not a mixed state.

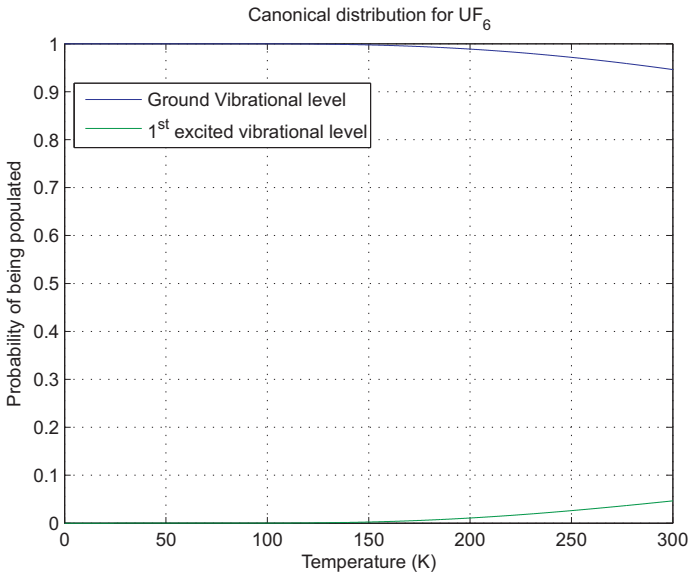

Figure B.1: The canonical distribution for UF_6 with the first two vibrational levels indicated.

Appendix C

Mixed States

The continuation of chapter 6, to prove that equation 6.85 for the pure case is the same for the mixed state case. The density matrix elements for a mixture of states are as follow,

$$\rho_{pn} = \sum_k p_k c_p^k (c_n^k)^* \tag{C.1}$$

assuming the set of probabilities, $\{p_k\}$, is independent of time and only the coefficients, c_n^k, are dependent on time. Then it follows that the total time derivative of this equation is given by,

$$\frac{d\rho_{pn}}{dt} = \sum_k \frac{dc_p^k}{dt}(c_n^k)^* + c_p^k \frac{d(c_n^k)^*}{dt} \tag{C.2}$$

Similar to equation 6.80, the case for a mixed state follow,

$$-\frac{i}{\hbar}\sum_{l=1}\ c_l^k(t)e^{i\omega_{r,l}t}I_{rl} = i\hbar\frac{dc_r^k(t)}{dt} \tag{C.3}$$

The proof now follow,

$$\frac{d\rho_{pn}}{dt} = \sum_k(-\frac{i}{\hbar}\sum_l\ p_k c_l^k (c_n^k)^* e^{i\omega_{p,l}t}I_{pl}) + \sum_k(\frac{i}{\hbar}\sum_l\ p_k c_p^k (c_l^k)^* e^{-i\omega_{n,l}t}I_{nl}^*) \tag{C.4}$$

$$\frac{d\rho_{pn}}{dt} = -\frac{i}{\hbar}(\sum_{k,l}\ p_k c_l^k (c_n^k)^* e^{i\omega_{p,l}t}I_{pl} - \sum_{k,l}\ p_k c_p^k (c_l^k)^* e^{-i\omega_{n,l}t}I_{nl}^*) \tag{C.5}$$

$$\frac{d\rho_{pn}}{dt} = -\frac{i}{\hbar}(\sum_{k,l}\ p_k c_l^k (c_n^k)^* e^{i\omega_{p,l}t}I_{pl} - \sum_{k,l}\ p_k c_p^k (c_l^k)^* e^{-i\omega_{n,l}t}I_{nl}^*) \tag{C.6}$$

$$\frac{d\rho_{pn}}{dt} = -\frac{i}{\hbar}(\sum_{k,l}\ \rho_{ln} e^{i\omega_{p,l}t}I_{pl} - \sum_{k,l}\ \rho_{pl} e^{-i\omega_{n,l}t}I_{nl}^*) \tag{C.7}$$

Appendix D

Code

D.1 GA run

Algorithm D.1 Code to run the genetic algorithm

```
options = gaoptimset(@ga);

NGen    = 100;
LB      = [zeros(1,1280) 80 80];
UB      = [ones(1,1280) 80 80];
Nvars   = numel(LB);

options = gaoptimset( options,'Generations',NGen);
options = gaoptimset( options,'UseParallel', 'always');
options = gaoptimset( options,'StallGenLimit', NGen);
options = gaoptimset( options,'TolFun', 1e-100 );
options = gaoptimset( options,'TolCon', 1e-100 );
options = gaoptimset( options,'FitnessScalingFcn', @fitscalingrank );
options = gaoptimset( options,'PlotFcns', @gaplotbestf );

[x fval]=ga(@SLM_GA, Nvars,[],[],[],[],LB,UB,[],options);
save SLM_DATA x;
```

D.2 SLM simulation code

Algorithm D.2 Code to run the genetic algorithm

```
function [func] = SLM_GA(x)

%physical constants
e       = 1.6*10^(-19);
hbar    = 1.05457159642*10^(-34);
c       = 299972458;
ps      = (10^(-12));
um   = 1e-6;
%physical constants

FWHM = 150e-15;
alpha= log(2)/(FWHM/2)^2;
t0   = -10000*FWHM;
tf   = +10000*FWHM;
T    = tf - t0;

vl   = 628;
wl   = (2*pi)*(100*c)*vl;
ws   = 10*wl;
ts   = 1/ws;

test = T/ts;
n    = nextpow2(test);
t    = linspace(t0,tf,2^n);
N    = numel(t);
w    = (0 : N - 1)*(2*pi/T);

ef1     = exp(-alpha*(t).^2).*exp(1i*wl*t) ;
EF1     = fft(ef1);

lamdaleft = 10*um;
lamdaright= 30*um;

wright    = 2*pi*c/(lamdaleft);
wleft     = 2*pi*c/(lamdaright);

posl      = find(w>wleft);
posr      = find(w>wright);

posL     = posl(1);
posR     = posr(1);
NumberPix= 640;
delNR    = posR - posL;
NumberFreq    = delNR/NumberPix;
NumberFreqnew = round(NumberFreq);

%%%%%%%%%%%%%%%%%%%%%%%%%%%%%%%%%%%%%%%%%%%%%%%%%%%%%%%%%%%%%%%%%%%%%%%%%%%%%%%
% define om numberfreq 'n integer te kry
delNRnew      = NumberFreqnew*NumberPix;
ΔNRs      = delNRnew - delNR;
half          = ΔNRs/2;

posL     = posL - half;
posR     = posR + half ;
% Region   = posR - posL;
%%%%%%%%%%%%%%%%%%%%%%%%%%%%%%%%%%%%%%%%%%%%%%%%%%%%%%%%%%%%%%%%%%%%%%%%%%%%%%%
```

```
am      = x(1:640);
ph      = x(641:1280);
am      = smoothvectorLudwigSLM(am,x(1281));
ph      = pi*smoothvectorLudwigSLM(ph,x(1282));

%replaces my for loop
amplHbuild   = ones(NumberFreqnew,1)*am;
amplHbuild   = reshape(amplHbuild,NumberFreqnew*640,1)';
phasesHbuild = ones(NumberFreqnew,1)*ph;
phasesHbuild = reshape(phasesHbuild,NumberFreqnew*640,1)';
%replaces my for loop

phasesHbuild = mod(phasesHbuild,2*pi);
Mask1        = amplHbuild.*exp(1i*( phasesHbuild ));

VecLeft  = zeros(1,posL-1);
length   = N - posR + 1;
VecRight = zeros(1,length);
MASK     = horzcat(VecLeft,Mask1,VecRight);
HregionTest2  = MASK;
efoutMask     = ifft(EF1.*HregionTest2);
efoutMask     = efoutMask/max(efoutMask);

%%%%%%%%%%%%%%%%%%%%%%%%%%%%%%%%%%%%%%%%%%%%%%%%%%%%%%%%%%%%%%%%%%%%%%%%%%%%

post     = find(t>-2*ps);
pos      = post(1);
dN       = abs(numel(t)/2 - pos);
tnew     = t(pos :pos + 2*dN -1 ) ;

t        = tnew;
N        = numel(t);
EF       = efoutMask(pos :pos + 2*dN -1 ) ;
EF       = real(EF);

%%%parameters
Fpulse      = 600;
I0          = (Fpulse /FWHM)*( 2*sqrt(log(2)/pi ));
%%%parameters

Intensity   = I0*EF.*conj(EF);
h           = t(2) - t(1);
area        = 0;
for k3 = 2 : numel(EF)
    intens  = real( Intensity(k3-1) );
    area    = area + h*intens;
end
facreduce   = (Fpulse/area);
I0new       = I0*facreduce ;
E0          = sqrt(188*I0new);

%%%%%%%%%%%%%%%%%%%%%%%%%%%%%%%%%%%%%%%%%%%%%%%%%%%%%%%%%%%%%%%%%%%%%%%%%%%%
clear tnew;
clear EF1;
clear ef1;
clear EF2;
```

```
clear EF1new;
clear Hreg;
clear Hregion;
clear HregionTest2;
clear Hshifted;
clear MASK;
clear Mask1;
clear VecLeft;
clear VecRight;
clear amplHbuild;
clear phasesHbuild;
clear wnew;
clear w;
clear lamtr;
clear posl;
clear posr;
clear ph;
clear am;
clear post;
clear efoutMask;
%%%%%%%%%%%%%%%%%%%%%%%%%%%%%%%%%%%%%%%%%%%%%%%%%%%%%%%%%%%%%%%%%%%%%%%%%%%%%%%

%%%%%%%%%%%%%%%%%%%%%%%%%%%%%%%%%%%%%%%%%%%%%%%%%%%%%%%%%%%%%%%%%%%%%%%%%%%%%%%
%%%%%%%%%%%%%%%%%%%%%%%%---MOLECULE-MODEL BEGIN---%%%%%%%%%%%%%%%%%%%%%%%%%%%%%

%molecular properties--begin-----------------------------------------
% This is where you have to do the following,
%input %input %input %input %input %input %input

%molecular properties %input
Num    = 17; % Number of levels to consider

%transition dipole moments
Debye       = 3.3356e-30;
eX12        = 0.394*Debye;
FirstTransX = (eX12)/e;
Scale2      = FirstTransX;

X11    = 0;
X12    = Scale2;
X13    = 0;
X14    = 0;
X15    = 0;
X16    = 0;
X17    = 0;
X18    = 0;
X19    = 0;
X110    = 0;
X111    = 0;
X112    = 0;
X113    = 0;
X114    = 0;
X115    = 0;
X116    = 0;
X117    = 0;
```

```
X21    = Scale2;
X22    = 0;
X23    = sqrt(0.444)*Scale2;
X24    = sqrt(0.222)*Scale2;
X25    = sqrt(0.666)*Scale2;
X26    = 0;
X27    = 0;
X28    = 0;
X29    = 0;
X210    = 0;
X211    = 0;
X212    = 0;
X213    = 0;
X214    = 0;
X215    = 0;
X216    = 0;
X217    = 0;

X31    = 0;
X32    = sqrt(0.444)*Scale2;
X33    = 0;
X34    = 0;
X35    = 0;
X36    = sqrt(1.029)*Scale2;
X37    = sqrt(0.500)*Scale2;
X38    = sqrt(0.137)*Scale2;
X39    = sqrt(0.278e-31)*Scale2;
X310    = 0;
X311    = 0;
X312    = 0;
X313    = 0;
X314    = 0;
X315    = 0;
X316    = 0;
X317    = 0;

X41    = 0;
X42    = sqrt(0.222)*Scale2;
X43    = 0;
X44    = 0;
X45    = 0;
X46    = sqrt(0.939)*Scale2;
X47    = sqrt(0.372e-27)*Scale2;
X48    = sqrt(0.7274)*Scale2;
X49    = sqrt(0.5434e-31)*Scale2;
X410    = 0;
X411    = 0;
X412    = 0;
X413    = 0;
X414    = 0;
X415    = 0;
X416    = 0;
X417    = 0;
```

```
X51    = 0;
X52    = sqrt(0.666)*Scale2;
X53    = 0;
X54    = 0;
X55    = 0;
X56    = sqrt(0.009)*Scale2;
X57    = sqrt(0.667)*Scale2;
X58    = sqrt(0.6658)*Scale2;
X59    = sqrt(0.333)*Scale2;
X510    = 0;
X511    = 0;
X512    = 0;
X513    = 0;
X514    = 0;
X515    = 0;
X516    = 0;
X517    = 0;

X61    = 0;
X62    = 0;
X63    = sqrt(1.029)*Scale2;
X64    = sqrt(0.939)*Scale2;
X65    = sqrt(0.009)*Scale2;
X66    = 0;
X67    = 0;
X68    = 0;
X69    = 0;
X610    = sqrt(0.095)*Scale2;
X611    = sqrt(0.190)*Scale2;
X612    = sqrt(0.2857)*Scale2;
X613    = sqrt(0.2857)*Scale2;
X614    = sqrt(0.19)*Scale2;
X615    = sqrt(0.095)*Scale2;
X616    = sqrt(0.2857)*Scale2;
X617    = 0;

X71    = 0;
X72    = 0;
X73    = sqrt(0.500)*Scale2;
X74    = sqrt(0.372e-27)*Scale2;
X75    = sqrt(0.667)*Scale2;
X76    = 0;
X77    = 0;
X78    = 0;
X79    = 0;
X710    = 0;
X711    = sqrt(0.2198)*Scale2;
X712    = sqrt(0.3297)*Scale2;
X713    = sqrt(0.3297)*Scale2;
X714    = sqrt(0.2198)*Scale2;
X715    = 0;
X716    = sqrt(0.3297)*Scale2;
X717    = 0;
```

```
X81    = 0;
X82    = 0;
X83    = sqrt(0.137)*Scale2;
X84    = sqrt(0.7274)*Scale2;
X85    = sqrt(0.6658)*Scale2;
X86    = 0;
X87    = 0;
X88    = 0;
X89    = 0;
X810    = sqrt(0.095)*Scale2;
X811    = sqrt(0.190)*Scale2;
X812    = sqrt(0.2857)*Scale2;
X813    = sqrt(0.2857)*Scale2;
X814    = sqrt(0.19)*Scale2;
X815    = sqrt(0.095)*Scale2;
X816    = sqrt(0.2857)*Scale2;
X817    = 0;

X91    = 0;
X92    = 0;
X93    = sqrt(0.278e-31)*Scale2;
X94    = sqrt(0.5434e-31)*Scale2;
X95    = sqrt(0.333)*Scale2;
X96    = 0;
X97    = 0;
X98    = 0;
X99    = 0;
X910    = 0;
X911    = 0;
X912    = 0;
X913    = sqrt(0.7143)*Scale2;
X914    = 0;
X915    = 0;
X916    = sqrt(0.7143)*Scale2;
X917    = 0;

%STUFF

X101    = 0;
X102    = 0;
X103    = 0;
X104    = 0;
X105    = 0;
X106    = sqrt(0.095)*Scale2;
X107    = 0;
X108    = sqrt(0.095)*Scale2;
X109    = 0;
X1010    = 0;
X1011    = 0;
X1012    = 0;
X1013    = 0;
X1014    = 0;
X1015    = 0;
X1016    = 0;
X1017    = sqrt(11/36)*Scale2;
```

```
X111    = 0;
X112    = 0;
X113    = 0;
X114    = 0;
X115    = 0;
X116    = sqrt(0.190)*Scale2;
X117    = sqrt(0.2198)*Scale2;
X118    = sqrt(0.190)*Scale2;
X119    = 0;
X1110    = 0;
X1111    = 0;
X1112    = 0;
X1113    = 0;
X1114    = 0;
X1115    = 0;
X1116    = 0;
X1117    = sqrt(11/36)*Scale2;

X121    = 0;
X122    = 0;
X123    = 0;
X124    = 0;
X125    = 0;
X126    = sqrt(0.2857)*Scale2;
X127    = sqrt(0.3297)*Scale2;
X128    = sqrt(0.2857)*Scale2;
X129    = 0;
X1210    = 0;
X1211    = 0;
X1212    = 0;
X1213    = 0;
X1214    = 0;
X1215    = 0;
X1216    = 0;
X1217    = sqrt(11/36)*Scale2;

X131    = 0;
X132    = 0;
X133    = 0;
X134    = 0;
X135    = 0;
X136    = sqrt(0.2857)*Scale2;
X137    = sqrt(0.3297)*Scale2;
X138    = sqrt(0.2857)*Scale2;
X139    = sqrt(0.7143)*Scale2;
X1310    = 0;
X1311    = 0;
X1312    = 0;
X1313    = 0;
X1314    = 0;
X1315    = 0;
X1316    = 0;
X1317    = sqrt(11/36)*Scale2;
```

```
X141    = 0;
X142    = 0;
X143    = 0;
X144    = 0;
X145    = 0;
X146    = sqrt(0.19)*Scale2;
X147    = sqrt(0.2198)*Scale2;
X148    = sqrt(0.19)*Scale2;
X149    = 0;
X1410    = 0;
X1411    = 0;
X1412    = 0;
X1413    = 0;
X1414    = 0;
X1415    = 0;
X1416    = 0;
X1417    = sqrt(11/36)*Scale2;

X151    = 0;
X152    = 0;
X153    = 0;
X154    = 0;
X155    = 0;
X156    = sqrt(0.095)*Scale2;
X157    = 0;
X158    = sqrt(0.095)*Scale2;
X159    = 0;
X1510    = 0;
X1511    = 0;
X1512    = 0;
X1513    = 0;
X1514    = 0;
X1515    = 0;
X1516    = 0;
X1517    = sqrt(11/36)*Scale2;

X161    = 0;
X162    = 0;
X163    = 0;
X164    = 0;
X165    = 0;
X166    = sqrt(0.2857)*Scale2;
X167    = sqrt(0.3297)*Scale2;
X168    = sqrt(0.2857)*Scale2;
X169    = sqrt(0.7143)*Scale2;
X1610    = 0;
X1611    = 0;
X1612    = 0;
X1613    = 0;
X1614    = 0;
X1615    = 0;
X1616    = 0;
X1617    = sqrt(11/36)*Scale2;
```

```
X171    = 0;
X172    = 0;
X173    = 0;
X174    = 0;
X175    = 0;
X176    = 0;
X177    = 0;
X178    = 0;
X179    = 0;
X1710    = sqrt(11/36)*Scale2;
X1711    = sqrt(11/36)*Scale2;
X1712    = sqrt(11/36)*Scale2;
X1713    = sqrt(11/36)*Scale2;
X1714    = sqrt(11/36)*Scale2;
X1715    = sqrt(11/36)*Scale2;
X1716    = sqrt(11/36)*Scale2;
X1717    = 0;

X      = ...
 [X11,X12,X13,X14,X15,X16,X17,X18,X19,X110,X111,X112,X113,X114,...
X115,X116,X117;X21,X22,X23,X24,X25,X26,X27,X28,X29,X210,X211,...
X212,X213,X214,X215,X216,X217;X31,X32,X33,X34,X35,X36,X37,X38,...
X39,X310,X311,X312,X313,X314,X315,X316,X317;X41,X42,X43,X44,...
X45,X46,X47,X48,X49,X410,X411,X412,X413,X414,X415,X416,X417;...
X51,X52,X53,X54,X55,X56,X57,X58,X59,X510,X511,X512,X513,X514,...
X515,X516,X517;X61,X62,X63,X64,X65,X66,X67,X68,X69,X610,X611,...
X612,X613,X614,X615,X616,X617;X71,X72,X73,X74,X75,X76,X77,X78,...
X79,X710,X711,X712,X713,X714,X715,X716,X717;X81,X82,X83,X84,...
X85,X86,X87,X88,X89,X810,X811,X812,X813,X814,X815,X816,X817;...
X91,X92,X93,X94,X95,X96,X97,X98,X99,X910,X911,X912,X913,X914,...
X915,X916,X917;X101,X102,X103,X104,X105,X106,X107,X108,X109,...
X1010,X1011,X1012,X1013,X1014,X1015,X1016,X1017;X111,X112,...
X113,X114,X115,X116,X117,X118,X119,X1110,X1111,X1112,X1113,...
X1114,X1115,X1116,X1117;X121,X122,X123,X124,X125,X126,X127,...
X128,X129,X1210,X1211,X1212,X1213,X1214,X1215,X1216,X1217;...
X131,X132,X133,X134,X135,X136,X137,X138,X139,X1310,X1311,...
X1312,X1313,X1314,X1315,X1316,X1317;X141,X142,X143,X144,...
X145,X146,X147,X148,X149,X1410,X1411,X1412,X1413,X1414,...
X1415,X1416,X1417;X151,X152,X153,X154,X155,X156,X157,X158,...
X159,X1510,X1511,X1512,X1513,X1514,X1515,X1516,X1517;X161,...
X162,X163,X164,X165,X166,X167,X168,X169,X1610,X1611,X1612,...
X1613,X1614,X1615,X1616,X1617;X171,X172,X173,X174,X175,X176,...
X177,X178,X179,X1710,X1711,X1712,X1713,X1714,X1715,X1716,X1717];
```

```
%molecular properties--end----------------------------------------
wn1 = 0;
wn2 = 627.71 ;
wn3 = 2*wn2 - 2.6080 ;
wn4 = 2*wn2 - 2.3560 ;
wn5 = 2*wn2 + 0.2120 ;
wn6 = wn5 + wn2 - 7.7916 ;
wn7 = wn5 + wn2 - 2.3960 ;
wn8 = wn5 + wn2 - 2.2204 ;
wn9 = wn5 + wn2 + 0.3330 ;
wn10 = 2495.75 ;
wn11 = 2495.76 ;
wn12 = 2503.73 ;
wn13 = 2504.20 ;
wn14 = 2506.60 ;
wn15 = 2506.87 ;
wn16 = 2509.42 ;
wn17 = 3132.17 ;

W1  = 2*pi*(wn2-wn1)*100*c ;
W2  = 2*pi*(wn3-wn2)*100*c ;
W3  = 2*pi*(wn4-wn3)*100*c ;
W4  = 2*pi*(wn5-wn4)*100*c ;
W5  = 2*pi*(wn6-wn5)*100*c ;
W6  = 2*pi*(wn7-wn6)*100*c ;
W7  = 2*pi*(wn8-wn7)*100*c ;
W8  = 2*pi*(wn9-wn8)*100*c ;
W9   = 2*pi*(wn10-wn9)*100*c ;
W10  = 2*pi*(wn11-wn10)*100*c ;
W11  = 2*pi*(wn12-wn11)*100*c ;
W12  = 2*pi*(wn13-wn12)*100*c ;
W13  = 2*pi*(wn14-wn13)*100*c ;
W14  = 2*pi*(wn15-wn14)*100*c ;
W15  = 2*pi*(wn16-wn15)*100*c ;
W16  = 2*pi*(wn17-wn16)*100*c; %lvl17

W      = [W1,W2,W3,W4,W5,W6,W7,W8,W9,W10,W11,W12,W13,W14,W15,W16];
%molecular properties

%simplification parameters
coef   = (e*E0)/hbar;
%simplification parameters
```

```
%the exp factor in the OBE's
factorE = ones(Num,Num,N);
for a = 1:Num
    for b = 1:Num
        Top = max(a,b);
        Bot = min(a,b);
        if (a == b)
                factorE(a,b) = 0;
        else
           for k = Bot:Top-1
               expTerm        = exp(-1i*W(k)*t*(abs( a-b )/(b-a)) );
               FactorEres     = reshape(factorE(a,b,:),1,N);
               factorE(a,b,:) = FactorEres.*expTerm;
           end
        end
    end
end
%the exp factor in the OBE's

%the Hamiltonian time discrete 3dim vector
H = zeros(Num,Num,N);

%iewers hier binne is n issue
for a = 1:Num
    for b = 1:Num
             if (a == b)
                 H(a,b) = 0;
             else
                 FactorEres  = reshape(factorE(a,b,:),1,N);
                 H(a,b,:)    = 1*coef*X(a,b)*EF.*(FactorEres) ;
            end
    end
end
%the Hamiltonian time discrete 3dim vector
%initialize the rho matrix for the numerical evaluation
clear FactorEres
rhoM = zeros(Num,Num,N);

%initial conditions that needs toe be entered by hand %input

%initialize all to zero
rhoM(a,b,:) = 0;
```

```
%initialize the physical levels to certain populations
rhoM(1,1,1) = 1.00 ;
rhoM(2,2,1) = 0.00 ;
rhoM(3,3,1) = 0.00 ;
rhoM(4,4,1) = 0.00 ;
rhoM(5,5,1) = 0.00 ;
rhoM(6,6,1) = 0.00 ;
rhoM(7,7,1) = 0.00 ;
rhoM(8,8,1) = 0.00 ;
rhoM(9,9,1) = 0.00 ;
rhoM(10,10,1) = 0.00 ;
rhoM(11,11,1) = 0.00 ;
rhoM(12,12,1) = 0.00 ;
rhoM(13,13,1) = 0.00 ;
rhoM(14,14,1) = 0.00 ;
rhoM(15,15,1) = 0.00 ;
rhoM(16,16,1) = 0.00 ;
rhoM(17,17,1) = 0.00 ;

%constructing the rho matrix in the form of the optical
%bloch equations.
%But becuase you cannot use a 3-dim array in the plot
%function step2 is done to decrease the dimension to two.
%STEP1
BracketF = 0;
gamma    = 1/(2*(1e-14));
Decay    = zeros(Num,Num,N);
for r = 1: N-1
    for a = 1:Num
        for b = 1:Num
            for l =1:Num
                BracketF = BracketF + ( rhoM(l,b,r)*H(a,l,r)...
                                        - rhoM(a,l,r)*H(l,b,r) );
            end
          %%% DECAY of level 17 into quasi continuum
          if (a ==17 && b==17)
              Decay(a,b,r) = Decay(a,b,r) -   2*gamma*rhoM(a,b,r);
          end
          %fix the off diagonal terms with only one decay in
          if (a ==17 && b≠17)
              Decay(a,b,r) = Decay(a,b,r) -   1*gamma*rhoM(a,b,r);
          end
          if (a ≠17 && b==17)
              Decay(a,b,r) = Decay(a,b,r) -   1*gamma*rhoM(a,b,r);
          end
           %%% DECAY of level 17 into quasi continuum

          rhoM(a,b,r+1) = rhoM(a,b,r) + h*( (-1i)*( BracketF  ) + ...
                                Decay(a,b,r) );
          BracketF = 0;
        end
    end
end
clear H
```

```
%STEP2
% rho_diff_form ( (1,:),(2,:),(3,:),(4,:),(5,:)... ) has this
% form where the : implies the time coordinate and the order
% is like the following format : p11,p12,p13,p21,p22,p23,p31,
% p32,p33. Thus I am creating a list here of the equations
% and therefore reducing the dimensions
rho_diff_form = zeros(Num^2,N);
tel1 = 1;
tel2 = 1;
for count = 1:Num^2 % al die eqns kom nou onder mekaar
        if (tel1 == Num+1)
           tel1 = 1;
           tel2 = tel2 + 1;
        else
           rho_diff_form(count,:) = rhoM(tel2,tel1,:) ;
        end
    tel1 = tel1 + 1;
end

f  = (real((rho_diff_form(37,N)+rho_diff_form(55,N)+...
      rho_diff_form(73,N))));
func = -f;

%%%%%%%%%%%%%%%%%%%%%%%%---MOLECULE-MODEL END---%%%%%%%%%%%%%%%%%
%%%%%%%%%%%%%%%%%%%%%%%%%%%%%%%%%%%%%%%%%%%%%%%%%%%%%%%%%%%%%%%%%
end
```

D.3 Smoothing

Algorithm D.3 Smoothing algorithm

```
function vecout=smoothvectorLudwigSLM(vecin,n)
    if n == 0
       vecout=vecin;
    else
        vecn=length(vecin);
        q=1;
        while q≤n
            if q/2==round(q/2)
                k=2;
            else
                k=3;
            end
            for j=k:2:vecn-1
               vecin(j)=(vecin(j-1)+vecin(j+1))/2;
            end
           q=q+1;
        end
        minvecin = min(vecin);

        if minvecin > 0
           vecin = vecin - minvecin;
        else
           vecin = vecin + abs(minvecin);
        end
        vecin = vecin/max(vecin);
        vecout=vecin;
    end
end
```

D.4 Husimi Plot

Algorithm D.4 Code for generating a Husimi plot.

```
function [step] = HusimiPlot(SIG,alpha,num,t,wnr)
c       = 299972458;
ps2     = 10^(-24);
fs2     = 10^(-30);
N       = num;
t0      = t(1);
tF      = t(numel(t));
wn_laser_set_to     = wnr;
wl                  = 2*pi*100*c*wn_laser_set_to;

t0v     = linspace(t0,tF,N);
t       = t0v;
dw      = (2*pi/(tF-t0));
w0v     = ( -N/2 : N/2 - 1 )*dw + wl;

sizeyEF = numel(SIG);
step    = sizeyEF/N;
EF      = SIG(1:step:N*step);

Q       = zeros(N,N);
for k1 = 1 : N
    parfor k2 = 1:N
        a  =  conj(exp( -1*alpha*(t-t0v(k1)).^2 + ...
              1i*w0v(k2)*(t-t0v(k1)) )).*( EF );
        ingrateV = trapz(a);
        Q(k2,k1) = (abs(ingrateV)^2);
    end
end
w      = w0v;

Points = 2500;
wnew   = w0v;
taun   = t;

w1I   = linspace(wnew(1),wnew(numel(wnew)),Points);
tau1I = linspace(taun(1),taun(numel(taun)),Points);
[w1I2,tau1I2] = meshgrid(w1I,tau1I);

YI    = interp2(wnew,taun,Q,w1I2,tau1I2);
YI    = YI/max(max(YI));

figure
imagesc(taun/1e-15,wnew/(100*c*2*pi),YI);
colormap(jet);
ylabel('Wavenumber (cm^{-1})')
xlabel('Time (fs)')
colorbar;
axis xy;
end
```

D.5 PG FROG

Algorithm D.5 Code for generating a PG-FROG plot.

```
function frog = FROG_PG(Sig,t,wl,fwleft,fwright,FWHM,ftl,ftr,Points)
N     = numel(t);
T     = t(N)-t(1);
w     = ((0 : N-1))*(2*pi/T);
%%%%%%%%%%%%%%%%%%%%%%%%%%%%%%%%%%%%%%%%%%%%%%%%%%%%%%%%%%%%%%%%%%%%%%%%%%%%
f     = [zeros(N,1); Sig(:) ; zeros(N,1)];
ix    = 1 : N;
tfix  = ix + N;
frog  = zeros(N,N);
parfor k1 = 1 : N
    tchange     = 2*N + ix - 2*k1 ;
    func        = f(tfix).*(f(tchange).*conj(f(tchange))) ;
    frog(k1,:)  = fft(func).*conj(fft(func));
end
%%%%%%%%%%%%%%%%%%%%%%%%%%%%%%%%%%%%%%%%%%%%%%%%%%%%%%%%%%%%%%%%%%%%%%%%%%%%
%Frog trace of the pulse
%%%%%%%%%%%%%%%%%%%%%%%%%%%%%%%%%%%%%%%%%%%%%%%%%%%%%%%%%%%%%%%%%%%%%%%%%%%%
wleft  = fwleft*wl;
wright = fwright*wl;

posr    = find(w>wright);
posl    = find(w>wleft);
posrt   = find(t≥ftr*FWHM);
poslt   = find(t≥ftl*FWHM);

wnew = w(posl(1):posr(1));
taun = t(poslt(1):posrt(1));
Ynew = frog(poslt(1):posrt(1),posl(1):posr(1));

w1I   = linspace(wnew(1),wnew(numel(wnew)),Points);
tau1I = linspace(taun(1),taun(numel(taun)),Points);
[w1I2,tau1I2] = meshgrid(w1I,tau1I);

YI    = interp2(wnew,taun,Ynew,w1I2,tau1I2);
YI    = YI/max(max(YI)); %normalize

%jet plot test interpolate
c= 2.998e8;
figure  %FIG4
imagesc(taun,wnew/(100*c*2*pi),YI');
colormap(jet);
title('PG Frog trace of pulse')
ylabel('Wavenumber (cm^{-1})')
xlabel('Delay (sec)')
colorbar;
axis xy;
```

Bibliography

[1] J. C. Whitehead. *Selectivity in chemical reactions*. Kluwer Academic Publishers, 1987.

[2] R. N. Zare. Laser control of chemical reactions. *Science*, 279:1875–1879, 1998.

[3] A. H. Zewail. Femtochemistry: Atomic-scale dynamics of the chemical bond. *Journal of Physical Chemistry A*, 104:5660–5694, 2000.

[4] M. Shapiro and P. Brumer. Coherent radiative control of unimolecular reactions. *Faraday Discussions of the Chemical Society*, 82:177–185, 1986.

[5] R. Kosloff D. J. Tannor and S. A. Rice. Coherent pulse sequence induced control of selectivity of reactions : Exact quantum mechanical calculations. *Journal of Chemical Physics*, 85:5805–5820, 1986.

[6] P. Brumer and M. Shapiro. Coherence chemistry: Controlling chemical reactions with lasers. *Accounts of Chemical Research*, 22:407–413, 1989.

[7] M. Shapiro J. L. Krause and P. Brumer. Coherent control of bimolecular chemical reactions. *Journal of Chemical Physics*, 92:1126–1131, 1989.

[8] L. Zhu R. J. Gordon and T. Seideman. Coherent control of chemical reactions. *Accounts of Chemical Research*, 32:1007–1016, 1999.

[9] National Research Council Committee on AMO 2010. *Controlling the Quantum World: The Science of Atoms, Molecules, and Photons*. National Academies Press, 2010.

[10] T. Chen W. Kiefer R. Pausch, M. Heid and H. Schwoerer. Selective generation and control of excited vibrational wave packets in the electronic ground state of K_2. *Journal of Chemical Physics*, 110:9560–9566, 1999.

[11] M. Oppel and G. K. Paramonov. Selective vibronic excitation and bond breaking by picosecond UV and IR laser pulses : application to a two-dimensional model of $HONO_2$. *Chemical Physics Letters*, 313:332–340, 1999.

[12] S. Chelkowski and A.D. Bandrauk. Raman chirped adiabatic passage: a new method for selective excitation of high vibrational states. *Journal of Raman Spectroscopy*, 28:459–466, 1997.

[13] R. de Vivie-Riedle and U. Troppmann. Femtosecond lasers for quantum information technology. *Chemical Reviews*, 107:5082–5100, 2007.

[14] S. Chelkowski and A. D. Bandrauk. Control of vibrational excitation and dissociation of small molecules by chirped intense infrared laser pulses. *Chemical Physics Letters*, 186:264–269, 1991.

[15] A. D. Bandrauk S. Chelkowski and P. B. Corkum. Effiecient molecular dissociation by a chirpeed ultrashort infrared laser pulse. *Physical Review Letters*, 65:2355–2358, 1990.

[16] M. Yamanouchi M. Sugawara and S. Yabushita. Laser field designing by evolutionary algorithm for coherent control of molecular dynamics. *Chemical Physics Letters*, 396:136–141, 2004.

[17] F. Fleming Crim. Vibrational state control of bimolecular reactions : Discovering and directing the chemistry. *Accounts of Chemical Research*, 32:877–884, 1999.

[18] D. C. Clary. Quantum theory of chemical reaction dynamics. *Science*, 279:1879–1882, 1998.

[19] R. Chakrabarti C. Brif and H. Rabitz. Control of quantum phenomena: Past, present, and future. submitted to: New Journal of Physics, in arXiv:0912.5121.

[20] R.K. Pathria. *Statistical Mechanics*. Elsevier, 2006.

[21] T. Uzer and W.H. Miller. Theories of intramolecular vibrational energy transfer. *Physics Reports*, 199:73–146, 1991.

[22] L. Holz S. M. Nikiforov V. V. Smirnov B. G. Sartakov. V. I. Fabelinskii S. S. Alimpiev, B. O. Zikrin and A. L. Shtarkov. Vibrational relaxation rate of sf_6 molecules excited in an intense ir laser field. *Jounal of Experimental and Theoretical Physics*, 38:421–425, 1984.

[23] P. Brumer and M. Shapiro. Control of unimolecular reactions using coherent light. *Chemical Physics Letters*, 126:541–546, 1986.

[24] M. Shapiro and P. Brumer. Quantum control of chemical reactions. *Journal of the Chemical Society, Faraday Transactions*, 93:1263–1277, 1997.

[25] D. J. Tannor. *Introduction to quantum mechanics: A time-dependent perspective*. University Science Books, 2007.

[26] Y. Y. Yin C. Chen and D. S. Elliott. Interference between optical transitions. *Physical Review Letters*, 64:507–510, 1990.

[27] K. Takahashi M. Kawasaki X. Wang, R. Bersohn and H. L. Kim. Phase control of absorption in large polyatomic molecules. *Journal of Chemical Physics*, 105:2992–2997, 1996.

[28] B. Walker B. Sheehy and L. F. DiMauro. Phase control in the two-color photodissociation of HD^+. *Physical Review Letters*, 74:4799–4802, 1995.

[29] X. Li V. D. Kleiman, L. Zhu and R. J. Gordon. Coherent phase control of the photoionization of H_2S. *Journal of Chemical Physics*, 102:5863–5866, 1995.

[30] D. J. Tannor and S. A. Rice. Control of selectivity of chemical reaction via control of wavepacket evolution. *Journal of Chemical Physics*, 83:5013–5018, 1985.

[31] B. M. Garraway and K. Suominen. Wave packet dynamics in molecules. *Contemporary Physics*, 43:97–114, 2002.

[32] E. A. Torres J. B. Ballard H. U Stauffer E. W. Lerch, X. Dai and S. R. Leone. Manipulation of ro-vibronic wave packet composition using chirped ultrafast laser pulses. *Journal of Physics B: Atomic, Molecular and Optical Physics*, 41:1–7, 2008.

[33] R. Thalweiser T. Baumert, M. Grosser and G. Gerber. Femtosecond time-resolved molecular multiphoton ionization: The Na_2 system. *Physics Review Letters*, 67:3753–3756, 1991.

[34] A. Materny J. L. Herek and A. H. Zewail. Femtosecond control of an elementary unimolecular reaction from the transition-state region. *Chemical Physics Letters*, 228:15–25, 1994.

[35] X. He A. F. Bell P. J. Tonge R. van Grondelle M. Vengri, I. H. M. van Stokkum and D. S. Larsen. Ultrafast excited and ground-state dynamics of the green fluorescent protein chromophore in solution. *Journal of Physical Chemistry A*, 108:4587–4598, 2004.

[36] J. Dods and P. Brumer. Two-color coherent control with SEP preparation: ekectronic branching in Na_2 photodissociation. *Canadian Journal of Chemistry*, 72:958–965, 1994.

[37] H. Theuer K. Bergmann and B. W. Shore. Coherent population transfer among quantum states of atoms and molecules. *Reviews of Modern Physics*, 70:1003–1025, 1998.

[38] A. Woody S. Shi and H. Rabitz. Optimal control of selective vibrational excitation in harmonic linear chain molecules. *Journal of Chemical Physics*, 88:6870–6883, 1988.

[39] S. Shi and H. Rabitz. Selective excitation in harmonic molecular systems by optimally designed fields. *Chemical Physics*, 139:185–199, 1989.

[40] M. Sugawara and Y. Fujimura. Control of quantum dynamics by a locally optimized laser field. application to ring puckering isomerization. *Journal of Chemical Physics*, 100:5646–5655, 1994.

[41] A. I. Solomon S .G. Schirmer and J. V. Leahy. Degrees of controllability for quantum systems and application to atomic systems. *Journal of Physics A: Mathematical and General*, 35:4125–4141, 2002.

[42] A. Albertini and D. D'Alessandro. Notions of controllability for bilinear multilevel quantum systems. *IEEE Transactions on Automatic Control*, 48:1399–1403, 2003.

[43] T. S.Ho M. Artamonov and H. Rabitz. Quantum optimal control of ozone isomerization. *Chemical Physics*, 305:213–222, 2004.

[44] R. S. Judson and H. Rabitz. Teaching lasers to control molecules. *Physical Review Letters*, 68:1500–1503, 1992.

[45] H. Rabitz I. Walmsley R. Kosut M. Grace, C. Brif and D. Lidar. Encoding a qubit into multilevel subspaces. *New Journal of Physics*, 8:1–29, 2006.

[46] D. V. Voronine F. J. Garcia de Abajo W. Pfeiffer T. P. Tuchscherer, C. Rewitz and Brixner. Analytic coherent control of plasmon propagation in nanostructures. *Optics Express*, 17:14235–14259, 2009.

[47] W. Zhu J.M. Geremia and H. Rabitz. Incorporating physical implementation concerns into closed loop quantum experiments. *Journal of Chemical Physics*, 113:10841–10848, 2000.

[48] W. Zhu and H. Rabitz. Closed loop learning control to suppress the effects of quantum decoherence. *Journal of Chemical Physics*, 118:6751–6757, 2003.

[49] Makoto Hasegawa Mitsutoshi Suzuki, Yasuaki Miyamoto and Yoshihiro Shimazaki. Selective excitation of branched vibrational ladder in uranium hexafluoride laser isotope seperation. *Journal of Nuclear Science and Technology*, 31:1006–1018, 1994.

[50] J. R. Baker. Infrared multiphoton decomposition: A comparison of approximate models and exact solutions of the energy-grained master equation. *Journal of Chemical Physics*, 72:3686–3694, 1980.

[51] *Jenoptik, SLM-S640d and SLM-S320d, Technical Documentation, 2009.*

[52] D. E. Goldberg. *Genetic Algorithms.* Addison Wesley, 2005.

[53] *GAVaPS-a genetic algorithm with varying population size*, 1994.

[54] A. M. Weiner. Femtosecond pulse shaping using spatial light modulators. *Review of Scientific Instruments*, 71:1929–1960, 2000.

[55] P. N. Kean D. E. Spence and W. Sibbett. 60-fsec pulse generation from a self-mode-locked ti:sapphire laser. *Optics Letters*, 16:42–44, 1991.

[56] S. A. Rice and M. Zhao. *Optical control of molecular dynamics*. John Wiley & Sons: New York, 2000.

[57] A. Galler F. Frei and T. Feurer. Space-time coupling in femtosecond pulse shaping and its effects on coherent control. *Journal of Chemical Physics*, 130:1–13, 2009.

[58] A.M. Weiner. Femtosecond optical pulse shaping and processing. *Progress in Quantum Electronics*, 19:161–237, 1995.

[59] V. Seyfried M. Strehle T. Baumert, T. Brixner and G. Gerber. Femtosecond pulse shaping by an evolutionary algorithm with feedback. *Applied Physics B*, 65:779–782, 1997.

[60] J.P. Heritage A.M. Weiner and E.M. Kirschner. High-resolution femtosecond pulse shaping. *Journal of the Optical Society of America B*, 5:1563–1572, 1988.

[61] J. S. Patel A. M. Weiner, D. E. Leaird and J. R. Wullert. Programmable femtosecond pulse shaping by use of a multielement liquid-crystal phase modulator. *Optics Letters*, 15:326–328, 1990.

[62] R. N. Bracewell. *The Fourier Transform and its Applications*. McGraw-Hill Kogakusha, 1978.

[63] R. Trebino. *Frequency-resolved optical gating: The measurement of ultrashort laser pulses*. KAP, 2000.

[64] T. C. Weinacht B. J. Pearson, J. L. White and P. H. Bucksbaum. Coherent control using adaptive learning algorithms. *Physics Review A*, 63:1–12, 2001.

[65] B. J. Pearson and P. H. Bucksbaum. Control of ramanlasing in the nonimpulsive regime. *Physical Review Letters*, 92:1–4, 2004.

[66] C. Meier V. S. Malinovsky and D. J. Tannor. Optical paralysis in electronically congested systems: application to large-amplitude vibrational motion of ground state na_2. *Chemical Physics*, 221:67–76, 1997.

[67] A. Douhal and J. Santamaria, editors. *Femtochemistry and femtobiology: ultrafast dynamics in molecular science*. 2002.

[68] F. L. H. Brown C. J. Bardeen, J. Cao and K. R. Wilson. Using time-dependent rate equations to describe chirped pulse. *Chemical Physics Letters*, 302:405–410, 1999.

[69] V. S. Malinovsky and J. L. Krause. General theory of population transfer by adiabatic rapid passage with intense, chirped laser pulses. *European Physics Journal D*, 14:147–155, 2001.

[70] A. E. Siegman. *Laser*. University Science Books, 1986.

[71] A. Hariharan D. Goswami J. S. Melinger, Suketu R. Gandhi and W. S. Warren. Adiabatic population transfer with frequency-swept laser pulses. *Journal of Chemical Physics*, 101:6439–6454, 1994.

[72] T. Feurer. Femtosecond light: Optics and interactions. Lecture Notes 2009.

[73] K. S. Viswanathan. Anharmonicity of vibration in molecules. *The Proceeding of the Indian Academy of Sciences*, XLVII:85–97, 1958.

[74] C. W. Patterson N. G. Nereson M. J. Reisfeld B. J. Krohn, R. S. McDowell and K. C. Kim. Analysis of the q branch of the $3\nu_3$ overtone of the uf_6 : the implied structure of the $n\nu_3$ ladder. *Journal of molecular spectroscopy*, 132:285–309, 1988.

[75] V. S. Letokov, editor. *Laser spectroscopy of highly vibrationally excited molecules.* Adam Hilger, 1989.

[76] R. Loudon. *The Quantum Theory of Light.* Oxford University Press, 1983.

[77] B. Diu C. Cohen-Tannoudji and F. Laloë. *Quantum Mechanics.* Wiley-VCH, 2005.

[78] P. W. Milonni and J. H. Eberly. *Lasers.* Wiley Interscience, 1988.

[79] J. C. Diels and S. Besnainou. Multiphoton coherent excitation of molecules. *Journal of Chemical Physics*, 85:6347–6355, 1986.

[80] M. M. Hsieh H. A. Rabitz and C. M. Rosenthal. Quantum optimally controlled transition landscapes. *Science*, 303:1998–2001, 2004.